POLITECNICO DI MILANO

Scuola di Ingegneria Industriale e dell'Informazione
Dipartimento di Energia
Corso di Laurea Magistrale in Ingegneria Energetica

POLITECNICO
MILANO 1863

DEVELOPMENT AND ASSESSMENT OF PHYSICAL BASED PROFILE LOSS MODEL FOR ORC TURBINE BASED ON BOUNDARY LAYER ANALYSIS

Relatore: Prof.Paolo Gaetani
Relatore estero: Prof.Dr. Matteo Pini

Tesi di Laurea di:
Federico Pizzi, matricola 852784

Anno Accademico 2016 - 2017

English Abstract

The Organic Rankine Cycles are receiving many attention since they make possible to exploit renewable source. In particular the necessity to establish a theoretical knowledge about the physical phenomena for this technology is the primary concern. In fact literature is poor of knowledge and there is not any general and solid specifications for the so called mean-line-design; moreover the classical loss models are not suitable for these new machine which processed such complex fluids. This thesis work is focused on the profile losses study in terms of physical based approach, analyzing in deep the fundamental phenomenon at the base: the boundary layer. The first part of this thesis was dedicated to the assessment of boundary layer code which has been the main instrument to obtain results and physical conclusion through a large amount of simulations. This code has been built with the original purpose to investigate the wall fluid-mechanics behavior of the nozzle belonging to the experimental facility ORCHID of the Power and Propulsion department of the Technische Universiteit Delft. The first results of this work concern the Smith's charts for the estimation of profile losses for axial machine through a physical based approach. However the core structure is the boundary layer analysis focusing on the behavior of the dissipation coefficient, crucial element for the estimation of whatever near wall phenomena. This dimensionless group represents the entropy generation inside the viscous fluid flows and it has been investigated under many aspects: incompressible case, with and without acceleration, compressible supersonic both for air and for other classes of fluids. Because it is a new parameter it has been performed a sensitivity analysis in order to determine quantitatively what is the most influencing parameter on the dissipation phenomena in the boundary layer. In the final part, all ours results have been compared, with good response, against a classical CDF code (SU2) suitable for the aerodynamic optimization.

Keywords: Boundary Layer; dissipation coefficient; ORC turbine; profile loss theory; CFD; boundary layer code;

Italian Abstract

I cicli Rankine utilizzanti fluidi organici stanno acquistando interesse poiché sono adatti allo sfruttamento di risorse energetiche rinnovabili. In particolare, oggi sorge la necessità di stabilire conoscenze solide circa i fenomeni fisici per questa tecnologia. In letteratura, infatti, c'è scarsezza di risultati generali in particolare per le cosiddette linee guida per il progetto preliminare della turbomacchina; inoltre i metodi classici di perdite non sono adatti a macchine di nuova generazioni che processano tale tipo di fluidi. Il presente lavoro di tesi si inquadra in quest' ottica, concentrandosi sull' analisi delle perdite di profilo ed investigando il fenomeno fondamentale alla base: lo strato limite. La prima parte di questa tesi è stata dedicata alla verifica di un codice di strato limite che poi è stato utilizzato per ottenere risultati attraverso molte simulazioni. Tale codice è stato elaborato con l' obiettivo di studiare tali fenomeni per l'ugello dell' apparato sperimentale ORCHID del dipartimento Power and Propulsion della Technische Universiteit Delft. Oltre alla presentazione di grafici tipo Smith per le perdite di profilo in macchine assiali, il presente lavoro si concentra soprattutto sullo studio dello strato limite e del coefficiente di dissipazione elemento fondamentale per la stima dell' efficienza di qualunque fenomeno fluido-meccanico a parete. Tale gruppo adimensionale è stato indagato sotto molti aspetti: casi incomprimibili, supersonici comprimibili sia per aria che per altre classi di fluidi, in particolare quelli a complessità molecolare alta. Data la novità dello studio, un analisi di sensibilità è stata effettuata per determinare quantitativamente qual è il parametro determinante sulle dissipazioni nello strato limite. Nella parte finale è stato fatto un confronto, con buon esito, tra i nostri risultati e quelli derivanti da SU2 classico codice CFD per l'ottimizzazione aerodinamica.

Keywords: Strato limite; Coefficiente di dissipazione; ORC turbine; teoria delle perdite di profilo; CFD; codice di strato limite;

A tutte le persone
che mi hanno accompagnato in questo viaggio
Amici, genitori e mentori...

Aknowledgement

Questo lavoro di tesi non sarebbe stato possibile senza la stima, il supporto e la guida di molte persone. In ordine temporale, vorrei ringraziare il Professor Paolo Gaetani che mi ha trasmesso la passione per l' ambito delle turbomacchine ed anche per la fiducia dimostratami dandomi la possibilità di svolgere la tesi all' estero. Un grazie speciale va al Professor Matteo Pini, supervisore estero, cha mi ha guidato in un mondo per me nuovo come la ricerca mostrando sempre entusiasmo ed interesse verso il lavoro svolto. Alla luce dei mesi trascorsi mi sono sentito veramente fortunato ad avere a disposizione un weekly supervisor come lui. I suoi input e consigli sono sempre stati importanti nel superamento di ostacoli e problematiche di ricerca. Ringrazio anche il Dottor Carlo de Servi per i suggerimenti e l'appoggio nella parte più complessa di tale lavoro. Nessun risultato sarebbe stato ricavato senza il codice scritto da lui. La mia riconoscenza va a Dominic, studente col quale abbiamo lavorato insieme durante questi dieci mesi al TU di Delft condividendo risultati ed entusiasmo per le scoperte. Ancora, senza i suoi sforzi nello svviluppo del programma non sarebbe stato possibile ricavare tali risultati. Non è stato solo un collega ma un caro amico che mi ha insegnato tanto non solo in termini scolastici ma anche su questo bellisimo paese che è l' Olanda. Un grazie generale va al gruppo di Power and Propulsion del TU di Delft, il quale mi ha fatto capire che il futuro a cui aspiro è quello della Ricerca e dell' Accademia. Infine un grazie va anche al Professor Rene Pecnik per i commenti e consigli sui concetti teorici presenti in questa tesi.

Naturalmente il lavoro di tesi è solo la parte culminante di un lungo e duro percorso in cui felicità, ed ogni tanto delusione, si alternano, ecco perchè sono fondamentali amici come quelli che ho avuto in questi ultimi anni. In particolare un sentito grazie va Mattia "Tia", Andrea "Rei" e Lorenzo "Means" per le giornate di studio/progetti e risate fatte insieme. Un grande grazie va a Gabriele "Gabra" per le scalate e per le escursioni fuori dall grigia Milano, ed al grande Corrado con cui per due anni si è fantasticato sulle turbomacchine ed il nostro futuro. Non meno importante è la riconoscenza verso i miei coinquilini, bravissimi ragazzi che hanno contribuito ad un clima allegro e rasserenante quindi grazie a Pasquale con cui si è condiviso per un paio d' anni "l'attico Bovisa" ed a Simone, per le serate e tutti i consigli che mi ha dato.

Naturalmente l' ultimo ringraziamento va ai miei genitori fonte di sostentamento non solo economico ma soprattuto morale essendoci sempre stati, e soprattutto avendo assecondato tutti i miei obiettivi e volontà appoggiandomi sempre...

Riassunto esteso

Scopo del lavoro

Il presente lavoro ha come scopo principale lo studio dei fenomeni fisici fluido dinamici relativi alle perdite di profilo in turbine di nuova concezione, ossia processanti fluidi a complessità molecolare alta (ORC). L' intento iniziale era quello di utilizzare un approccio physical-based in quanto l'unico valido per nuove applicazioni, con l' obiettivo di riprodurre dei diagrammi adimensionali di effeicienza tipo-Smith mostrando l' impatto del fluido. Tale obiettivo non solo è stato raggiunto ma è servito come introduzione ad uno studio più fondamentale e generale: analisi qualitativa e quantitativa dei fenomeni di strato limite per una lamina piana (flat plate). Al centro di questa analisi c'è lo studio del parametro fondamentale di questo modello: il *dissipation coefficient*. Il lavoro portato a termine si vuole porre come il primo studio completo riguardo a questo coefficiente in quanto in letteratura ci sono solo due grafici riportati dal Denton nel suo *Loss mechanisms in turbomachines*. Il bisogno di estendere la conoscenza di questo parametro risulta cruciale per qualsiasi approccio con fenomeni di strato limite, in particolare per i campi di aero-fluidodinamica delle turbomacchine. La possibilità di studiare, analizzare i fenomeni e produrre risultati riguardo allo strato limite è stato possibile grazie allo strumento che il Dr. Carlo De Servi, lo studente del TU Delft Dominic Dijkshoorn ed il sottoscritto hanno rispettivamente creato, validato-verificato, migliorato ed adattato a casi applicativi. Con una conoscenza profonda dei fenomeni fisici siamo in grado di predire il comportamento di qualsiasi applicazione, in particolare per flussi in turbine trovando un ottimo in cui le perdite di profilo potrebbero essere minimizzate. In ottica di ORC la scoperta interessante è stata riguardo al comportamento di tali fluidi in strato limite: essi per quanto non-convenzionali in alcuni campi quale la gas-dinamica, dimostrano l' andamento più classico possibile in regime laminare in prossimità della parete, seguendo la teoria analitica di Blasius vale a dire comportamento incomprimibile anche ad alti numeri di Mach (high speed flow) ed in zone di forte non-realità del gas. La conclusione fondamentale è che la natura del fluido influenza fortemente i fenomeni viscosi a parete (strato limite). Le conseguenze sono naturalmente interessanti in quanto:

- semplifica significativamente i futuri studi riguardo a questi fluidi in campo aerotermodinamico
- riduce le variabili di ottimizzazione per le perdite di profilo poichè il C_d non ha

margini di riduzione, al contrario di fluidi più semplici.

Tali risultati saranno importanti per il gruppo di *Power and Propulsion* della Technische Universiteit Delft (NL) per lo studio dell' apparato ORCHID in particolare per il nozzle.

Le domande di ricerca, "impalcatura" e tracciato su cui si è sviluppato il presente lavoro sono:

- Qual è l' andamento del C_d, sorgente delle perdite di profilo, per flussi incomprimibili e successivamente con effetti di comprimibilità (high speed flow)?
- Qual è l' effetto della non idealità del fluido?
- Qual è l' accuratezza dei risultati di un modello di perdite fisico basato su questi risultati confrontato con la CFD?

Struttura del lavoro

Il presente lavoro di tesi si struttura come segue:

Ricerca-lavoro individuale

Nel periodo iniziale è stata svolta un' ampia rassegna della letteratura. Gli argomenti ed i campi coinvolti in questa tesi sono molteplici ergo la bibliografia ha una notevole estensione. Il riferimento principale, spunto di tutto questo lavoro è stata la produzione di Denton (ed in generale del Whittle Lab. di Cambridge) relativo ad una nuova concezione di modelli di perdita. Altra parte teorica importante è legata alla letteratura riguardante le applicazioni ORC, non ideal gas - dynamic. Infine uno studio generale dei modelli classici della teoria delle turbomacchine e dei principali e più famosi modelli di perdita è stato fatto. In parallelo a ciò i primi calcoli di generazioni entropiche seguendo il modello del Denton sono sati condotti: partendo da un profilo isolato e ricavando una formulazione per gas perfetti si è approcciato il modello physical - based. Come passo successivo lo studio di un tipico stadio a reazione stata condotta, utilizzando approcci convenzionali quali Zweifel, Smith e correlazioni angoli di flusso-coefficienti adimensionli. Tutto ciò rappresenta l' introduzione allo studio del coefficiente di dissipazione, necessario per chiudere il modello fisico di perdite di profilo.

Lavoro in collaborazione con lo studente Dominic Dijkshoorn (TU Delft 3ME)

In questa sezione i risultati sono stati ottenuti da una ricerca in parallelo operata sul BOUNDARY LAYER CODE. In questa fase è stata necessaria una conoscenza approfondita dei fenomeni di strato limite e dei codici classici per studiare lo stesso. In particolare la letteratura su questo argomento è molto vasta quindi è stato importante seguire la produzione di tre autori principali: Cebeci, Clutter, Smith. In questa sezione si collocano i primi risultati riguardanti la verifica del C_d. Il lavoro congiunto ha portato infine alla costruzione di un codice più efficiente della versione originale di Clutter-Smith:

- Implementazione del metodo Keller-Box di ultima versione: accoppiamento delle equazioni del trasporto in unica matrice 5x5 (3 quantità di moto e 2 per le energia) derivanti dalla linearizzazione delle equazioni originali. Grande riduzione del tempo computazionale.
- possibilità di integrazione di una libreria per le proprietà di fluidi (FluidProp). Ciò consente lo studio di qualsiasi stato gassoso.
- integrazione dell' ultima versione del modello di turbolenza Cebeci - Smith. Modello di turbolenza a 0-equazioni abile di individuare inner e outer layer e capace di governare fenomenologie comprimibili.

Infine la parte turbolenta è stata condotta in parallelo con lo scopo di arricchire lo studio dei fenomeni in tale regime.

Boundary layer study

Attraverso il codice di strato limite è stato possibile studiare molteplici casi di flussi viscosi su lamina piana e in condizione di flusso accelerato. Il centro dello studio del regime laminare è rappresentato dalla sensitivity analisys riguardo all' impatto del fluido sullo strato limite in particolare sulla dissipazione operata dallo stesso.

Parte finale: Validazione risultati tramite con CFD code

Al fine di valutare quantitativamente la bontà dei risultati ottenuti si utilizza in questa sessione il software SU2 sotto la supervisione del Prof.Dr Matteo Pini. Uno studio aerodinamico riguardante le perdite per strato limite è stato condotto con tre strumenti differenti: il nostro codice, SU2 e il modello di Denton. I risultati sono ragionevoli e molto vicini tra loro.

Originalità del lavoro e dei risultati

La caratteristica principale di questo lavoro è stata quella di produrre una quantità consistente di risultati nuovi. Tutto ciò che ruota intorno al C_d è sostanzialmente nuovo, essendoci fino ad oggi in letteratura solo i grafici collezionati dal Denton nel suo articolo. Lo studio del comportamento in laminare dei fluidi ad alta complessità molecolare presenta anche originalità e la correttezza dei risultati è stata ricontrata durante il periodo di lavoro grazie ad un paper uscito in parallelo (2017). L' autore, Kluwick arrivava a conclusioni perfettamente in linea con i risultati di questa tesi.

Software utilizzati

L'importanza degli strumenti di lavoro è cruciale per correttezza dei risultati. Nel presente lavoro buona parte del tempo è stata dedicata allo sviluppo di un proprio codice specifico per gli studi fenomenologici dello strato limite.

- **Excel**: foglio di calcolo della release OFFICE®raccolta dati e tabelle per i fluidi; prove sull' equazione entropica gas perfetti.
- **Visual Studio**: ambiente Windows per la compilazione e simulazione basato su diversi linguaggi: usato solo due volte nel passaggio da FORTRAN a MATLAB per il codice turbolento.
- **Matlab**: principale programma utilizzato. Boundary layer code, grafici termodinamici e calcolo dei grafici tipo-Smith per le perdite primarie.
- **FluidProp**: Programma contenente librarie termodinamiche di una vasta gamma di fluidi e miscele. Rilasciato da Asymptote®
- **SU2**: Stanford University Unstructure open source CFD code usato per la parte finale di validazione
- **TecPlot**: Ambiente di grafica per plottare ed analizzare i risultati CFD (post-processing).

Conclusioni e Sviluppi futuri

In quanto questo lavoro è uno dei primi (se non il primo) nel suo genere, vale a dire studio del C_d per flussi comprimibili e per fluidi diversi dall' aria, è chiaro che esso rappresenta il primo passo di un lungo percorso. Lo scopo iniziale è la determinazione quantitativa del coefficiente di dissipazione per una lamina piana in regime adiabatico, stazionario: lo studio più semplice possibile. Il primo punto di ricerca ha mostrato la verifica dei risultati riportati in letteratura sottolineando come gli effetti di comprimibilità siano importanti

solo per alcune classi di fluidi (semplici). Ciò è stato fatto mostrando come dipenda dalla natura del fluido: in regime laminare tale studio è corretto in quanto è una teoria analitica. Il panorama cambia totalmente in regime turbolento poichè i fluidi semplici o classici quali aria e vapore acqueo dimostrano forti gradienti delle proprietà di trasporto, ergo un modello di turbolenza più complesso andrebbe implementato.
La non-idealità, rappresentata da due coefficienti principali Z e Γ, rispettivamente fattore di comprimibilità e derivata fondamentale della gas-dinamica, non porta alcuna deviazione nella fenomenologia e trend del C_d essa semmai ha un impatto su:

- proprietà del fluido al cambiare della temperatura; quindi solo ad alti Mach si iniziano a ravvisare effetti
- calore specifico, numero di Prandtl e distribuzione di densità all' interno dello strato limite dipendono dalla zona del diagramma di compressibilità.
- i fluidi complessi spostandoci nel piano di comprimibilità non mostrano deviazione in tutti i parametri di stato limite: rapporto di temperatura, rapporto di pressione, parametro di viscosità (parametro di Chapman-Rubesin) rimangono fissati sull' unità. Ciò perchè tale tipologia di fluidi riesce ad incamerare grandi quantità di energia senza modificare significativamente la temperatura; quindi la dissipazione di energia cinetica in termica (fenomeno descritto e quantificato dal C_d) rimane costante in tutti i casi.

Per concludere la non idealità del gas non ha alcun impatto sui fluidi candidati per applicazioni ORC (silossani in testa) e con questo si è risposto al secondo punto. Per quanto riguarda la verifica utilizzando SU2 si può dire con certezza che il codice di strato limite dà buoni risultati anche se non coglie fenomeni quali punto di stagnazione, fenomeni di miscelazione al vertice di uscita della pala, quindi tende a sottostimare leggermente le perdite di profilo. Al contrario il metodo di Denton tende a sovrastimare fissando un limite superiore per il coeffciente di dissipazione (0.002).
Con la presente tesi ci siamo spinti fino allo studio turbolento a numeri di Mach non troppo elevati (2) . Molti sviluppi potrebbero essere ancora indagati su tutti i fronti, sia da un punto di vista fisico che numerico-implementativo. In particolare la non-adiabaticità impatta fortemente sui fenomeni di dissipazione in quanto la generazione di entropia è direttamente correlata con lo scambio di calore con la parete. Anche la non stazionarietà del flusso cambia totalmente il valore del C_d quindi tale studio è cruciale. Sempre nel primo punto di ricerca si intendeva analizzare gli effetti di comprimibilità. Essi sono stati analizzati in modo fisicamente corretto in regime laminare, tuttavia nel caso turbolento un modello più complesso va integrato nel codice al fine di descrivere fenomenologie complesse quali la distribuzione dell' energia cinetica turbolenta o il tasso di dissipazione (ε) con tutti i concetti statistici ad essi correlati.

Contents

List of Figures

List of Tables

Nomenclature

Symbols

A	Area, Van Driest parameter in turbulence model	m^2, [-]
b	Blade camber line	m
c	Speed of sound (S.o.S) $\sqrt{\left(\frac{\partial p}{\partial \varrho}\right)_s}$,	m/s
c_p	Specific heat at constant pressure	J/kgK
c_v	Specific heat at constant volume	J/kgK
C	Chord, Chapman-Rubesin parameter $\frac{\varrho\mu}{(\varrho\mu)_e}$	m, [-]
C_d	Dissipation coefficient $\frac{T_e \dot{S}_a}{(\varrho u^3)_e}$	[-]
c_D	Drag coefficient	[-]
C_L	Lift coefficient	[-]
C_x	Axial chord	m
c_f	skin friction coefficient	[-]
C_{ft}	Zweifel coeffcient (0.8 or 0.9)	[-]
D	Diameter, Drag	m, N
$\dot{D}$	Dissipation integral $\int_0^e \frac{\tau_{xy}}{T}\frac{\partial u_x}{\partial y}$	W/m^2
$\overline{e}_{2D}$	Glassman loss coefficient	[-]
e	Specific internal energy	J/kg
$\overline{e}_{2D}$	Energy thickness (Glassman model)	[-]
Ec	Eckert number $\frac{U^2}{\Delta h}$	[-]
F_x	Specific friction force	N/kg
f	Boundary layer dimensionless stream funtion	[-]

f'	Boundary layer first parameter (velocity ratio) $\frac{u}{u_e} = \frac{\partial f}{\partial \eta}$	[-]
f''	Boundary layer shear parameter $\frac{\partial f'}{\partial \eta}$	[-]
G	Turbulence model parameter	[-]
H	Blade height, Boundary layer shape parameter $\frac{\delta^*}{\theta}$	m, [-]
H_2	Boundary layer second shape parameter $\frac{\delta^{**}}{\theta}$	[-]
h	Specific enthalpy	J/kg
i	Incidence angle	deg
K_{is}	Head coeffcient	[-]
l	chord length, mixing length in 0-equation turbulence model	m, m
L	Lift, Characteristic length, Flat plate length	N, m, m
Ma	Mach number $\frac{u}{c}$	[-]
N	Inner layer turbulence parameter, Revolution speed	[-], rpm
$\dot{P}$	Power	W
P	Production terms in transport equation	
p^+	Pressure gradient coefficient in Cebeci-Smith model (eq.2.62)	[-]
Pr	Prandtl number $\frac{\mu c_p}{\lambda} = \frac{\nu}{\alpha}$	[-]
Pr_t	Turbulent Prandtl number $\frac{\nu_t}{\alpha_t}$	[-]
q	Heat flux	W/m^2
r	Boundary layer recovery factor $\frac{T_{ad\ w}-T_e}{T_T-T_e}$	[-]
r^*	Stage Degree of reaction	[-]
R	Radius, Rothalpy	m, J/kg
Re	Reynolds number $\frac{Lu}{\nu}$	[-]
Re_θ	Reynolds number based on momentum thickness $\frac{\theta u_e}{\nu}$	[-]
Re_τ	Reynolds number based on friction velocity $\frac{\delta u_\tau}{\nu}$	[-]
Re^*_τ	Semilocal Reynolds number $Re_\tau \sqrt{\frac{\bar{\varrho}}{\bar{\varrho_w}}}$ / $\frac{\bar{\mu}}{\mu_w}$	[-]
s	Specific entropy, pitch	J/kgK, m
$\dot{S}$	Entropy generation per unit length $\dot{S} = \int_l \frac{C_d(u_e^3 \varrho)_e}{T_e} dx$	W/mK

$\dot{S}_a$	Entropy generation per unit area $\int_0^e \dot{S}_v dy$	W/m^2K
$\dot{S}_v$	Entropy generation per unit volume $(\frac{\tau_{xy}}{T}\frac{du_x}{dy} - \frac{dq}{dy})$	W/m^3K
S_0	Blade suction surface	m
T	Temperature	K
t	Blade trailing thickness	m
U	Peripheral speed	m/s
u	Velocity	m/s
u^+	Scaled velocity (Van Driest law of the wall) $\frac{u}{u_\tau}$	m/s
u_τ	Friction velocity $\sqrt{\frac{\tau_w}{\varrho}}$	m/s
$\dot{V}$	Volumetric flow rate	m^3/s
V	Velocity of the stage	m/s
v	Specific volume	m^3/kg
x	Spatial coordinate. Boundary layer axial direction	m
y	Spatial coordinate. Boundary layer vertical direction	m
Z	Compressibility factor $\frac{v}{v^0}$	[-]
y^+	Scaled coordinate for turbulent boundary layer $\frac{yu_\tau}{\nu}$	[-]
y^*	Semilocal scale coordinate for turbulent boundary layer $\frac{y}{\delta}Re_\tau^*$	[-]
Y	Pressure loss coefficient $\frac{\Delta P_T}{\text{reference dynamic pressure}}$	[-]
∇	Hamiltonian operator $\begin{bmatrix} \frac{\partial}{\partial x}\vec{i} \\ \frac{\partial}{\partial y}\vec{j} \\ \frac{\partial}{\partial z}\vec{k} \end{bmatrix}$,	

Greek Symbols

α	Absoulute flow angle, thermal diffusivity, outer layer turbulence factor	degree, m^2/s, [-]
β	Relative flow angle, pressure ratio	degree, [-]
γ	Specific heat ratio, intermittency factor (Klebanoff factor), stagger angle	[-], [-], deg
Γ	Fundamental Derivative of gas dynamic, Aerodynamic circulation	[-], m^2/s
δ	Boundary layer thickness	m

δ^*	Boundary layer displacement thickness	m
δ_{ij}	Kronecker delta	[-]
∂	Partial derivative	
ε	Dissipation rate (turbulence), deflection angle, eddy kinetic viscosity, blade loading	m^2/s^3, rad/degree, m^2/s, [-]
ζ	Loss coefficient	[-]
η	Efficiency, Blasius transformed coordinate $y\sqrt{\frac{u}{\nu x}}$	[-] , [-]
κ	Von Karman universal constant in log wall 0.41	[-]
θ	Boundary layer momentum thickness, fluid complexity	m, [-]
λ	Thermal conductivity, Bulk viscosity (Lamè const), Work coefficient	W/mK, Pa s, [-]
Λ	Boundary layer Pohlausen parameter $\frac{\delta^2}{\nu}\frac{du_e}{dx}$	[-]
μ	Dynamic molecular viscosity	Pa s
μ_t	Eddy viscosity	Pa s
ν	Kinematic vicosity (mechanical diffusivity),	m^2/s
π	Pi greek (≈ 3.14), Buckingham thorem symbol	[-]
ϱ	Density	kg/m^3
τ	shear stress	Pa
τ'_{ij}	Reynolds shear stress $-\varrho\overline{u'_i u'_j}$	Pa
χ	Reynold number correction for profile loss models	
ϕ	Flow coeffcient	[-]
ψ	Loading coeffcient, general transport property	[-],[-]
ω	Turbulence frequency, revolution speed	s^{-1}, rad/s

Subscript, Superscript and Abbreviation

δ	Evaluated at Boundary layer edge
∞	Related to free-stream
$\overline{()}$	Average quatity
^{0}	Ideal gas quantitiy
S_0	related to blade suction side

’	Fluctuation quantity
0	Inlet of turbine stage
1	Outlet of stator cascade
2	Outlet of turbine stage
AM	Ainley Mathieson
ax	Axial
B-Z-T	Bethe, Zel’dovich, Thompson
c	Critical (thermodynamic)
CFD	Computational fluid dynamics
DC	Dunham Came
DF	Diffusion Factor
DNS	Direct Numerical Simulation
e	Evaluated at Boundary layer edge
gen	Generation
HMC	High Molecular Complexity
ij	Tensorial notation: i, rows; j: columns
irr	Irreversibilitie(in terms of II principle of thermodynamic)
Ko	Kacker Okapuu
LMC	Low Molecular Complexity
m	Meridian
max	Maximum quantity
ORC	Organic Rankine Cycle
PS	Pressure side
r	Reduced quantity
RANS	Reynolds Averaged Navier Stokes
ref	Reference
SA	Spalart Allmaras
SS	Suction side

SST	Shear Stress Transport
SU2	Stanford University Unstructured
T	Total
t	Turbulent quantity
tg	Tangential
TR	Transition
TS	Total-to-static
TT	Total to total
w	Wall quantity
x, y, z	Vectorial components

" I too can see the stars on a desert night, and feel them. But do I see less or more? The vastness of the heavens stretches my imagination — stuck on this carousel my little eye can catch one-million-year-old light. A vast pattern — of which I am a part... What is the pattern, or the meaning, or the why? It does not do harm to the mystery to know a little about it. For far more marvelous is the truth than any artists of the past imagined! Why do the poets of the present not speak of it? What men are poets who can speak of Jupiter if he were a man, but if he is an immense spinning sphere of methane and ammonia must be silent? "

Richard Feynman

Chapter 1

Introduction

This part presents a general introduction about the ORC (Organic Rankine Cycle) technology topic. The first part deals with the thermodynamic features. The second section analyzes the turbomachinery characteristics . The chapter will end with the presentation of the goal and motivation of this work and the point of originality.

1.1 Organic Rankine Cycle (ORC): thermodynamic point of view

The Organic Rankine Cycle (ORC) is one of the most interesting technology in the energy scenario. This thermodynamic asset allows to exploit sources hardly or impossible to use with cycles employing common working fluids such as water or air. The possibility to select a different fluid represents an additional degree of freedom for the design of a thermodynamic cycle, therefore the optimization is based on more variables. Each element of the cycle is influenced by the typology of the fluid: heat exchangers, turbomachines. Nowadays the necessity to exploit new energetic sources has a primary importance in order to accomplish the task of new energy saving: biomass, geothermal and solar power plants are only the most important classes to achieve this goal. Since the primary source is poor from an energetic point of view (low enthalpy source), the classical steam power plant would be inappropriate: impossibility to design expander [5] or the problems related to efficiency drop are so relevant mainly due to the extremely small mass flow rate. The main characteristics of ORC power plant are resumed in the figures (a) and (b) 1.1.

As we can see, the plant's layout can include a regeneration part. The right chart 1.1(b) shows the working region of ORC technology. The benefits related to the exploitation of ORC cycles are summarized in the following points:

- pressure and density levels within the cycle can be decoupled from the cycle tem-

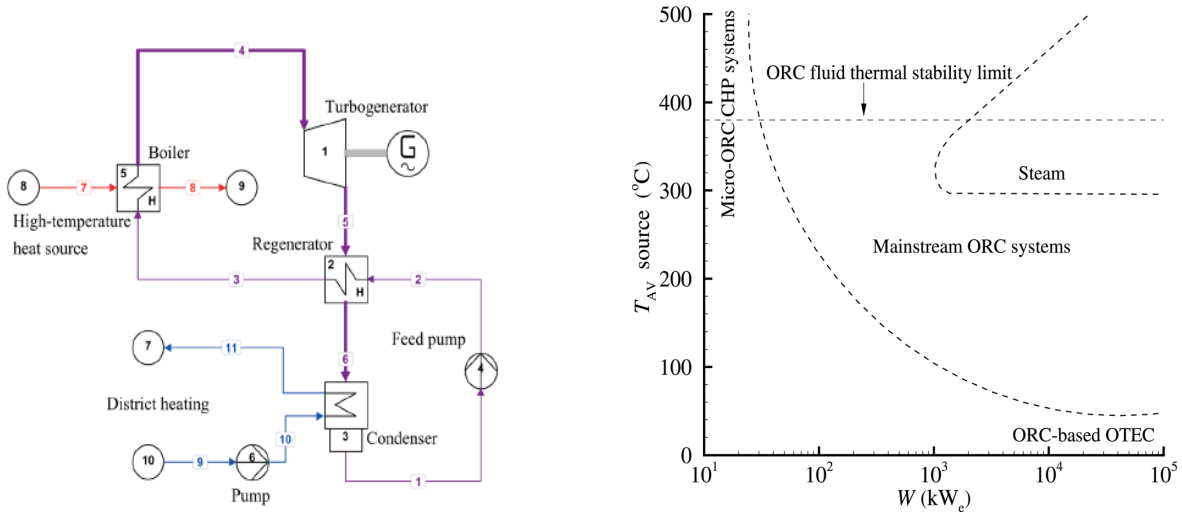

Figure 1.1: General features for ORC technology: (a) Typical plant layout; (b) Working region of application; [5]

perature having the possibility to choice the working fluid, therefore it is possible optimize the cycle.

- the chance of a thermal regeneration through a de-super-heating process. This asset increases the cycle efficiency (from first principle point of view):

$$\eta = \frac{\dot{P}}{\dot{Q}}$$

With a fixed useful effect $\dot{P}$, if the thermal power entering in the cycle is reduced the efficiency increases having an important consequence on energy savings.

- the nature of the fluid manifests its behavior in the saturation curve. More complex is the fluid the steeper is the curve. The consequence is the possibility to perform a dry expansion with the benefit of a higher expansion efficiency and reliability due to the lack of liquid droplets.

- For a low power output, between the range of kW to MW, the realization of the expanders could be problematic if not impossible since the mass flow rate is extremely small: axial or radial turbine would present a difficult design with a very low efficiency. Other type of machines (volumetric) add other problems, therefore, this is not the right pathway. The ORC is the solution. The dry expansion avoids the blade erosion and efficiency issue due to condensation. Moreover many ORC working fluids are also suitable as lubricant for rotating machine.

- possibility to operate at smaller temperature than conventional fluid because the freezing point is much lower than water.

About the thermodynamic characteristics:

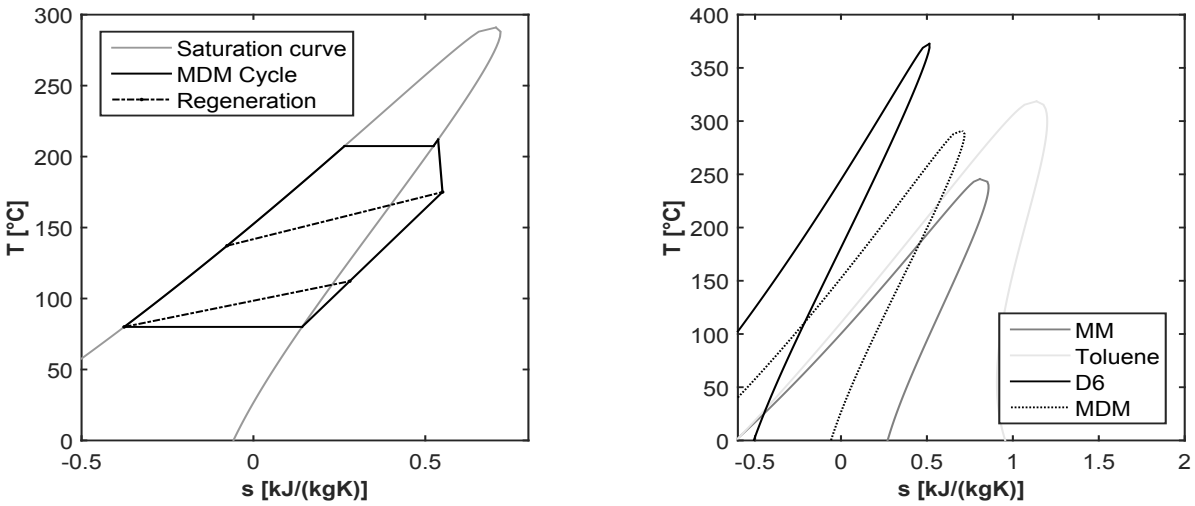

Figure 1.2: T-s diagram for ORC: (a) Optimized Cycle for MDM, regeneration process is allowed (data taken from [5]); (b) influence of molecular complexity on saturation curve for the most important candidate fluids (computation made through FluidProp [6])

In the fig.1.2 the fundamental characteristics of ORC cycle are shown: the typical inclined saturation curve, influenced by fluid molecular complexity. Moreover the complexity has huge impact on the thinness of evaporation path. The general tendency is the increasing of economizer process and decreasing of evaporator rate. Looking at the MDM cycle is clear how it is possible to exploit a pure dry expansion, utilizing a de-super-heating equipment to regenerate the fluid (reducing the economizer's task). To conclude the analysis, the expansion curve is much lower with respect to the classical gas or steam cycles. The reason is purely thermodynamic; for perfect gas model is already possible to check the behavior:

$$\Delta h = \frac{R_u}{MW\theta} T_{IT}(1-\beta^{-\theta}) \qquad \text{where} \qquad c_p = \frac{R_u}{MW\theta} \tag{1.1}$$

with R_u is the universal gas constant 8.314 $\frac{J}{molK}$, T_{IT} is the turbine inlet temperature and

$$\gamma = \frac{c_p}{c_v} \qquad \theta = \frac{\gamma - 1}{\gamma} \qquad \beta = \frac{pressure\ inlet}{pressure\ outlet} \tag{1.2}$$

For high molecular weight (MW) and high complexity ($\gamma \rightarrow 1$) the specific enthalpy drop decreases and specific heat increases (only due to complexity) because θ tends to 0. Therefore, for a fixed power output, the mass flow rate (i.e geometry) is larger than a common steam expansion. The following plots shows clearly the great difference in heat exchanger equipment between classical steam cycle and a ORC asset. The available source is the same and the optimization is made in terms of pinch point and saturation iso-thermobaric.

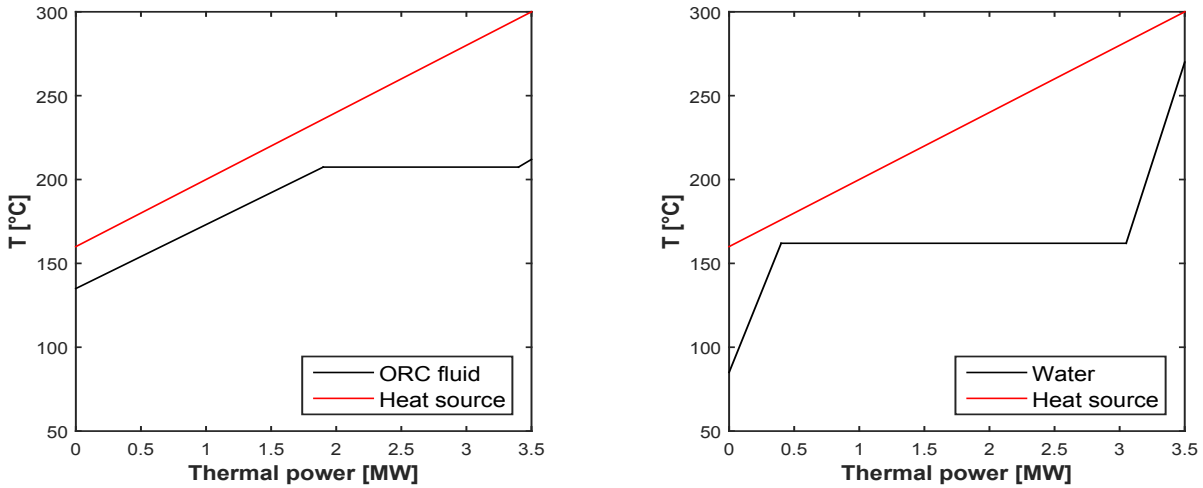

Figure 1.3: Comparison between heat exchanger process in (a) siloxane fluid; (b) water. Data taken from [5]

Other important characteristics which must be accomplished by a complex working fluid are summarized in the following points:

- environmental aspects due to pollution, human safety (risk of flammability)
- economic aspect, cheap fluids are preferable
- fluid choice based on thermodynamic optimization

The problem concerning the speed of sound is relevant for the expander. This aspect is strictly correlated with the molecular characteristics:

$$c = \sqrt{\left(\frac{\partial p}{\partial \varrho}\right)_s} = \sqrt{\gamma R_{gas} T} \tag{1.3}$$

where the last equality is valid only for perfect gas. The speed of sound tends to decrease a lot with the molecular weight and the complexity therefore it is very easy to achieve

transonic or supersonic regime in these machines in particular for one stage asset. Focusing the attention on the type of plant two general classifications (on power or temperature sources) can be set as shown in table 1.1:

Cycle max Temperature [°C]	**Power capacity [kW]**
High > 250	Micro <2
	Mini 3-50
Medium 150-250	Small 50-500
	Medium 500-5000
Low <150	Large > 5000

Table 1.1: Categories of ORC power plant [5]

Depending on the available sources a different machine is selected with the goal to achieve the best efficiency. In the following section a brief presentation of this topic will be given.

1.2 ORC Turbine design aspects

The expander element is very important for the sake of efficiency. The design criteria for the ORC turbines are very different from conventional steam and gas turbines because the organic fluids exhibit certain peculiar characteristics such as small enthalpy drop, low speed of sound and large expansion ratio. In the ORC technology research field one of the the pioneering works and studies of the turbine were made by the Politecnico of Milano researchers and the rising correlated company [7]. In particular in the article of Prof. Macchi [8] a first rigorous efficiency study was set with the aim of building dimensionless charts in Balje-style. The major hypothesis was that the comparison between conventional and complex fluids must be set at the same volumetric ratio, in this way the efficiencies are not so different with respect to classical fluid like steam water. In the table 1.2 the positive and negative aspects about ORC fluids are summarized [9]:

The architecture of the turbo-expander can be whatever, depending on the source. The high expansion ratio together with a high density ratio suggests the use of a radial configuration for the turbine to handle the high volumetric flow ratio not feasible for an axial machine. Although radial machines are preferred, also some axial configuration are investigated. There are two categories of radial turbines: a Radial Outflow Turbine (ROT), so called centrifugal turbine or a Radial Inflow Turbine (RIT), so called centripetal turbine or mixed flow turbine. The axial-flow geometry is the common one, it is suitable to exploit high power (large plant) therefore it is employed for CSP, biomass and binary geothermal plant. The centrifugal solution is very interesting since it allows to use a multi-stage solution, in contrast to the centripetal one, even if the design from aerodynamic point of view is challenging. An important aspect which must be optimized is the number of stages for both axial and centrifugal solutions; in many works [8, 10, 11]

PRO	CONS
small Δh, fixing $\dot{P}$ high mass flow rate: no issues about scaling effect in the geometry	large volume ratio: high flaring angles, huge compressibility effect: Balje theory no suitable
reduced number of stages: compact machine	low S.o.S: tendency to having high Mach number so strong deflection and risk of shock-waves
limited peripheral speed: no structural issue due to centrifugal forces	Challenge aerodynamic design
dry expansion: absence of droplets	

Table 1.2: Comparison between positive and negative aspects for an axial ORC turbine

this aspect has been discussed in order to find the best configuration in terms of efficiency and fluid dynamic characteristics.

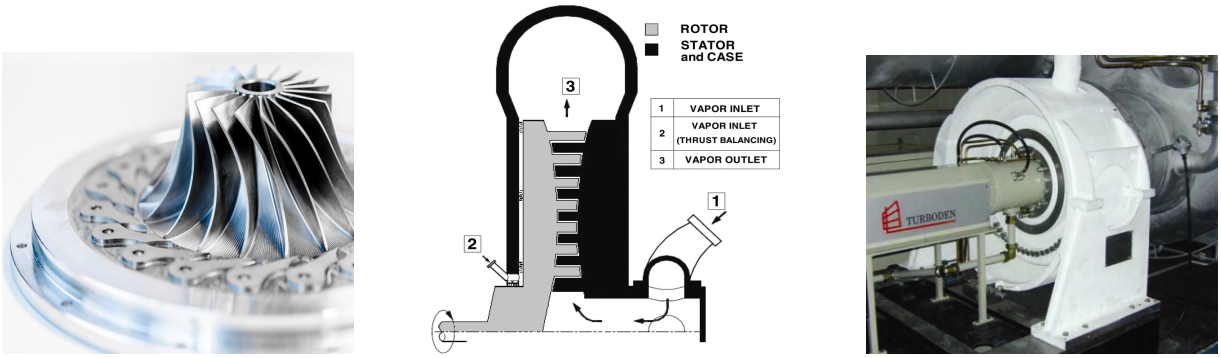

Figure 1.4: Three different assets: (a) Radial inflow turbine [12]; (b) Centrifugal turbine [13]; (c) axial turbo-expander for large power plant https://www.turboden.com/

The positive aspects related to the radial inflow turbine have been investigate in a thesis work of Power and Propulsion department TU Delft [14]. To conclude this section, a

crucial aspect is the choice of equation of state to describe the non ideality phenomena during expansion process. The work made by Colonna and Rebay [15] is focused on the importance of a suitable thermodynamic model for such complex processes. The state of the art is represented by the Span - Wagner EoS.
In this thesis the library FluidProp®is used, in particular the RefProp® by NIST will be employed for computation https://www.nist.gov/programs-projects/reference-fluid-thermodynamic-and-transport-properties-database-refprop.
The experimental facility ORCHID [16] and TROVA of Politecnico of Milano https://crealab.polimi.it/2017/09/presentation-of-experimental-results-from-trova-at-orc-2017.html are conceived with the task to analyzing the correlation between NICFD(Non Ideal Compressible Fluid Dynamic) concept and nozzle/turbine apparatus.

1.3 NICFD: Non Ideal Compressible-Fluid Dynamic

One of the most peculiar characteristics of complex fluid utilized for ORC applications is the non-ideal behavior shown in certain zones. In particular the compressibility factor Z diverges from unity often. The density is different with respect to the one compute using the ideal gas equation of state (E.o.S). The appellative *dense gas* is due to the high density of the fluids and the phase state which shows strong real effect, the repulsion and attraction forces between molecules become relevant. One of the common assumption made on the shear stress for Newtonian fluid i.e neglecting the bulk viscosity some times could fall close to critical point in particular flow regime.

$$\tau_{ij} = [\mu(\frac{\partial u_i}{\partial x_j} + \frac{\partial u_i}{\partial x_j}) + \lambda \frac{\partial u_k}{\partial x_k} - p\delta_{ij}] \tag{1.4}$$

In some cases the working region can be close to the critical one and therefore the explosion of transport properties as specific heat c_p and dynamic viscosity μ happens, in this cases the Prandtl number $(\frac{\mu c_p}{\lambda})$ becomes one order of magnitude bigger than a for a normal gas. The theoretical instrument to predict such phenomena are the real gas equation of state such as Peng-Robinson or Van der Waals [17, 18], cubic equations suitable for an analytical description also in close-to-critical zone.
The compressibility factor is defined as the specific volume of real gas with respect to the ideal one and it is a quantitative indicator of the deviation in the thermodynamic behavior compared with the ideal:

$$Z = \frac{v}{v^0} = \frac{pv}{R_{gas}T} \tag{1.5}$$

For general purposes it is possible to consider ideal gas behavior when the reduce pressure is smaller than 0.1 (fig. 1.5). The physical explanation is due to molecular interaction that are very weak for small pressure, the distance between molecules is too large therefore there is not reciprocal interaction as repulsion or attraction. The convenience to use ideal gas model is multiple: simple equation, dependence of specific heat, enthalpy and internal energy only from temperature. Unfortunately ORC fluid have tendency to operate outside

this one.
Another important aspect from gas-dynamic point of view is the non common behavior in terms of Γ, the so called fundamental derivative of gas-dynamic. This parameter comes directly from physics study. The first who formulated and defined this quantity was Hans Bethe [19]. During the decades other important authors continued to refine the theory in particular Zeldovich and Thomson. Nowadays many efforts deal with this concept related to fluid at high molecular complexity [15, 20]. Here the definition is given [21, 19, 22]):

$$\Gamma = 1 + \frac{\varrho}{c}\left(\frac{\partial c}{\partial \varrho}\right)_s = 1 + \frac{\varrho}{2c^2}\left(\frac{\partial^2 p}{\partial \varrho^2}\right)_s = \frac{v^3}{2c^2}\left(\frac{\partial^2 p}{\partial v^2}\right)_s \tag{1.6}$$

Where: p is the pressure, ϱ is the density with the inverse v (specific volume) and c is the speed of sound (S.o.S). An interesting point of view is the differentiation of fluids with respect to Γ [17]:

- $\Gamma > 1$ **Low molecular complexity**: monotonic trend of the speed of sound which can only increase on isentropic compression and decrease on isentropic expansion, independently of the thermodynamic region where the process takes place. The qualitative features of fluid flows are always similar to the ones of a flow of an ideal gas.
- $0 < \Gamma < 1$ **High molecular complexity**: existence of a thermodynamic region where the speed of sound decreases on isentropic compressions and increases upon isentropic expansions. This may lead, for example, to the non-monotone behavior of the Mach number and speed of sound in compressible flows through nozzles.
- $\Gamma < 0$ **Highest molecular complexity**: the exotic region of non conventional gas-dynamic appears: B-Z-T (Bethe Zeldovich Thompson). For these fluids, in a limited thermodynamic region at high reduced temperature and pressure near the dew-line, the reversed dependency of the speed of sound with respect to density in isentropic flows is so pronounced, that gas-dynamic behavior is reversed with respect to the gas dynamics of perfect gases; for example, rarefaction shock waves become theoretically permissible. No experience of this phenomena has ever been detected. In fig. 1.5 (b) it is possible observing a typical HMC fluid which presents zone with $\Gamma < 1$.

This behavior of complex fluid must be taken into account for a turbomachine design since shock wave due to sonic condition appear often. In the chapter 4 a study about this phenomena will be presented: for B-Z-T region a deceleration can cause a huge increase of Mach number producing shock wave. In the following entire work the candidate complex fluids presented will be MM, MD2M for HMC and D6 for B-Z-T.

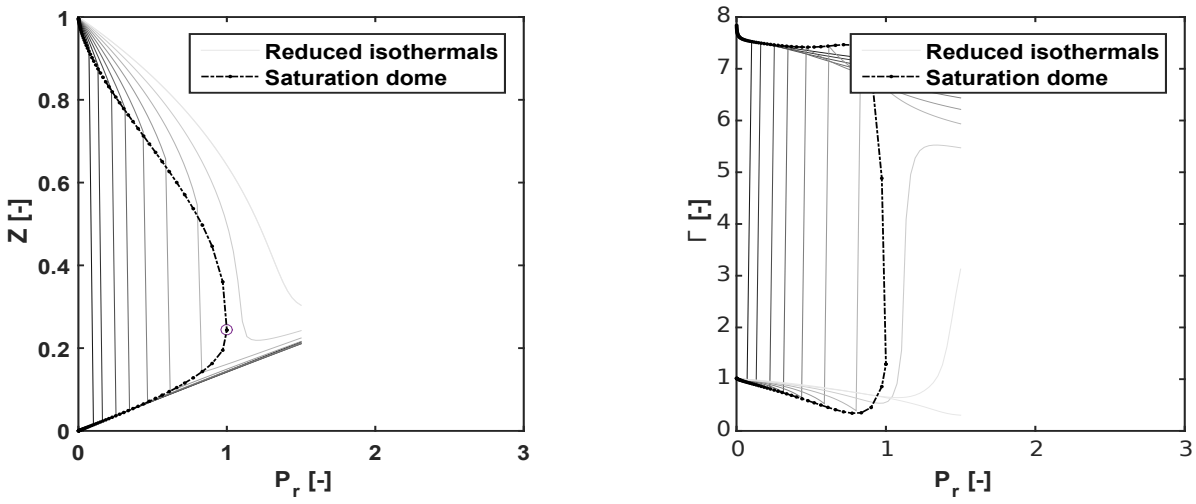

Figure 1.5: Two most relevant phenomena of real gas nature for complex fluid, in this case MM siloxane computed with RefProp library [6]: (a) compressibility factor Z; (b) Fundamental derivative of gas dynamic. Possibility of having $\Gamma < 1$ therefore non-monotonic trend of Mach number.

1.4 Motivation and scope of this thesis

The fraction of energy which cannot be converted to work in a turbine is termed as loss and it is usually expressed in terms of a non-dimensional quantity called loss coefficient. The computation of losses (estimation of efficiency) is the most important aspect for turbomachines. The aim of this work is to determine the trend of profile losses through Smith's chart and to show that the nature of the fluid plays a major role on it. In order to achieve this task we must computing and understand the dissipation coefficient C_d. The necessity of a physical solid comprehension is mandatory to investigate the phenomena in general terms abandoning the classical limited approach of semi-empirical loss model (Ainley - Mathieson [23], Soderberg [24], Kacker-Okapuu [25]...). The generality given by a boundary layer study linked with simplified profile loss model will overcome also the limitation of standard CFD (computational fluid dynamic) optimization analysis which is machine-specific therefore it is not suitable to extract a general trend in terms of dimensionless diagram in a resonable amount of time.
Moreover the boundary layer code has allowed a general study focused on the interaction between compressibility effects and fluid nature in laminar and turbulent regime. The link between the fundamental study about boundary layer phenomena and the more applied turbine field is represented by the dissipation coefficient C_d, core of Denton physical based model [26, 2].

1.5 Research Questions

This work aims to answer the following research questions:

1. What is the C_d, dissipation coefficient (i.e source of losses), trend of boundary layer for incompressible flow and then with respect to compressibility effects?
2. What is the influence of non-ideality effects on the C_d?
3. What is the accuracy of physical- based profile loss model results as compared to CFD?

1.6 Points of originality

The main points of originality of this work are as follows:

1. Investigated and determined the C_d trend for compressible flow in the laminar and turbulent regime.
2. Investigated the effects of the real gas on C_d [27].
3. Described all the physical phenomena behind the dissipation in boundary layer such as fluid nature and pressure gradient effects.
4. Final connection between C_d and the physical profile loss mode.

1.7 Thesis outline

The structure of the present thesis is the following:

1. **Chapter 1: Introduction** General background in terms of energy field and ORC technology with the related scientific/engineering problems. In the final part the motivation and scope of the work, the research questions and the points of originality are presented.
2. **Chapter 2: Theoretical background** for turbomachinery field and for boundary layer. For the first group the similarity concept (Buckingham theory) and the efficiency study will be presented. Then a general overview on loss models, first the classical ones then the physical approach will be done. The boundary layer topic is presented with its main concepts and parameters.

3. **Chapter 3: Profile charts** The results for turbomachinery loss will be presented. The general form is the Smith's chart style. The classical model will show bad behavior in high speed zone otherwise the physical approach is very good and it is able to catch also real gas phenomena. Moreover there are other important features for blade concepts such as lift, velocity triangles and diffusion coefficients. All these studies are performed on a pure reaction stage with the same inlet used by Smith for his work [28].

4. **Chapter 4: Dissipation coefficient in Laminar boundary layer** The results for dissipation coefficient in laminar will be shown. The first step is the verification of Denton reference chart. After this the compressibility effect (Mach number increase) and the effects of the nature of the fluid will be investigated. Moreover another important flow phenomenon will be challenged: the pressure gradient. The last part is dedicated to the analysis of real gas effects, also in B-Z-T zone.

5. **Chapter 5: Dissipation coefficient in Turbulent Boundary layer** The results for dissipation coefficient in turbulent regime is the core of this chapter, moreover many other studies will be presented such as the effect of pressure gradient, the compressibility effect and some verification cases. We will try to understand the physical causes for the various deviation in dissipation phenomena such as the eddy viscosity variation with respect to the different regimes.

6. **Chapter 6: Applications** In the end an open source code built for aerodynamic optimization will be used to compare the results of our BL code versus the Denton relations and the losses directly given by the SU2 [29].

7. **Conclusions and Recommendations:** This final chapter includes the conclusion from scientific and engineering point of view. In particular the importance of C_d is underlined in terms of boundary layer and profile loss field. The recommendations are for the possible future works in terms of turbomachinery, boundary layer code and fluid mechanics phenomena.

8. **Appendix A: Critical phenomena in boundary layer** could be important for certain advanced technology (supercritical power plant) however more advanced computational instrument are necessary.

9. **Appendix B: Transcription of part of the code and its general utilization** Instruction and discussion of the Laminar part of the Boundary layer code.

10. **Appendix C: On the nature of the dissipation** A general discussion on the basic assumption of Navier-Stokes and the derivation of dissipation coefficient with the discussion about the difficulties to govern the dissipation phenomena from theoretical point of view in such complex case as turbulence is.

11. **Appendix D: Turbulence model in CFD validation** The SST turbulence model used in SU2 is explained.

12. **Appendix E: Similitude concept and classical loss models** A list of profile loss model. Craig Cox, Glassman, Traupel. And also a description of the Buckingham theory for the similitude charts.

Chapter 2

Theoretical background

The core of this chapter is the theoretical background of this the topic presented in this thesis work. The first section deals with the turbomachinery concepts related to efficiency diagrams and loss model computations. After this, the necessity to develop a physical based approach is discussed following the Denton point of view. In the second section the classical theory of boundary layer, fundamental phenomenon at the base of blades profile losses, is briefly introduced.

2.1 Turbomachinery theory

The turbomachinery theory is a wide field which includes many fundamental topic: fluid mechanics, thermodynamic analysis and many others. The study of efficiency for a machine is the primary objective since it is the parameter of the thermodynamic quality. In particular the fluid dynamic design of turbomachinery is of primary concern to meet the requirements of highly-efficient power and propulsion systems. The design process is very long and complex and it is characterized by many steps: from a rough estimation of the most important parameters to complex optimization CFD study for the blade aerodynamic [30]. The base of the design chain is the so-called mean line or 0-dimensional design, through which the designer selects the turbine configuration, the number of stages, the velocity triangles, and the basic geometrical parameters. This first part is important not only for the design of classical machine but also for the new applications since it is desirable to have a rough estimation of the performance and dimensions of the turbomachinery already at the beginning of the design level in order to assess whether the machine could be one of the limiting factor from thermodynamics and economic point of view. For unconventional power applications, like ORC, super-critical CO_2, it is fundamental having roughly estimation and reliable correlations for sizing and efficiency prediction of turbomachinery. Because of the nature of fluids processed, all these systems can often operate in compressible and significant non-ideal regimes, for which design experience and experimental informations are much more limited, if not totally existent. The lack of knowledge from experimental and simulation point of view it makes necessary a design approaches

based on the similarity theory: a very powerful and widely tool. A classical example are the Balje's diagrams or the Smith's chart. These efficiency maps based on similarity have a duble function:

- select and help the preliminary design of the machine
- identify efficiency trends with respect to dimensionless group

In turbomachinery field this concept is expressed through the computation and consequently minimization of the losses. In order to set-up a general theory in such complex subject, a dimensionless approach based on the Buckingham theory (π theorem) is necessary.

2.1.1 Similitude analysis for turbine

With the aim of defining the efficiency of the machine [30] we can write the following expression:

$$\eta_{TS} = f\Big(\underbrace{\lambda, \phi_0, \phi_1, \phi_2}_{\text{duty coefficients}}, \underbrace{r*}_{\text{degree of reaction}}, \underbrace{\pi_{stator}, \pi_{rotor}}_{\text{volumetric flow ratios}}, \underbrace{\frac{R_0}{R_1}, \frac{R_2}{R_1}}_{\text{radial evolution}}, \underbrace{Ma_0, Ma_1, Ma_2, Re_{stator}, Re_{rotor}}_{\text{flow regime}}, \underbrace{\zeta_{stator}, \zeta_{rotor}}_{\text{loss coefficient}}\Big) \tag{2.1}$$

A further simplification is adopted defining the $K_{is} = \frac{\Delta h_{TS}}{\frac{U^2}{2}}$ head coefficient and imposing the dependency of loss coefficient by Reynolds and Mach numbers and geometrical quantities.

$$\eta_{TS} = f(P_r, T_r, \pi, K_{is}, \phi_0, \phi_1, \phi_2, r*, \frac{R_0}{R_1}, \frac{R_2}{R_1}, Re_{stator}, Re_{rotor}, \vec{\sigma}, \vec{\pi}). \tag{2.2}$$

The equation 2.2 is the most general form for whatever turbine stage, any geometry (axial, radial inflow and outflow), size and flow regime. For the purpose of this work it is important underlying that this expression takes into account also non ideal flow effects. From this expression is possible extract simpler sub cases like axial flow machine or incompressible fluid machine simply reducing the number of variables. Many authors have worked on this field finding diagram characterized by generality behavior. The most important are the Balje's diagram, the Smith's chart [28] and the Chaines-Baines' diagram [31]. The parameters plotted on these map are different and there is not an universal analytical correlation between themselves:

$$\begin{cases} \omega_s = \omega \frac{\sqrt{\dot{V}_{out}}}{\Delta h_{is}^{\frac{3}{4}}} \text{ specific speed} \\ D_s = D \frac{\Delta h_{is}^{\frac{3}{4}}}{\sqrt{\dot{V}_{out}}} \text{ specific diameter} \end{cases} \tag{2.3}$$

For Smith chart [28] (related to a stage):

$$\begin{cases} \Phi = \frac{V_{m,1}}{U} \\ \Psi = \frac{\Delta h_{TT}}{U^2} \end{cases} \tag{2.4}$$

The formulations are different and there is not any correlations between these two approach. Balje uses volumetric flow rate ($\dot{V}_{out}$)

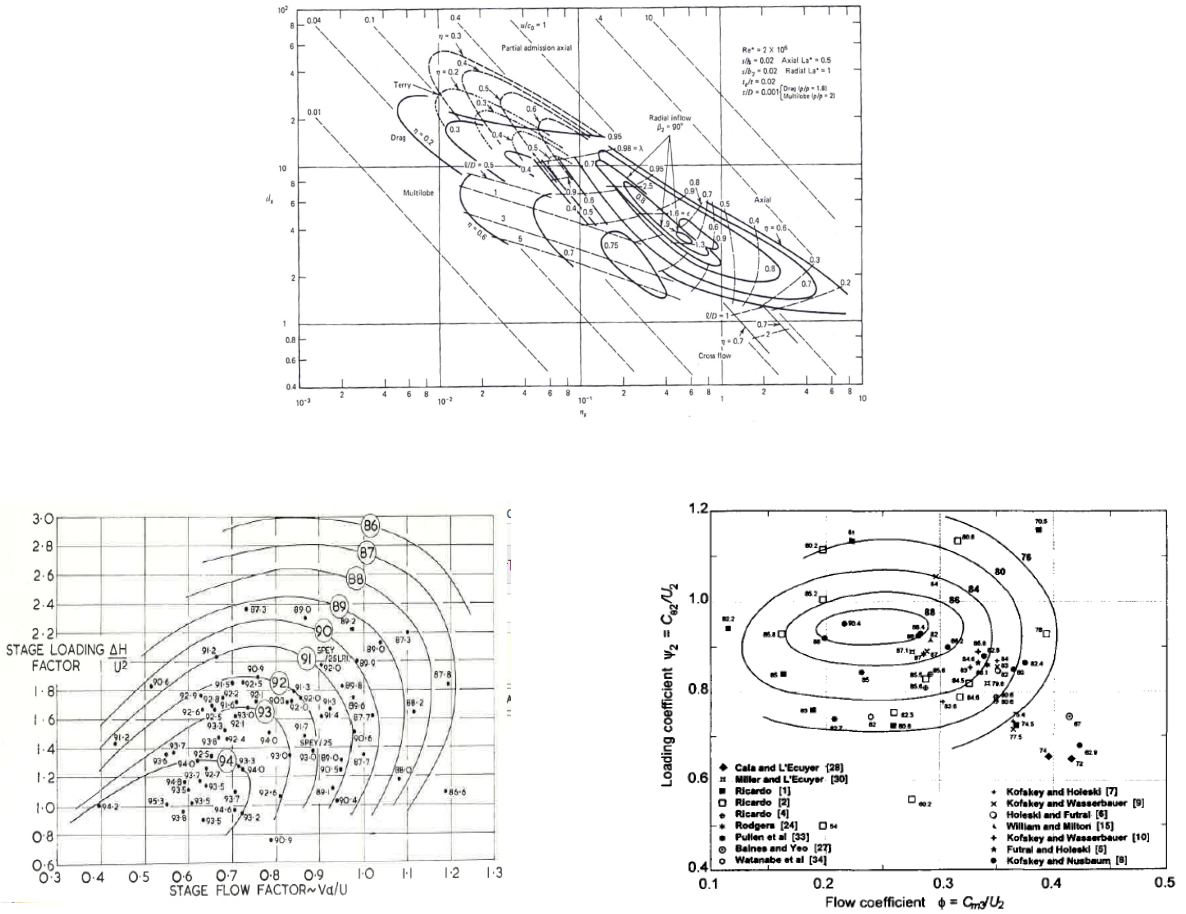

Figure 2.1: Most important similitude diagrams for turbine: (a) Balje; (b) Smith-chart ; (c) Chen-Baines

All of these charts have great limitations: the main assumptions in the Balje one is to consider incompressible flow machines, Smith chart is based on experimental campaign on axial turbine therefore is valid in principle only for axial gas turbine at low speed flow ($Ma < 0.3$). Moreover both are quite old (1965 Smith). This assumption can be neglected in the first phase of the preliminary design in order to have just a rough idea on which machine configurations should be selected. Then, more reliable charts must be used to obtain a more precise insight of the machine performance and dimensions

2.1.2 Loss breakdown and loss estimation

The expander's thermodynamic process is generally diagrammed in the Mollier's plane fig.2.2.

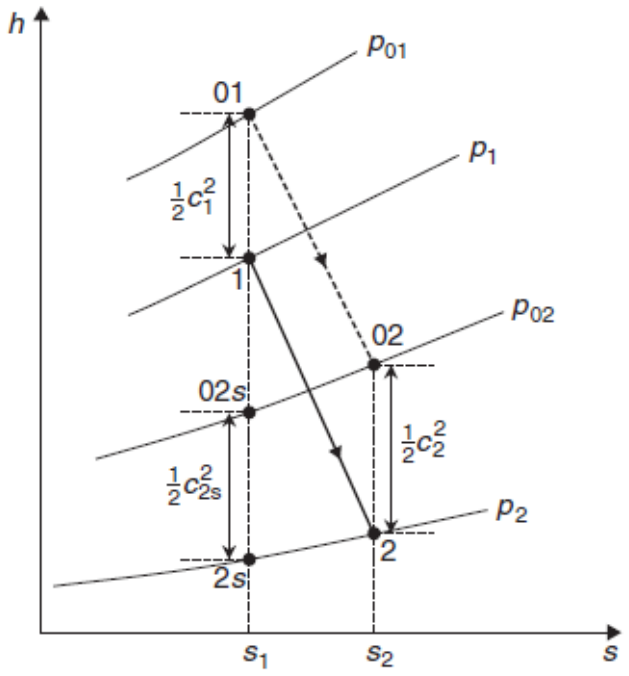

Figure 2.2: Mollier diagram for turbine process [53].

Historically the breakdown of loss into "profile loss," "endwall loss," and "leakage loss" has always been the general theory and nowadays it continues to be widely used although it is now clearly recognized that the loss mechanisms are seldom really independent [1]. Profile loss is usually taken to be the loss generated in the blade boundary layers well away from the end walls. It is often assumed that the flow here is two dimensional so the loss may be based on two-dimensional cascade tests or boundary layer calculations this is the purpose of this work. The extra loss arising at a trailing edge is usually included as profile loss. Endwall loss is still sometimes referred to as "secondary" loss because it arises partly from the secondary flows generated when the annulus boundary layers pass through a blade row. It is often difficult to separate endwall loss from profile loss and leakage loss. Tip leakage loss arises from the leakage of flow over the tips of rotor blades and the hub clearance of stator blades. The relative magnitudes of the above three categories of loss are dependent on the type of machine and on such details as blade aspect ratio and tip clearance. However, in many machines the three are comparable in magnitude, each accounting for about 1/3 of the total loss [1].

In the flow chart 2.3 it is possible to analyze the common division between losses. This work is focused only on the studying of boundary layer (the blue one) therefore for the other categories please refer to common literature [32, 24, 2].

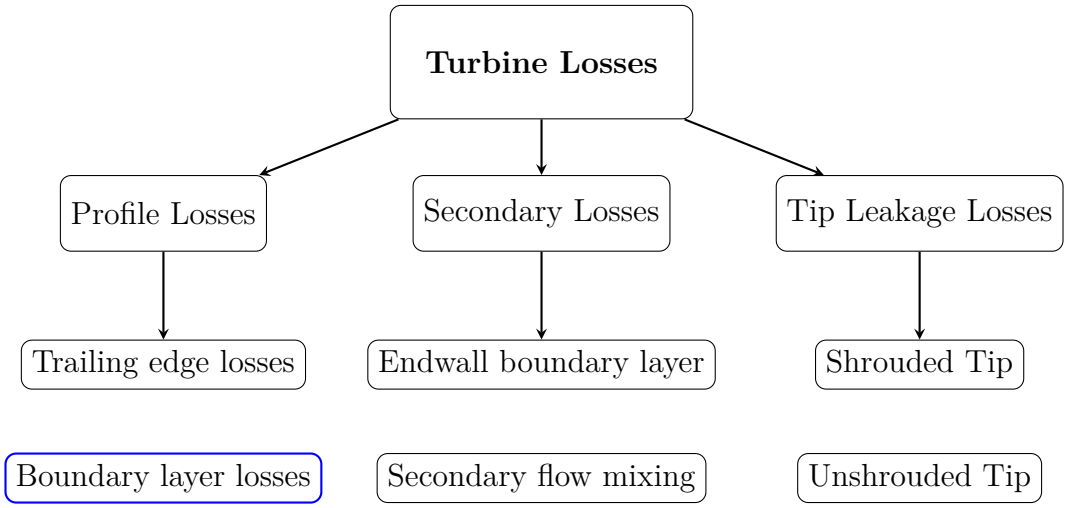

Figure 2.3: Turbine categories of losses

In order to estimate quantitatively the losses on the machine there are many different point of view, resulting in several loss coefficient definitions; the most important are:

Stagnation pressure loss coefficient

It is the most famous and it is the one computed by the family Ainley-Mathieson, Dunham-Came, Kacker-Okapuu (see 2.1.2). The definition is the following:

$$Y_P = \frac{p_{01} - p_{02}}{p_{02} - p_2} \ , \tag{2.5}$$

which represents the difference in total pressure between the inlet and outlet of a blade rows over the dynamic pressure at the outlet. Denton states that it is not the most convenient for a design but it is the simplest to compute, this is why it is widely used.

Energy loss coefficient

It is very useful for design purposes. It is defined as:

$$\zeta = \frac{h_2 - h_{2s}}{h_{02} - h_2} \ , \tag{2.6}$$

Which is the comparison between the difference in real and isentropic process over the specific kinetic energy at the outlet of the row. The physically superiority of the enthalpy coefficient is the independence by Mach number (compressibility effects) therefore it is more general than the pressure one [33].
The classical loss models are characterized by different approaches. In the following paragraphs a briefly description of classical loss models will be given in the vision only

of profile phenomena. A detailed description of profile losses along blade will be given in terms of physical based approach. We discard the Soderberg model since it does not take into account a precise separation between the different groups. More refined methods are Ainley-Mathieson, Dunham-Came and Kacker-Okapuu developed from the same statistical basis, Craig-Cox, Traupel and Chen-Baines.

Ainley-Mathieson, Dunham e Came, Kacker Okapuu

They take into account several phenomena inside the turbine. Ainley and Mathieson (1951) reported a way of estimating the performance of an axial flow turbine, and it should be noted, the method has been widely used ever since. In essence the total pressure loss and gas efflux angle for each row of a turbine stage is determined at a single reference diameter and under a wide range of inlet conditions. This reference diameter was taken as the arithmetic mean of the rotor and stator rows' inner and outer diameters. When the blading is completely designed the revised method has been found to give reliable predictions of efficiency to within 2 % over a wide range of designs, sizes, and operating conditions Focusing only on profile losses also called primary losses [23]:

$$Y_{p(i=0)} = \{Y_{p(\alpha_1=0)} + \left(\frac{\alpha_1}{\alpha_2}\right)^2 [Y_{p(\alpha_1=\alpha_2)} - Y_{p(\alpha_1=0)}]\} \left(\frac{t_{max}/l}{0.2}\right)^{\frac{\alpha_1}{\alpha_2}}, \tag{2.7}$$

Eq. 2.7 represents an intermediate function between a nozzle blades and impulse ones. The loss coefficient for both are obtained by chart (a) and (b) fig. 2.4, initially at zero incidence ($i = 0$); at any other incidence the profile loss ratio $\frac{Yp}{Yp_{(i=0)}}$ is assumed to be defined by a unique function of the incidence ratio 2.4 (c) where is is the stalling incidence. Next, correlated the profile losses of turbine blade rows against space–chord ratio $\frac{s}{l}$, fluid outlet angle α_2, blade maximum thickness–chord ratio $\frac{t_{max}}{l}$, and blade inlet angle.

This profile loss method presents many limitations: correlation estimated on very old machine, roughly estimation of Reynolds correction and finally no Mach number effects (fundamental for an ORC expander).

Dunham and Came

Dunham and Came [35] improved this methodology adding several correction factors:

- Mach number correction:

$$Y_P = [1 + 60(Ma_{out} - 1)^2]Y_{P(i=0)} \; ; \tag{2.8}$$

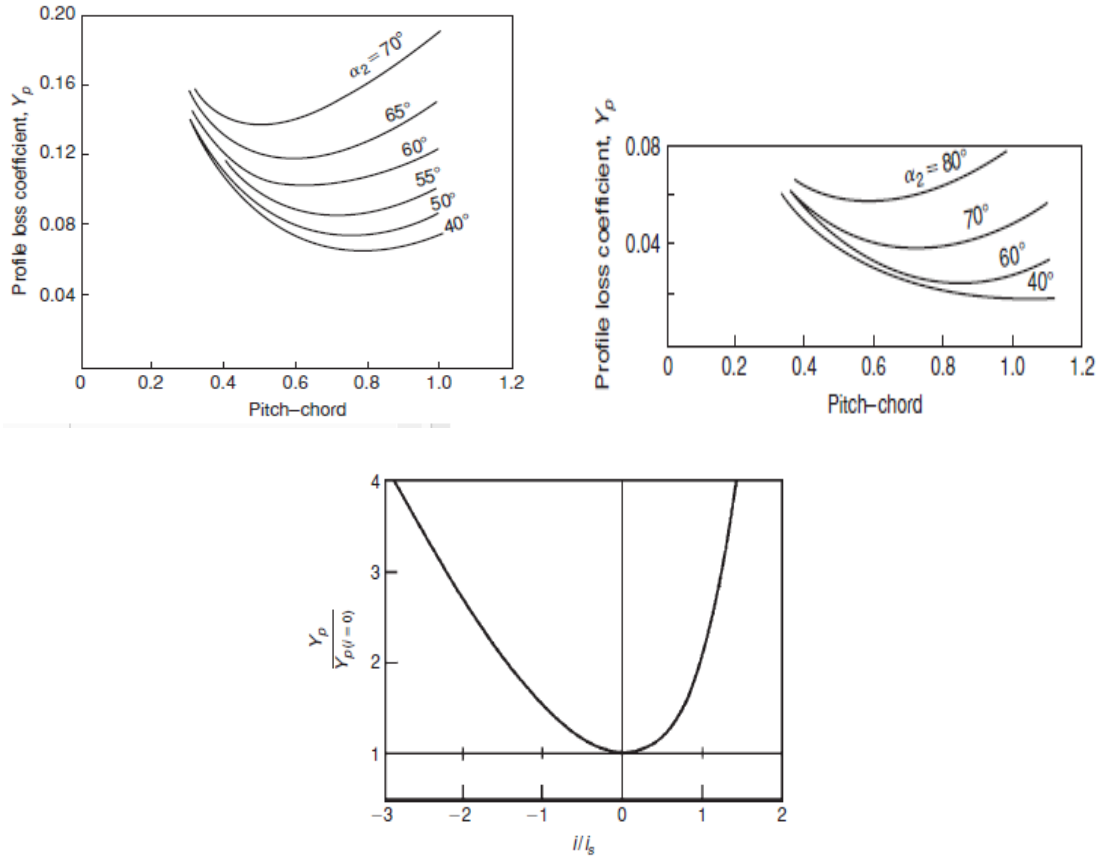

Figure 2.4: Ainley-Mathieson charts correlation: (a) Rotor losses; (b) Nozzle losses; (c) Correction respect to incidence [53]. An analytical function is proposed by Aungier [34]

- trailing edge correction χ_{Te} ;
- Reynolds correction $(\frac{Re}{210^5})^{0.2}$;

Kacker Okapuu

Finally the most refined one is Kacker-Okapuu [25], which is based on an evolution of the older method adding a deeper physical point of view. The first change is about an absolute value in contrast to the square in the losses at zero incidence:

$$Y_{p(i=0)} = \{Y_{p(\alpha_1=0)} + \left(\frac{\alpha_1}{\alpha_2}\right)|\frac{\alpha_1}{\alpha_2}|[Y_{p(\alpha_1=\alpha_2)} - Y_{p(\alpha_1=0)}]\}\left(\frac{t_{max}/l}{0.2}\right)^{\frac{\alpha_1}{\alpha_2}}, \tag{2.9}$$

Moreover a more complex correction for Reynolds number is then introduced:

$$\chi_{re} = \begin{cases} (\frac{Re}{2\ 10^5})^{-0.4}, & \text{for } Re < 2\ 10^5 \\ 1, & \text{for } 2\ 10^5 < Re < 10^6 \\ (\frac{Re}{10^6})^{-0.2}, & \text{for } Re > 10^6 \end{cases} \tag{2.10}$$

The profile losses according to Kacker and Okapuu are:

$$Y_P = 0.914 \left(\frac{2}{3} K_P \chi_i Y_{P(i=0)} + Y_{Shock}\right) \tag{2.11}$$

It is appreciable the increase in the complexity in the formulation 2.11 with respect to the other models. In particular two more phenomena both related to compressibility effects affect the profile losses:

- shock could happen at blade leading edges ,
- the flow acceleration within the blade channel.

The shock process (Y_{Shock}) has an intrinsically 3-D formulation since

$$\left(\frac{\Delta P}{q_1}\right)_{Hub} = 0.75(Ma_{1,HUB} - 0.4)^{1.75} , \tag{2.12}$$

therefore at midspan:

$$\left(\frac{\Delta P}{q_1}\right)_{Shock} = \left(\frac{R_H}{R_T}\right)\left(\frac{\Delta P}{q_1}\right)_{Hub} , \tag{2.13}$$

Finally the subsonic losses coefficient:

$$Y_{Shock} \equiv \left(\frac{\Delta P}{q_2}\right)_{Shock} = \left(\frac{\Delta P}{q_1}\right)_{Shock}\left(\frac{p_1}{p_2}\right) = \frac{1 - (1 + \frac{\gamma-1}{2} Ma_1^2)^{\frac{\gamma}{\gamma-1}}}{1 - (1 + \frac{\gamma-1}{2} Ma_2^2)^{\frac{\gamma}{\gamma-1}}} , \tag{2.14}$$

The second contribution related to acceleration in a channel is described by:

$$K_P = 1 - K_2(1 - K_1) , \tag{2.15}$$

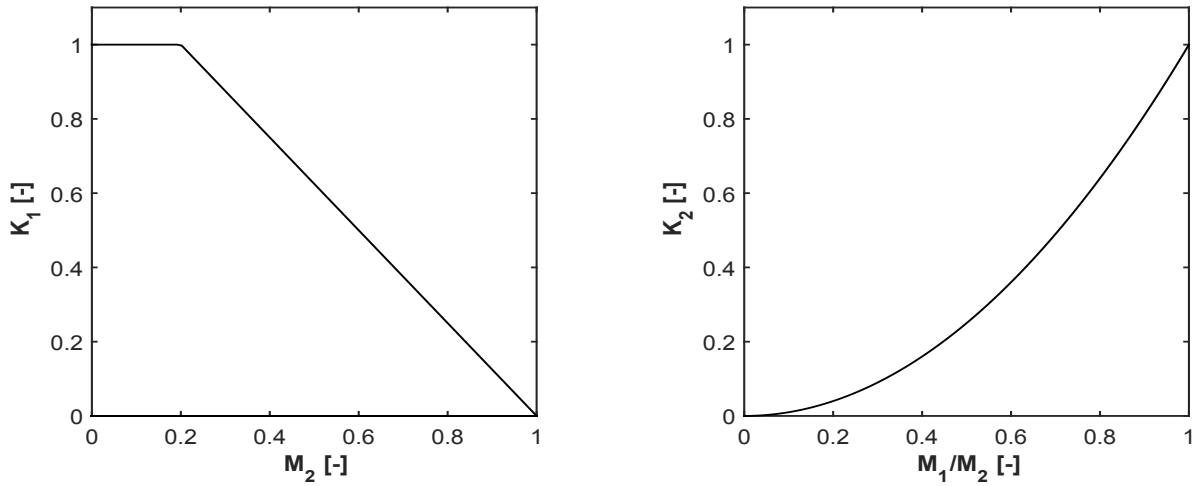

Figure 2.5: (a) The factor K1 depending by the outlet cascade Mach; (b) Correction due to the accelerating effects coupled with compressibility ([25] pag.114)

The two terms are Mach corrections 2.5:

The graphs in fig.2.5 are the plot of the following analytical expression:

$$K_1 = 1 - 1.25|Ma_2 - 0.2| \quad for \ M_2 > 0.2 \ , \tag{2.16}$$

$$K_2 = |\frac{M_1}{M_2}|^2 \tag{2.17}$$

The Kacker-Okapuu modification to Ainley Mathieson has the goal to make coincidence with Smith profile chart. Correctly these authors state that the Dunham Came correction (eq. 2.8) are the major shortcoming of that theory. The meaning of this term is supersonic Drag rise in the regime of supersonic exit velocities additional pressure losses occur as a result of shocks originating in the trailing edge wake.
For total losses the results were compared with Smith's chart and with 33 turbine and the prediction were estimated to be in $\pm 3\,\%$. These models will be used in chapter 3 with the aim to show their limitations for ORC turbines.
Other important models (Glassman, Traupel and Craig-Cox) are in the Appendix E.

2.1.3 Physical based loss model

Unlike the majority of the authors, Denton proposed a physical-based method to account for the various loss sources in turbomachinery cascades [2, 26]. The essence of the method relies on fundamental principles (first and second law of thermodynamics) and control volume analysis based on Navier-Stokes equations, applied between proper cascade sections. The main idea of this approach is that a good physical understanding of the flow, and particularly of the origins of loss, is more important to the designer than is the availability of a good but oversimplified loss correlation. The first great quantitative introduction is a new loss coefficient based on entropy, for turbines is defined as:

$$\zeta_s = \frac{T_2 \Delta s}{h_{02} - h_2} \ , \tag{2.18}$$

The coefficient defined in 2.18 derives from the necessity to define a dimensionless parameter related to the entropy. The necessities to develop a new point of view, different from the previous ones are summarized in the table 2.1

About the last point of table 2.1, Denton shows in his paper how to pass from entropy to enthalpy loss (eq.10 [1]) or from entropy to aerodynamic friction force, a sum of skin friction and pressure drag (eq.7 [1]):

$$\Delta h = \frac{T_{ref} \Delta s}{\zeta} \qquad\qquad \Delta F = -T \Delta s (\varrho A) \tag{2.19}$$

All the coefficients collapse to the same value for incompressible flow, therefore the discriminant is high speed phenomena. In fact for perfect gas:

$$\zeta - \zeta_s \approx 0.25(\gamma - 1) Ma^2 \zeta \zeta_s \tag{2.20}$$

This last one Denton explains as follows the choice of entropy as universal quantity to estimate losses: in fact the classical blade row loss coefficients are perfectly satisfactory for cascade tests but are not directly applicable in rotating machines due to the change of stagnation quantity. Since the isentropic efficiency is defined as the ratio of the actual work to the isentropic work, the only factors that change this efficiency are departures from isentropic flow. These may be due to either heat transfer or to thermodynamic irreversibilities directly. For most machines the flow is closely adiabatic and so only entropy creation by irreversibilities contributes significantly to the loss of efficiency: the most reasonable measure of loss in an adiabatic machine is entropy creation. Any irreversible flow process creates entropy and so inevitably reduces the isentropic efficiency. Even if entropy is an unfamiliar quantity because it cannot be seen or measured directly, its value can only be inferred by measuring other properties (by just knowing two parameters the thermodynamic state is completely defined for a single substance). The entropy generation is then related to the efficiency of the machine:

$$\eta_t \approx \frac{h_{in} - h_{out}}{h_{in} - h_{out} + T_{out} \Delta s_{gen}} \ . \tag{2.21}$$

Entropy approach	**Empirical approach**
Thermodynamically sound, valid for each flow regime	Discrepancy between different definition: pressure vs. energy at high Mach numbers
Easy to measure, by just knowing the thermodynamic state	The drag definition depends by the direction in which it acts. For turbomachinery flow it is very complex because tangential and axial direction accomplish two different task: the former is about work transfer, the latter is about pressure change
Invariant with respect to reference frame Easy to convert in the other coefficient (both momentum and energy)	Drag and energy coefficients depend by system: stationary or rotating

Table 2.1: Superiority of entropy approach and comparison of the coefficients with classical parameters

The main mechanisms of entropy creation are summarized in the following chart:

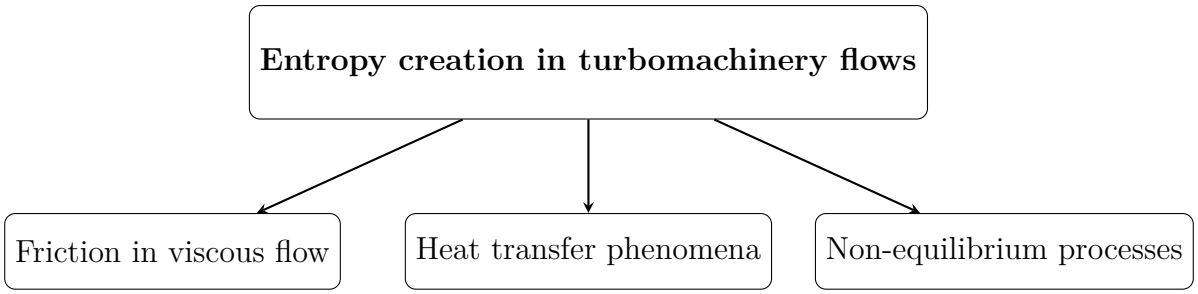

Figure 2.6: Mechanisms for entropy generation [1]

Entropy production inside the boundary layer

In the case of turbine stages, the dissipation mechanisms in which we are interested is the one related to the boundary layer phenomena in physical sense, then we will apply this concept only to profile losses (i.e boundary layer along the blade). The first step is represented by the derivation of the production of entropy $\dot{S}$ [1]:

$$\frac{ds}{dx} = \frac{dh}{dx} - \frac{1}{\varrho}\frac{\partial p}{\partial x} = \frac{dh_0}{dx} - u_x\frac{u_x}{dx} - \frac{1}{\varrho}\frac{\partial p}{\partial x} \qquad \text{II Principle of thermodynamic} \tag{2.22}$$

$$F_x - \frac{1}{\varrho}\frac{\partial p}{\partial x} = u_x\frac{\partial u_x}{dx} \qquad \text{Momentum} \tag{2.23}$$

$$\frac{D}{Dt}(e + \frac{u^2}{2}) = -p\frac{D}{Dt} + u_x(F_x - \frac{1}{\varrho}\frac{\partial p}{\partial x}) + \frac{1}{\varrho}(\tau_{xy}\frac{\partial u_x}{\partial y} + \tau_{yz}\frac{\partial u_z}{\partial y}) - \frac{1}{\varrho}\frac{\partial q}{\partial y} \qquad \text{Energy} \tag{2.24}$$

Where p is the pressure, h enthalpy, s entropy, τ the shear stress q heat transfer and u velocity. The F is friction forces. The previous equations (2.22, 2.23, 2.24) are the base of physical based model; notice that they are valid for whatever case (compressible and incompressible) and for whatever flow regime (for turbulent a RANS approach combined with the Boussinesq's hypothesis allows to add only the eddy viscosity to the velocity gradient). Moreover for our purpose these formulations are valid for each type of fluid molecule therefore the real gas effect can be inserted inside.[1]
Working on the energy equation, combining it with the other relations and using the following concepts:

- for steady phenomena, expliciting the eulerian total derivative $\frac{D}{Dt} = u_x\frac{\partial}{\partial x}$;
- continuity equation $\dot{m} = u_x\varrho A = \text{constant}$

$$T\frac{\partial}{\partial x}(\varrho u_x s\Delta A) = \Delta(\tau_{xy}\frac{\partial u_x}{\partial y} + \tau_{yz}\frac{\partial u_z}{\partial y} - \frac{\partial q}{\partial y}) \ ; \tag{2.25}$$

For 2-D boundary layer the component in z direction is canceled out :

$$\tau_{yz}\frac{\partial u_z}{\partial y} = 0 \ , \tag{2.26}$$

[1] only critical region in extreme gas dynamic condition could present the bulk viscosity in the formulation of τ but it is outside the purpose of this study

The final step is the integration of this differential formulation over the boundary layer thickness:

$$\frac{d}{dx}\int_0^{\delta}(\varrho u_x(s-s_\delta))dy = \int_0^{\delta}(\frac{\tau_{xy}}{T}\frac{du_x}{dy} - \frac{dq}{dy})dy. \tag{2.27}$$

The equation 2.27 is not only the principal instrument to compute the entropy generation in boundary layer but it has a general validity from thermodynamic point of view: in whatever process in whatever system there are only two ways to increase the entropy [32, 36, 37]:

1. by irreversibilities related to reality of the process
2. by heat transfer

This is nothing but the general formulation of second principle of thermodynamic:

$$d\dot{S} = \underbrace{\frac{\delta\dot{Q}}{T}}_{\text{heat transfer}} + \underbrace{d\dot{S}_{irr}}_{\text{irreversibilities}} \tag{2.28}$$

The equation 2.27 represents two ways to compute the entropy per unit area $\dot{S}_a$ and is the source of all profile losses computation. The core of Denton model is the dimensionless coefficient based on the above quantity mentioned: the *dissipation coefficient*. In this thesis work a general estimation and comprehension about this parameter will be given. The function of this group is to compute the generation of entropy in whatever fluid-solid interaction so also in turbomachinery application. Once the entropy along blade surfaces is computed, it is possible estimated the profile losses for row or stage. All these steps are described in the flow chart 2.7:

The model is completely described and it does not present any simplification or semi-empirical relation, all the quantities are based on the physics of the phenomena. The physical based approach is more "robust" with respect to other models as Chain and Glassman in the optic of boundary layer: C_d is better with respect to the most suitable coefficient for this purposes: Glassman chooses friction coefficient which is intrinsically limited since it represents only the phenomena at the wall neglecting the importance of the entire span of boundary layer (fundamental in turbulence regime); Baines uses two physical concepts, H shape factor and E energy coefficient but the problem is the great sensitiveness of both, therefore the results are strongly dependent by flow condition (i.e H has a huge compressibility dependence). The best point of view for physical based model is the entropy one, in dimensionless term dissipation coefficient. We need a tool to investigate the C_d since the knowledge of boundary ayer state is necessary: this instrument is a boundary layer code.

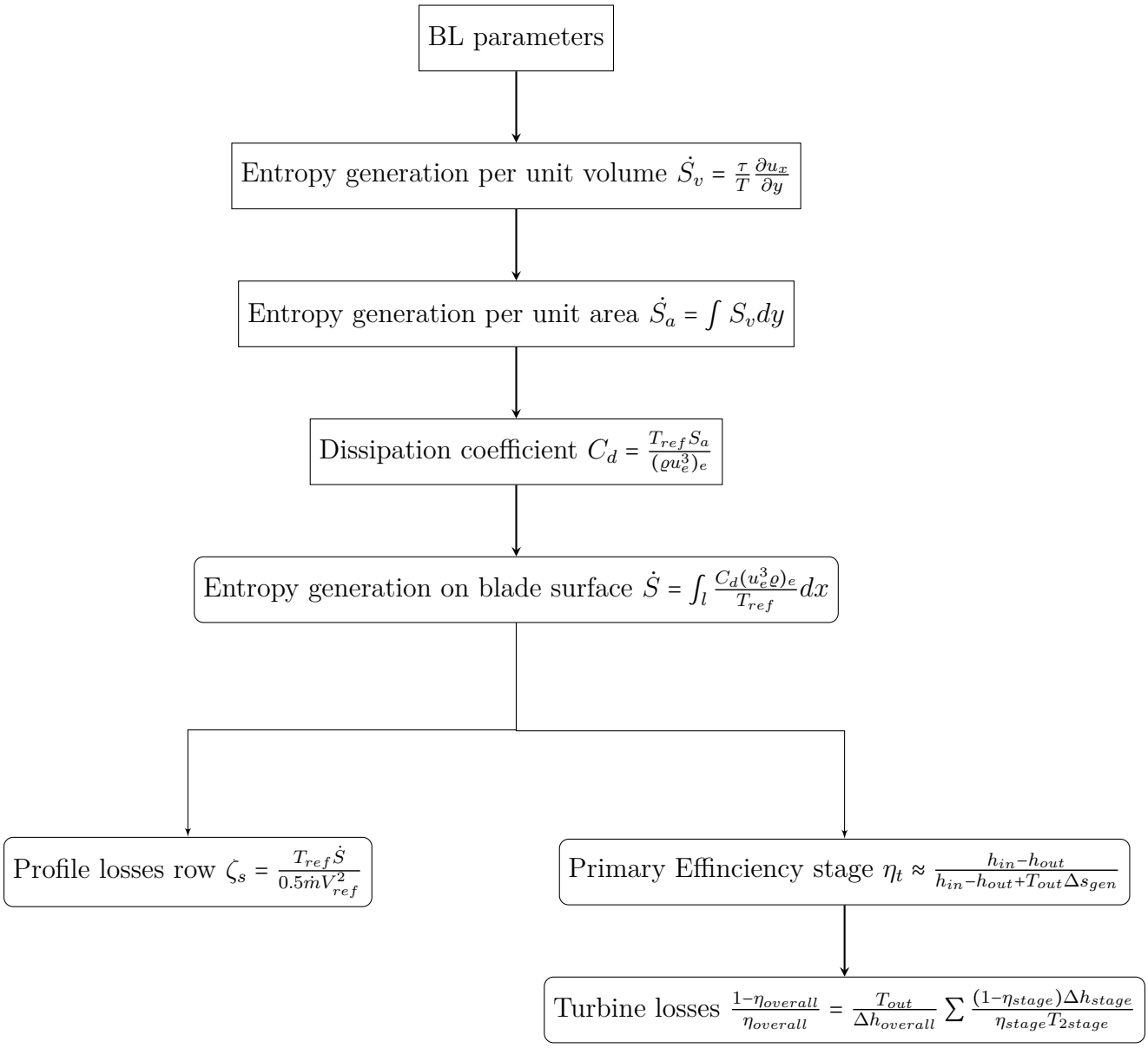

Figure 2.7: Computational process for boundary layer profile losses [2]

2.2 Boundary Layer theory

The theory of boundary layer is one of the most important branches of fluid mechanics. In the optic of turbomachines, this field is the natural basis of profile losses along blade surfaces and it is historically based on 2-dimensional approach. The fundamental equations of boundary layer derives from the Navier-Stokes ones with some simplifications:

- Pressure along vertical is constant due to absence of high stresses which pushes (only stratification effects) the viscous layer $\frac{\partial p}{\partial y} \approx 0$;
- Through the magnitude analysis the derivatives along mean stream line direction

are negligible $\frac{\partial}{\partial x} \gg \frac{\partial}{\partial y}$

- High Reynolds number at the edge of the flow

With these assumption the set of fundamental equations are computed, in particular for compressible flow [37]:

$$\frac{\partial \varrho}{\partial t} + \frac{\partial}{\partial x}(\varrho u) + \frac{\partial}{\partial y}(\varrho u) = 0 \qquad \text{continuity,} \tag{2.29}$$

$$\varrho(\frac{\partial u}{\partial t} + u\frac{\partial u}{\partial x} + v\frac{\partial u}{\partial y}) \approx \frac{\partial p_e}{\partial x} + \frac{\partial}{\partial y}(\mu\frac{\partial u}{\partial y}) \qquad \text{momentum x,} \tag{2.30}$$

$$\frac{\partial p}{\partial y} \approx 0 \qquad \text{momentum y,} \tag{2.31}$$

$$\varrho(\frac{\partial h}{\partial t} + u\frac{\partial h}{\partial x} + v\frac{\partial h}{\partial y}) \approx \frac{\partial p_e}{\partial t} + u_e\frac{\partial p_e}{\partial x} + \frac{\partial}{\partial y}(\lambda\frac{\partial T}{\partial y}) + \mu(\frac{\partial u}{\partial y})^2 \qquad \text{energy} \tag{2.32}$$

Through these parameters all the coefficient of aerodynamic or fluid dynamic are computable (i.e c_f, drag, dissipation etc.). A boundary layer code must be able to calculate these elements. In particular whatever validation of the code is based on the comparison of this parameters with the classical works results (Blasius, Cohen and Reshotko, Howarth, Götler) for this code this step is represented by the other thesis [38]. The famous typologies of boundary layer are:

- Blasius for incompressible with zero pressure gradient; the transformed coordinate is $y\sqrt{\frac{u}{\nu x}}$. The analytical solution is computed from the momentum equation which is an ordinary equation of third degree obtained from the partial derivative one.
- Cohen-Reshotko which introduced compressibility and accelerating flow
- Howarth: transformation for compressible boundary layer [39] this is used also in the Boundary layer code useful to stretch the vertical coordinate for high change in density inside the BL;

$$\eta = \sqrt{\frac{u_e}{\varrho_e \mu_e x}} \int_0^e \left(\frac{\varrho}{\varrho_e} dy\right) \tag{2.33}$$

With η is the transformed coordinate, sub-script "e" represents the edge.

Parameter	Description	Formulation
BL thickness δ	Height of boundary layer. In general « flow characteristic length	
Velocity profile f'	actual velocity inside BL with respect to the edge one	$\frac{u}{u_e}$
Displacement thickness δ^*	defect of mass flow rate due to viscous nature compare to the inviscid Eulerian case	$\int_0^e (1 - \frac{\varrho u}{\varrho_e u_e})$
Momentum thickness θ	defect of momentum of viscous flow with respect to the Eulerian case	$\int_0^e (1 - \frac{u}{u_e}) \frac{\varrho u}{\varrho_e u_e}$
Kinetic displacement δ^{**}	defect of momentum of viscous flow with respect to the Eulerian case	$\int_0^e (1 - \frac{u^2}{u_e^2}) \frac{\varrho u}{\varrho_e u_e}$
Shape factor H	Ratio of displacement over momentum thickness: measure of defect of mass with respect to the momentum one	$\frac{\delta^*}{\theta}$
Second shape factor H_2	Ratio of kinetic displacement over momentum thickness: measure of defect of kinetic energy with respect to the momentum one	$\frac{\delta^{**}}{\theta}$
Chapman-Rubesin parameter	Ratio of density and viscosity inside viscous flow with respect to the inviscid edge	$\frac{\mu\varrho}{\mu_e \varrho_e}$
shear parameter f"	derivative of velocity ratio, it represents a dimensionless shear quantity	$\frac{\partial f'}{\partial \eta}$

Table 2.2: Fundamental parameters of boundary layer

2.2.1 Integral method

Integral methods are based on the solution of the integral equations of motion. They avoid the complexity of solving the differential form of the boundary layer equations, and they provide, with very short computation times, a solution of the boundary-layer

equations [40]. Due to the complexity of the subject, a theory developed by Von Karmàn and Pohlausen deals with integral formulation [41, 42, 36]:

$$\frac{d\theta}{dx} + (H + 2 - Ma_e^2)\frac{\theta}{u_e}\frac{dU_e}{dx} = \frac{c_f}{2} \qquad \text{Momentum integral,} \tag{2.34}$$

$$\frac{d\delta^{**}}{dx} + (3 - Ma_e^2)\frac{du_e}{dx} = \frac{2\dot{D}}{(\varrho u)_e^3} = 2C_d \qquad \text{Mechanical Energy integral,} \tag{2.35}$$

$$\frac{d([\varrho hu]_e\delta_h)}{dx} + (u_e^2\varrho_e\delta_h)\frac{du_e}{dx} = \dot{D} + \dot{q} \qquad \text{Enthalpy integral,} \tag{2.36}$$

Where θ is the momentum thickness, δ^{**} the kinetic displacement, $\dot{q}$ is thermal power per unit area and $\dot{D}$ is the dissipation integral defined for whatever flow:

$$\dot{D} = \int_0^\infty (\mu\frac{\partial u}{\partial y} - \varrho\overline{u'v'})dy = \int_0^\infty (S_v T)dy \tag{2.37}$$

This last parameter 2.37 is particularly important since it represents the numerator of the dissipation coefficient and it is related to the entropy generation per unit volume. It is important to underline that this formulation is a little different from the one of Denton since the temperature in compressible high speed flow or for non adiabatic case are strongly variable inside the boundary layer. The dissipation $\dot{D}$ skips directly the division by temperature and the consequently multiplication for a reference one. This set of equation are valid for laminar and turbulent boundary layer, for laminar regime the eddy viscosity represented by the average of the fluctuation component of the velocity is equal to zero. Through simplified Boussinsesq's hypothesis [43, 44]:

$$-\varrho\overline{u'v'} = \tau' = \mu_t(\frac{\partial u}{\partial y}) \ , \tag{2.38}$$

it is possible to use the gradient of velocity multiplied by a total viscosity.

2.2.2 Boundary Layer code

The boundary layer code [45] is based on the works made by NACA between '50 and '80 years. In particular the paper of Clutter and Smith [39] coupling with the numerical method of Keller [46, 40] are the theoretical background of it. Even if the integral method presented in the previous section is very useful point of view, the code is based on differential approach, in other words, finite difference method.

Structure of the code

The main structure of the code is in chart 2.8:

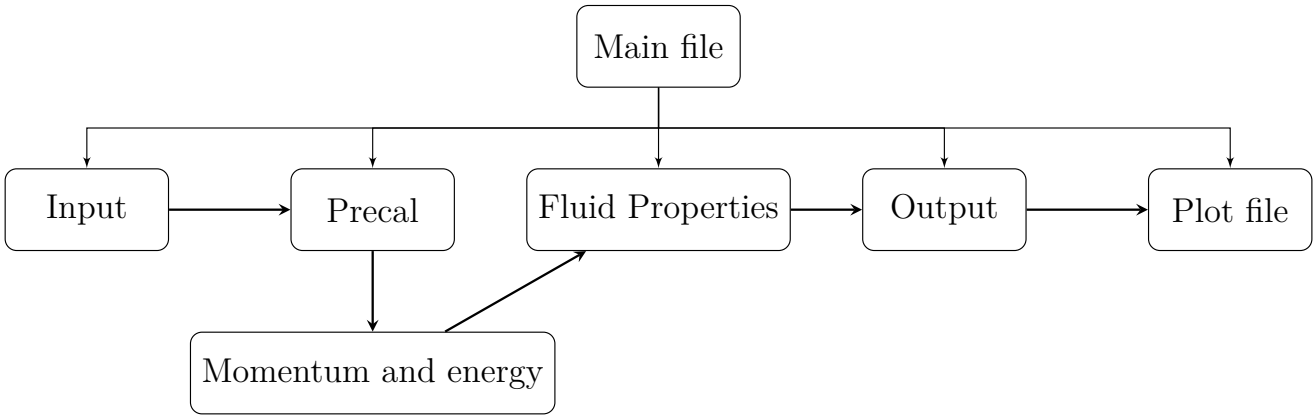

Figure 2.8: Structure of the code for Boundary layer computation

The main files of 2.8 are:

- Main: file which commands all the other, through this one it is possible to run the code.
- Input file: the input for a certain boundary layer study must be inserted here plus boundary condition
- Precal computation of all thermodynamic quantities along the edge and at the wall using the boundary condition and physics relations or libraries (FluidProp)
- output file: is the script which contains the implementation of all parameter (H, θ , c_f, C_d...)
- Plot file: the several values are diagrammed.

The explanation of the numerical core of the code, Momentum and energy files, is contained in [38].

Keller's box method

The mathematical method is an alternative to the Crank-Nicholson and it is an implicit scheme very polyvalent since it can be solved with several order of accuracy and for a wide class of problems. The name "box" derives from the typical computational structure 2.9.

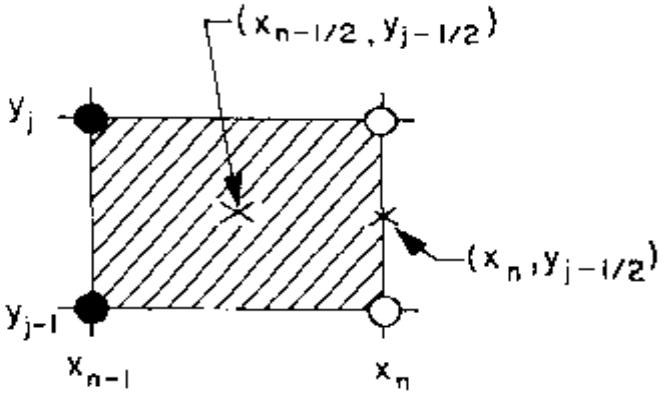

Figure 2.9: The "Box" structure based on numerical method of boundary layer code [46].

The linearization allows to speed up the computation and the solution is computed iteratively using Newton's method. The convergence velocity is proportional to the square of the residual. Because the truncation errors have expansions in the squares of the mesh widths, thus Richardson extrapolation is employed (only for laminar study), therefore improvement by two orders of accuracy can be obtained for each application. This numerical method should be suitable also for more complex study as separation flow and unsteady boundary layer phenomena [46, 47].

Transition model

For the sake of simplicity the model used to estimate transition is the one proposed by Wazzan [48]. This is the so called $H - Re_x$ method since the transitional Reynolds number is a function of shape factor H. Even if it is a semi-empirical expression, the physical root of this method is the phenomenon for which laminar and turbulent regime are characterized by two different values of shape factor in boundary layer field: between 2.1 and 2.8 for laminar and close to 1.5 for turbulent, therefore if H drop down from the laminar range transition is started.

$$\log_{10}(Re_{xTR}) = -40 + 64.8066H - 26.7538H^2 + 3.3819H^3 \quad \text{for } 2.1 < H < 2.8 \tag{2.39}$$

The limitation of this model is respect to Mach effect since it is valid only for low speed flow and for adiabatic phenomena. The author states that the model is valid only for a ΔT until 23 C°. Using the adiabatic wall temperature formulation:

$$\Delta T = T\ rMa^2 \frac{\gamma - 1}{2}, \qquad \text{r is the recovery factor } f(Pr) \tag{2.40}$$

We can appreciate why high Mach flows are problematic for this method: because the wall temperature increase a lot due to viscous dissipation. In the turbulence part an artificial transition or fully turbulent flow will be used.

Turbulence model: Cebeci-Smith model

The Cebeci-Smith model is an algebraic model, evolution of the original Prandtl - Mixing length [43]. It is a two layer model able to describe viscous laminar (sub-layer) and the outer one without any need of transport turbulence equations (0-equation).
There are several versions of the turbulent model by Cebeci-Smith. The first one was made in 1967 [49] and it was valid for incompressible boundary layer without any thermal phenomena computed. The characteristics of the latest version [50] is to be able to compute the thermal quantities of boundary layer such as temperature profile and change in density. The positive aspects are related to the simplicity and the lightness from computational point of view. Despite his simplicity, many physical concepts like the various layers inside the viscous flow (viscous laminar sub-layer, buffer layer and outer) can be described. A more refined turbulent Prandtl number influenced by molecular aspects close to the wall is used. Another interesting concept is the intermittency factor γ_{tr} related to the statistical behavior of turbulence. This part was formulated after a campaign of experiment by Klebanoff from this the other name "*Klebanoff factor*". The intermittency factor is the probability that the flow at (x, t) is turbulent [44]:

$$\gamma_{tr}(\vec{x},t) = \langle I(\vec{x},t)\rangle = Prob|\omega(\vec{x},t)| > \omega_{treshold} \tag{2.41}$$

Where ω is the turbulence frequency. Figure 2.10 shows clearly this concepts.

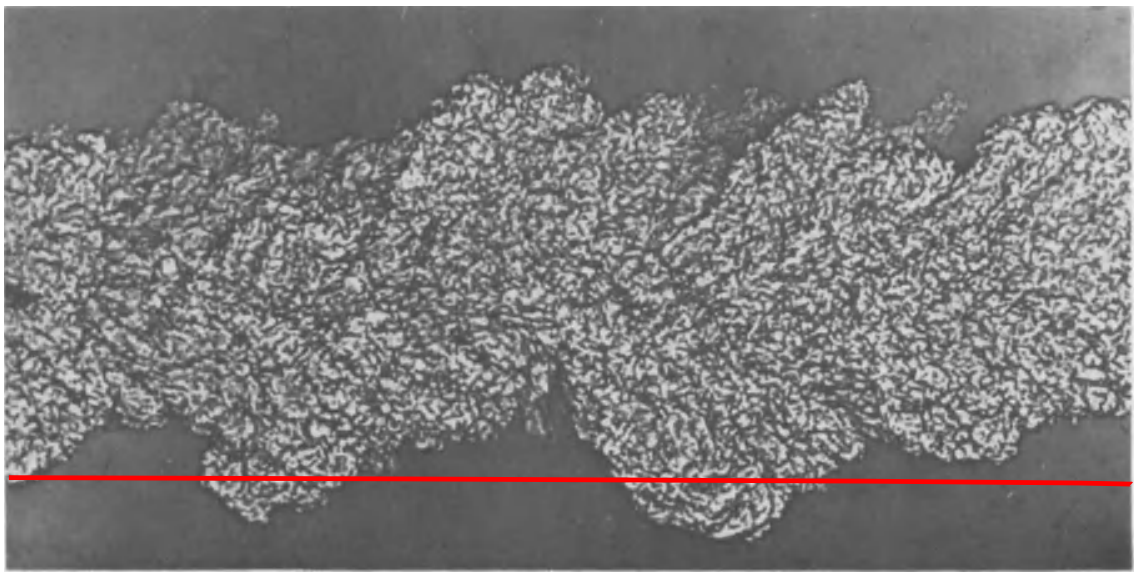

Figure 2.10: Concept of intermittency at the super-layer of the shear flow: red line (—) is the average separation between free flow and shear layer [51]

The general formulation of Cebeci-Smith model is the following:

$$\begin{cases} (\varepsilon_m)_i = l^2 |\frac{\partial u}{\partial y}| \gamma_{tr} \gamma, & 0 < y \ y_c \\ (\varepsilon_m)_o = \alpha |\int_0^e (u_e - u) dy| \gamma_{tr} \gamma, & y_c < y < \delta \end{cases} \tag{2.42}$$

These are the two equation to compute the eddy (turbulence) viscosity in the inner and the outer layers. For a standard incompressible case the result of our code is in the figure 2.11:

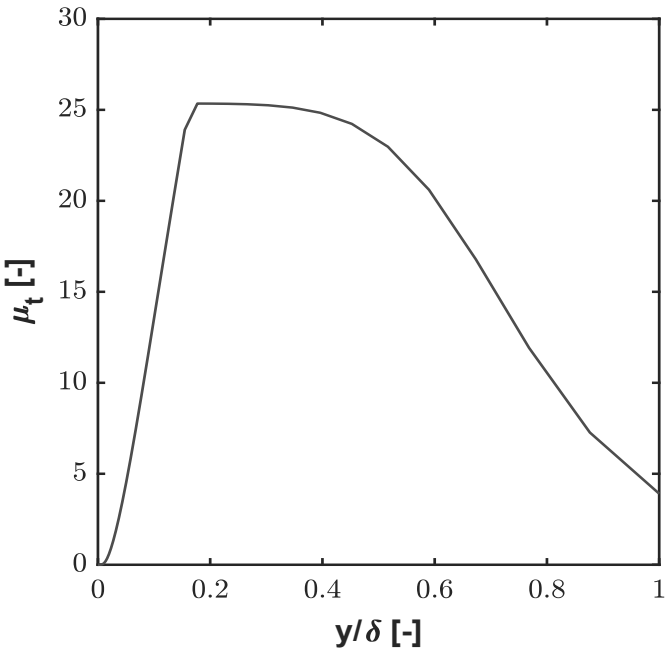

Figure 2.11: Trend of turbulent viscosity with respect to molecular one inside the boundary layer: steep increase close to the wall and smooth decrease towards the edge

About the other terms:

Mixing length

$$l = \kappa y \left[1 - exp\left(-\frac{y}{A}\right)\right], \tag{2.43}$$

Van Driest damping parameter: semi-empirical relation based on the experiment

data at the wall

$$A = 26\frac{\nu}{N}u_\tau^{-1}(\frac{\varrho}{\varrho_w})^{1/2} \ , \tag{2.44}$$

Friction velocity and N parameter and pressure gradient: characteristic velocity; semi-empirical relation based on the experiment data at the wall

$$u_\tau = \sqrt{\frac{\tau_w}{\varrho_w}} \qquad N = \sqrt{1 - 11.8\frac{\mu_w}{\mu_e}\left(\frac{\varrho_e}{\varrho_w}\right)^2 p^+} \qquad p^+ = \frac{\nu_e u_e}{u_\tau^3}\frac{du_e}{dx} \tag{2.45}$$

Intermittency, factor G and supplementary intermittency: see figure 2.10 only for adiabatic case and until Mach =5:

$$\gamma_{tr} = 1 - exp[-G(x - x_{tr}\int_{x_{tr}}^{x}\frac{dx}{u_e})]; \qquad G = 8.33\ 10^{-4}\frac{u_e^3}{\nu^2}Re_x^{-1.34}; \tag{2.46}$$

$$\gamma = [1 + 5.5(\frac{y}{\delta})^6]^{-1} \ , \tag{2.47}$$

outer layer factor general case until Re_θ:

$$\alpha = 0.0168\ Re_\theta^{-1/4} \tag{2.48}$$

All the theoretical concepts which serves as background for this work have been presented in this chapter, also the instrument set to obtain the results. In the next chapters the results will be show and discussed both for turbomachinery field 3 and boundary layer phenomena 4 and 5.

Chapter 3

Profile charts

The first part of the results of this work will be presented in this chapter, in particular the ones related to applicative field: profile losses in an axial turbine stage. The profile losses field is complex and, as shown in chapter 2 and Appendix E there are several methods to compute the relative efficiency. Following the relations presented by the authors it is possible to estimate what is the best model in particular for new applications such as ORC expanders.
The following study has the purpose to generate the Smith's charts focusing only on boundary layer profile losses: this analysis is very important for the mean line design and it is a difficult task for a common CFD code since it is machine specific. In particular a 2-D approach is implied using the profile at the midspan. The first step is introducing the stage terminology 3.1:

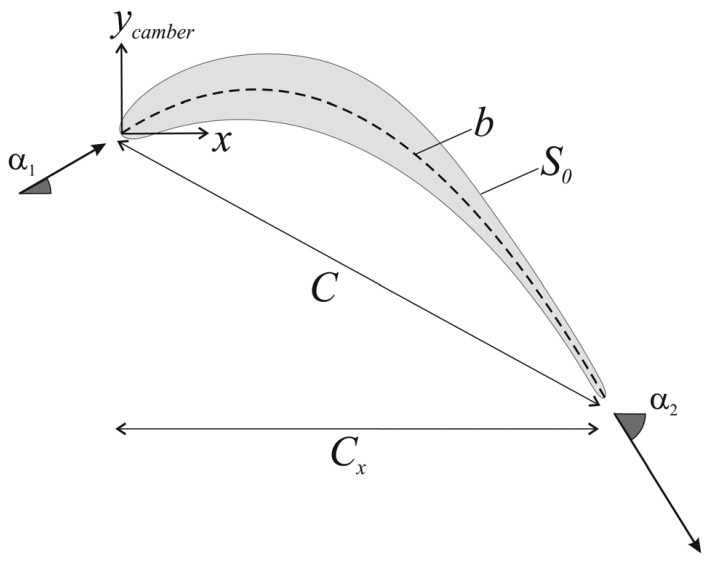

Figure 3.1: Definitions and conventions of the blade nomenclature [52]

3.1 Features of the stage

The common turbomachinery stage theory [53] gives the general relation between the coefficient of the Smith's chart and the flow angles. The problem studied is a common reaction stage (r^* = 0.5) with a pressure ratio β_{TT} of 2.5 (it will be varied only in one study to see the effect).
First the general characteristics of the stage are presented.

Dimensionless parameter

The first choice is the pressure ratio total-to-total of the stage β_{TT}. For a classical gas turbine stage is 2 or 2.5. The range in flow coefficient and the loading coefficient is respectively between 0.5-1.3 and 0.6-3 with 50 values for both range so 2500 points will be computed.

Thermodynamic values

In this group total temperature, total pressure and the typology of the fluid are chosen. In particular:

- T_{T0} = 500 K common temperature for low pressure axial stage also because the original experiments made by Smith were performed with a TIT (turbine inlet temperature) of 200° C [28];
- P_{T0} = 2 atm (202650 Pa);
- Fluid parameter: starting from a perfect gas air approach,

$$\gamma = 1.4 \qquad MW = 28.97 \ \frac{kg}{kmol} \qquad R_u = 8.314 \frac{J}{molK} \qquad \theta = \frac{\gamma - 1}{\gamma} \ . \tag{3.1}$$

Velocity triangle

They are built through the general angle relation and the magnitude of the vectors. The relations which link the dimensionless Smith coefficients to the flow angle are presented by Dixon [24] for a reaction stage:

$$\alpha_2 = \beta_1 \qquad\qquad \alpha_1 = \beta_2 \tag{3.2}$$

$$\beta_2 = atan\left(\frac{\psi + 1}{2\phi}\right) \qquad\qquad \beta_1 = atan\left(\frac{\psi - 1}{2\phi}\right) \tag{3.3}$$

And the velocities magnitude from ϕ and ψ.

Blade geometry

The geometry chosen is based on two concept: the classical formulation made by Zweifel based on the optimization of blade aerodynamic load for the axial solidity and a classical parabolic camber line geometry for the blade. The Zweifel criterion is [54];

$$C_{ft} = 2cos^2\alpha_1 \left(\frac{V_{0ax}}{V_{1ax}} tan(\alpha_{in}) - tan(\alpha_{out})\right) \frac{s}{C_x} \ , \qquad \text{with } C_{ft} = 0.8 \tag{3.4}$$

The camber line formulation is based on the assumption of zero incidence and zero deflection therefore the flow angles are equal to the geometrical ones;therefore for a pure parabolic camber shape:

$$A = 4\left(\frac{tan(\alpha_{in}) - tan(\alpha_{out})}{2}\right)^2$$

$$B = 4\left(\frac{tan(\alpha_{in}) - tan(\alpha_{out})}{2}\right)(-tan(\alpha_{in}))$$

$$C = 1 + tan^2(\alpha_{in})$$

$$D_1 = \frac{(B+2A)\sqrt{A+B+C} - B\sqrt{C}}{4A} \tag{3.5}$$

$$D_2 = \frac{4AC - B^2}{8A^{1.5}} \ ln\left(\frac{2A + B + 2\sqrt{A^2 + AB + AC}}{B + 2\sqrt{AC}}\right)$$

$\frac{b}{C} = cos(\gamma)(D_1 + D_2)$ camber line over chord;

$\gamma = \frac{tan(\alpha_{in}) + tan(\alpha_{out})}{2}$ stagger angle;

This blade shape is quite simplified since in the reality the geometry could be very complex: in figure 3.2 two examples of blade are reported.

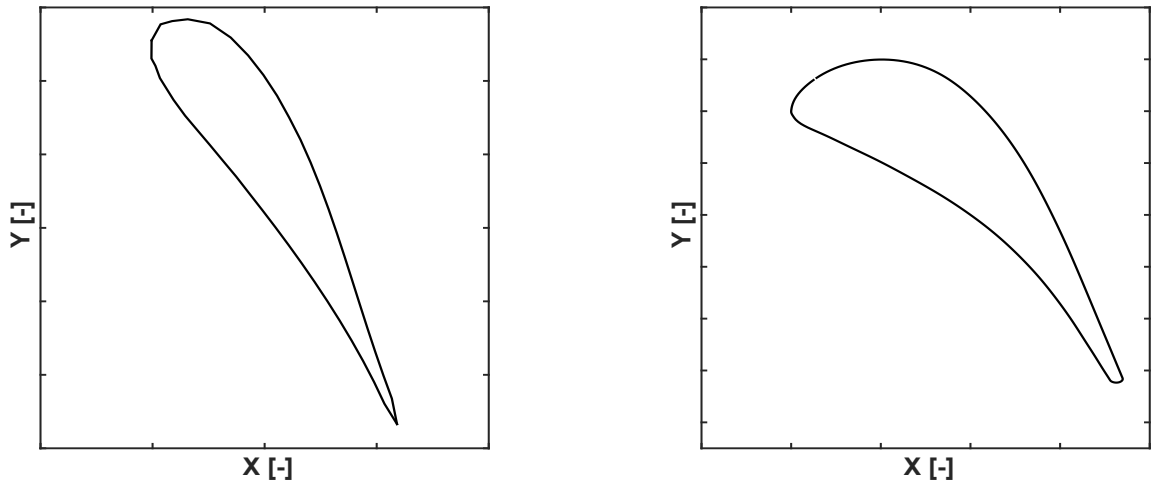

Figure 3.2: Typical stator blade profile of two different families: (a) A3K7 reaction blade for a gas turbine [32]; (b) LS89 used in ORC application [16]

Aerodynamic concepts

Once the geometry of the rows is defined and the flow angles are known, through the theorem of Kutta-Jukowsky and the conservation of momentum in tangential direction it is possible to compute the velocity distribution along the blade surfaces, either for pressure and suction side.

$$V_{PS} = \overline{V} - \Delta V \tag{3.6}$$

$$V_{SS} = \overline{V} + \Delta V \tag{3.7}$$

Through Kutta-Joukowsky theorem applied [55]:

1. In the blade pitch direction

$$\Gamma = \Delta V_t s \tag{3.8}$$

2. in the camber-line direction

$$\Gamma = (V_{SS} - V_{PS})b = (\overline{V} + \Delta - \overline{V} + \Delta)C_s = 2b\Delta V \ ; \tag{3.9}$$

Manipulating the two last equations:

$$\Delta V = \frac{\Delta V}{2\frac{b}{s}} = \frac{\Delta V}{\frac{b}{C}\frac{C}{C_x}\frac{C_x}{s}} \; ; \tag{3.10}$$

The terms are respectively: $\frac{C}{C_x}$ is the inverse of the cosine of stagger angle (γ), $\frac{C_x}{s}$ is the axial solidity (computed by the Zweifel criterion) and finally $\frac{b}{C}$ is the so called blade shape factor, parameter which describes the geometry of the blade 3.5.
The average velocity of the blade is computed through the conservation of the momentum, starting from the concept of lift:

$$L = \varrho V_{ax} s \Delta V_t = \oint_{blade} p\vec{n}d\vec{l} \; , \tag{3.11}$$

Managing the formulation and introducing the assumption of low speed flow therefore $\varrho \approx constant$:

$$\overline{V} = \frac{V_{ax}\Delta V_t}{2\frac{C_x}{s}\Delta V} \; , \tag{3.12}$$

A parameter related to the blade load is the ratio of the difference in velocity over the average velocity:

$$\varepsilon = \frac{\Delta V}{\overline{V}} \; , \tag{3.13}$$

In fact the ΔV represents the discrepancy with respect to the average value. Notice that this parameter relates to the primary losses. Normally high ε means high load coefficient (top left corner in the Smith chart). Figure 3.3 presents the idealized profile used by Denton as base for his model.

We can conclude that the type of fluid and therefore the load on the blade is the determinant factor for the shape of the blade. Also the degree of reaction directly connected to the load is a fundamental parameter.

In this way it is possible to build a Smith-type-chart.

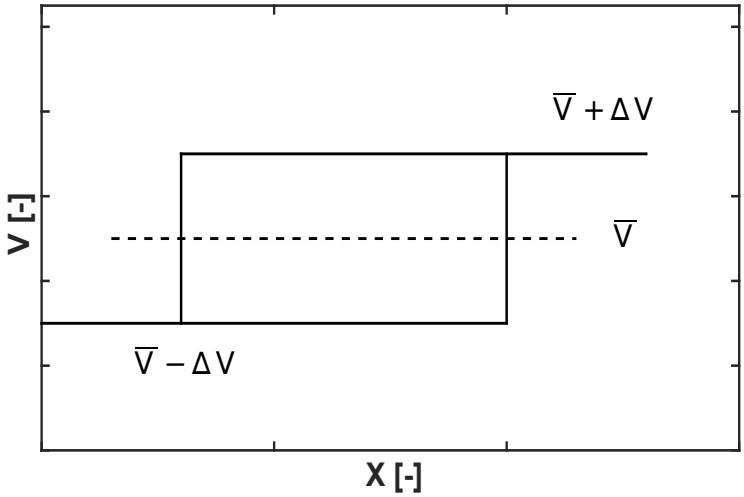

Figure 3.3: Idealized velocity surface distribution [1]

3.1.1 General results for the stage

First we plot the general characteristics of the axial stage: deflection angles fig.3.4, velocity triangles fig. 3.5 aerodynamic fig. 3.6 and geometry parameters fig. 3.7.

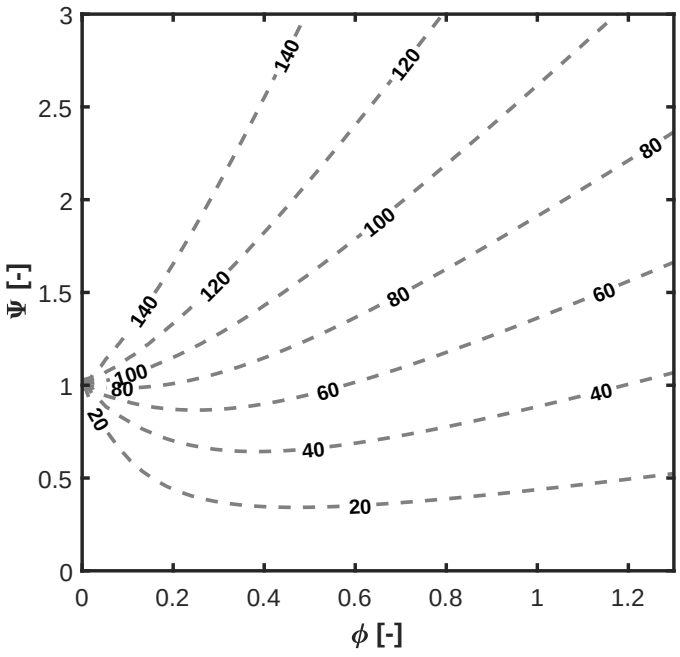

Figure 3.4: Deflection trend of the angle;A general collapse in the unity of load coefficient happens when the flow coefficient is zero

In particular one of the most important steps of the mean line design is the computation of the velocity triangles. In this case they are shown in dimensionless version using the peripheral speed U to scale all vectors (fig.3.5).

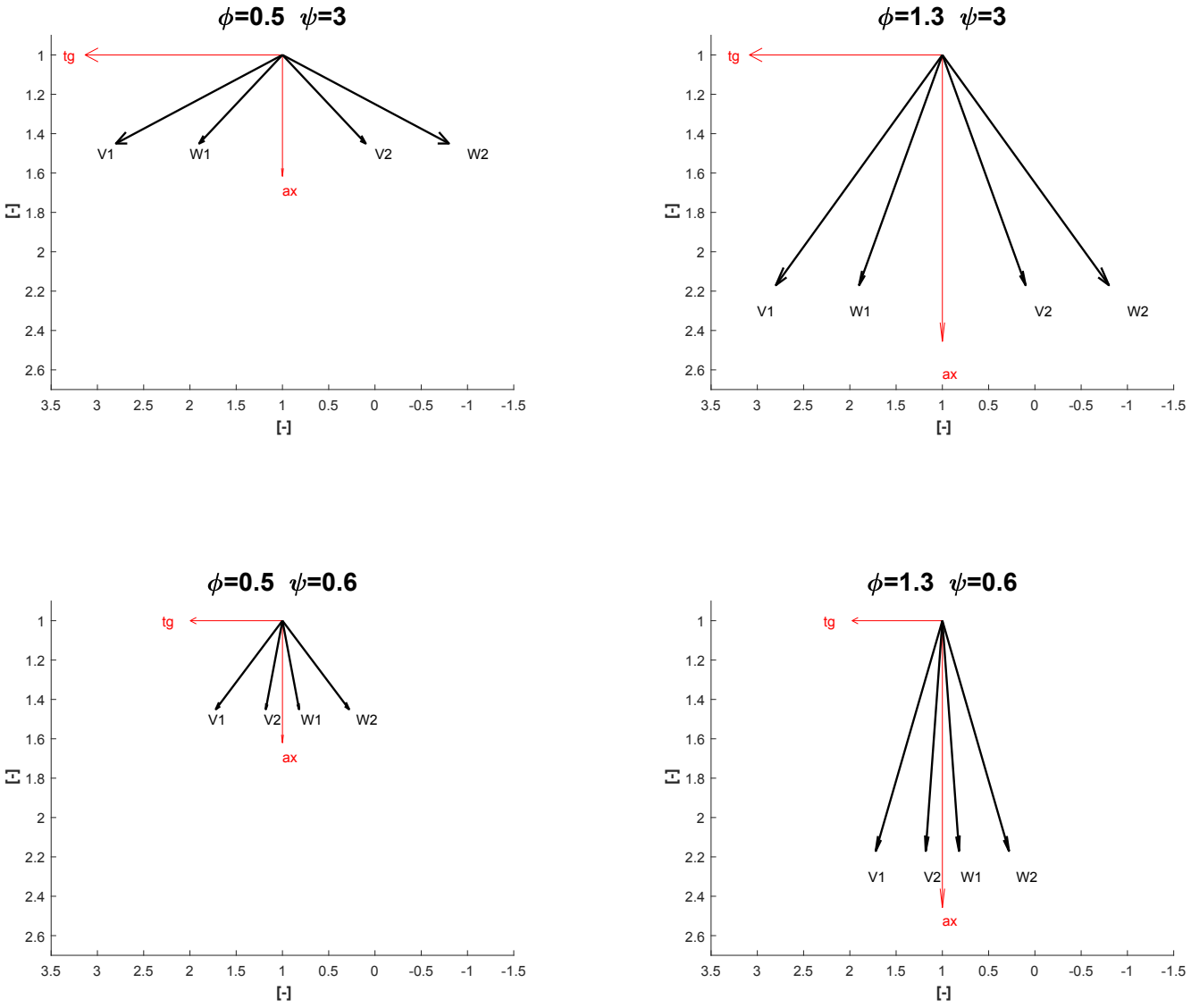

Figure 3.5: Velocity triangles computed in the extreme points of the Smith charts: the load coefficient ψ and flow coefficient ϕ influence the direction and the openings of the vector.

We can check the concept of high load in the shape of the top-left velocity triangles: very high flow deflection happens in this working zone. In contrast high ϕ means high axial

component and in general very high velocities and so the reason for the high Mach in the bottom right corner 3.5.
Due to the symmetry given by the reaction degree equal to 0.5 the following parameters are the same for stator and rotor cascades. Following the analysis of Coull and Hodson [52] a series of Smith charts for aerodynamic concepts and geometry are proposed in fig 3.6:

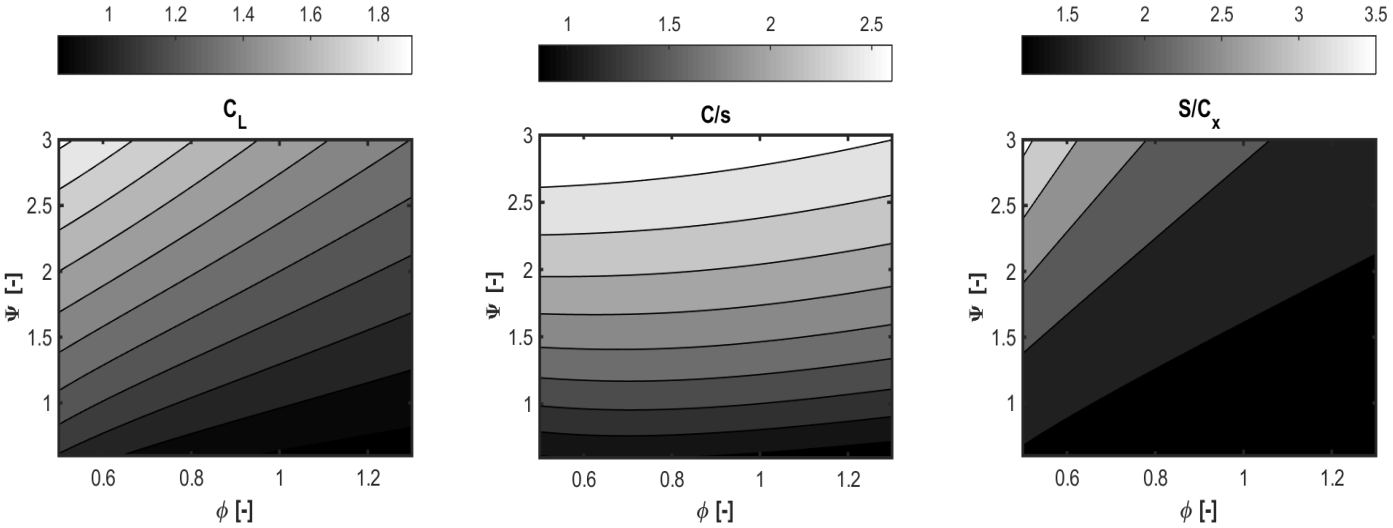

Figure 3.6: Parameters of the cascade: (a) Lift coefficient on the blade; (b) Solidity; (c) Suction surface over axial chord, description of the blade geometry. Results consistent with the one presented by Coull and Hodson [52]

It is important to underline the common trend of this factors: at high load the solidity (b) is the maximum one therefore the length of the blade is much higher with respect to the pitch. Moreover in the left-top corner the most extreme conditions are achieved in terms of lift (a) and the most curved geometry of camber line (c). The definition of lift coefficient is the classical one for turbine blades [52](at low speed):

$$C_L = 2\left(\frac{s}{C}\right)(tan(\alpha_{in}) - tan(\alpha_{out})) - tan(\alpha_{out}))cos(\alpha_m) \tag{3.14}$$

where:

$$\alpha_m = atan(tan(\alpha_{in}) + tan(\alpha_{out})) \tag{3.15}$$

This variable must be known in order to optimize the stage selecting the right work zone. The other set of important parameters are those related to thermodynamic quantities, Mach number and Reynolds number.

It is clear that in the bottom right corner of the Smith chart is characterized by highest kinematic aspect i.e maximum velocity. This is caused by the elevated flow coefficient

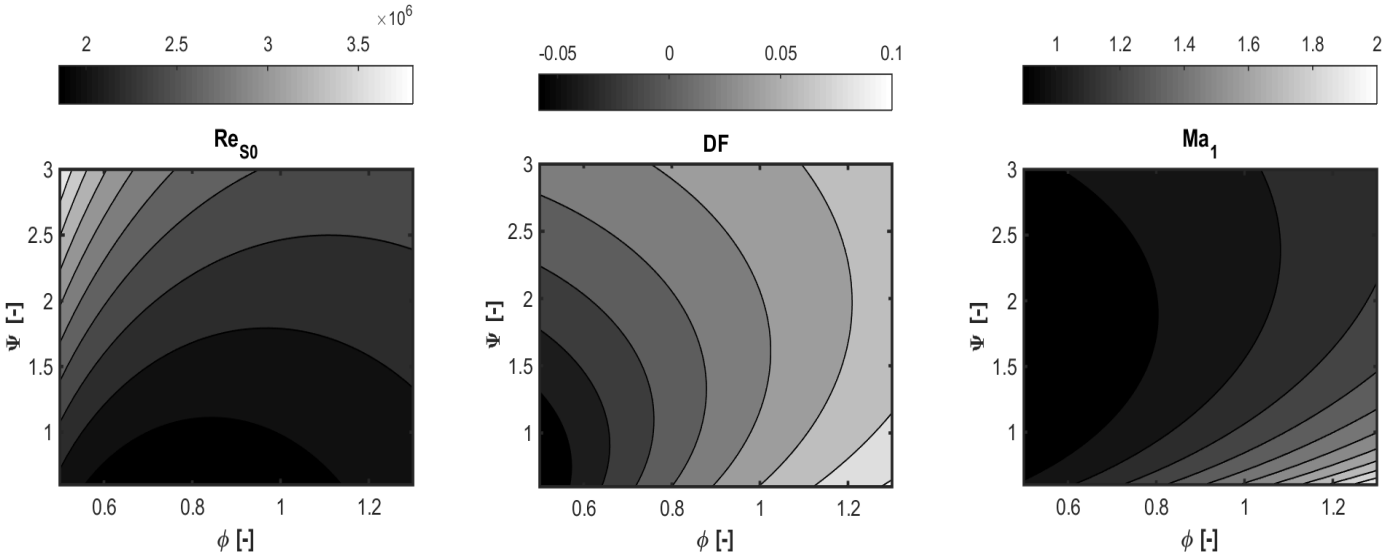

Figure 3.7: Features of the cascade: (a) Reynolds based on suction side surface $\frac{U_{SS}S_0}{\nu}$; (b) Diffusion factor defined as: $\frac{u_{peak}-u_{TE}}{u_{peak}}$; (c) Mach number at the stator exit

and minimum load. Therefore the peak velocity becomes the 10 % higher than the trailing edge one fig.(b)3.7 producing high acceleration which causes strong dissipation in boundary layer (Chapter 4). Moreover the risk of shock wave is very elevated since the Mach tends to be large. This aspect will be the major weakness of the classical models, in particular Dunham-Came which tends to over estimate it. As stated by many authors the aerodynamic and the design optimization are necessary in order to increase the efficiency in particular this has huge impact on primary loss phenomena. From the previous graphs 3.7 we can conclude that the extreme zones (high ψ and ϕ) should be excluded as the working zone starting from the preliminary mean line design because they present high losses, in other words a moderate flow and in particular load coefficient must choose following the criterion already presented by the original work of Smith [28]. Therefore the profile loss field follows the general trend of stage efficiency.

3.2 The limitations of classical loss models

The task of this section is showing the limitations of the classical approaches for the profile loss computation. For this stage the following models are used:

- Ainley Mathieson
- Dunham Came

- Kacker Okapuu

The relations used are the one already presented in the section 2.1.2. In the following plots 3.8 the Smith chart computed with three classical model belonged to the AM family:

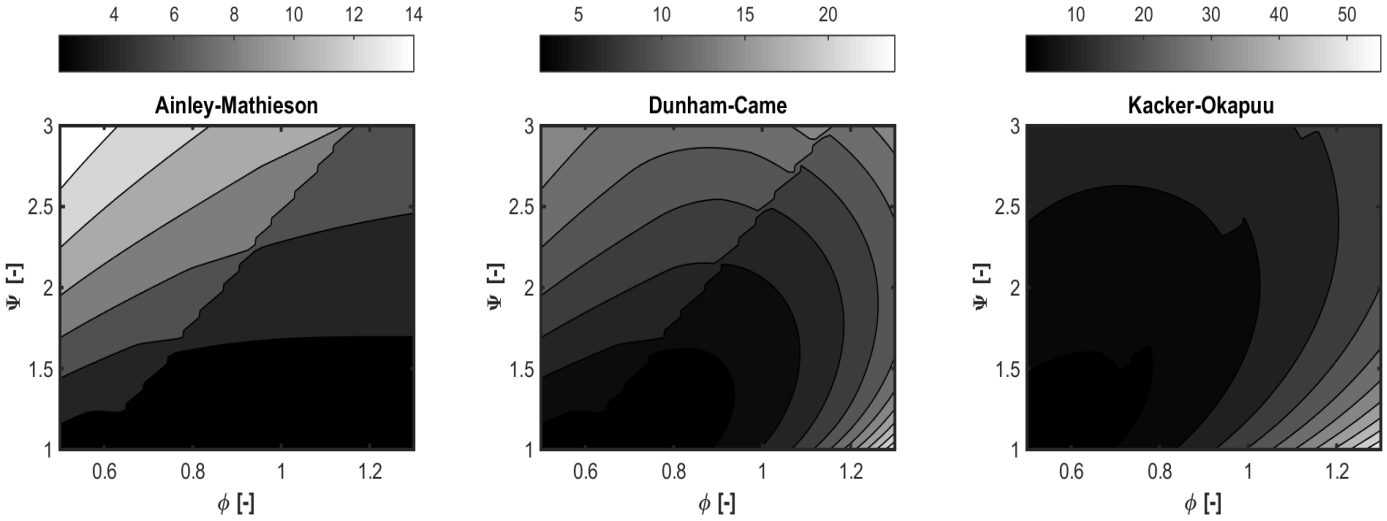

Figure 3.8: Profile losses computed through classical model: (a) Ainley-Mathieson ; (b) Dunham-Came ; (c) Kacker-Okapuu. Discontinuities and jump due to interpolation of extraction formulas [34].

The limitation of all three methods are evident:

- Ainley-Mathieson uses only a simple relation and a blending function between nozzle and propeller
- Dunham-Came is characterized by over simplified and raw compressibility function which causes an increase of loss estimated in the high Mach zone.
- Kacker-Okapuu is the most sensitive to Mach losses. The increase in the bottom right corner is mainly due to the factor Y_{SHOCK} in fact this term related to shock wave is based on a perfect gas assumption 2.14.

In order to show this phenomena, we plot the parameter of DC and KO fig. 3.9.

A noticeable work in this optic is the paper of Lozza and Macchi [56] on the comparison between the Ainley-Mathieson family and the Craig Cox method. The final thesis is that this latter is better for many aspects in particular for turbine which process vapor. Since the ORC application are characterized by dense gas with non ideality effects and often.

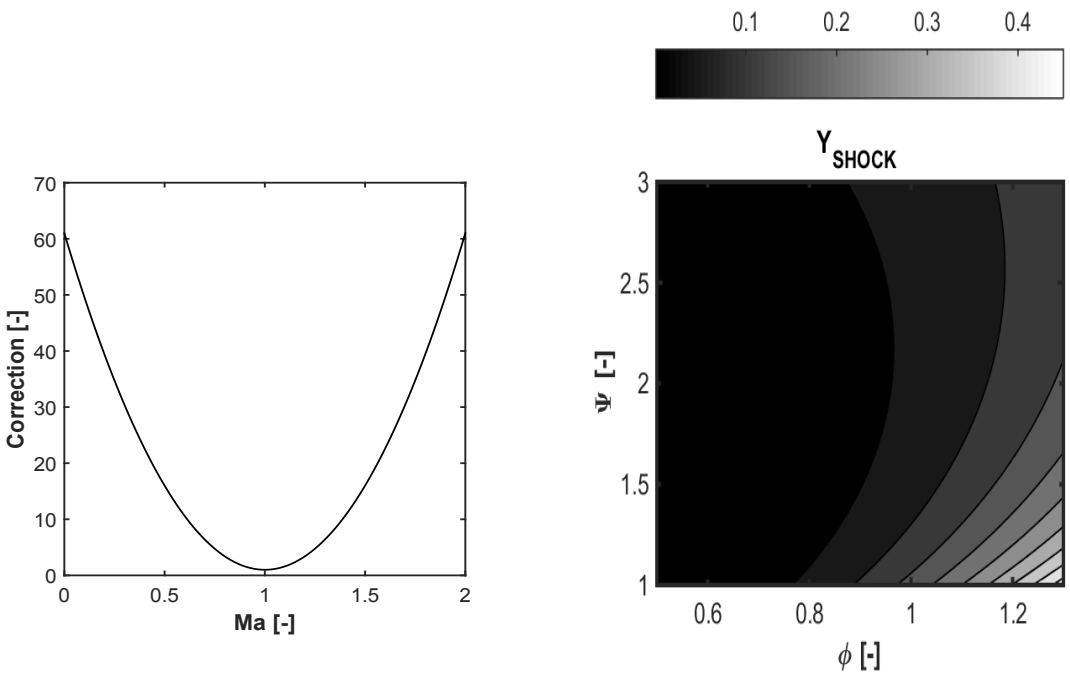

Figure 3.9: (a) Dunham Came correction function; (b)Y_{SHOCK} shock wave correction introduced by Kacker Okapuu

3.3 Physical-Based Model results

The model proposed by Denton is based on computation of entropy. This is a physically sound approach which allows to understand all the computational passages. No semi-empirical relations are employed.
The chart 3.10 shows the entire computation process. Notice that until the velocity triangles step we follow the same pathway as the previous classical model. Then more concept are introduced since they are necessary to compute the surface side losses. Through the fundamental expression shown 3.16 it is possible estimate the generation of entropy along whatever solid body i.e the blade.

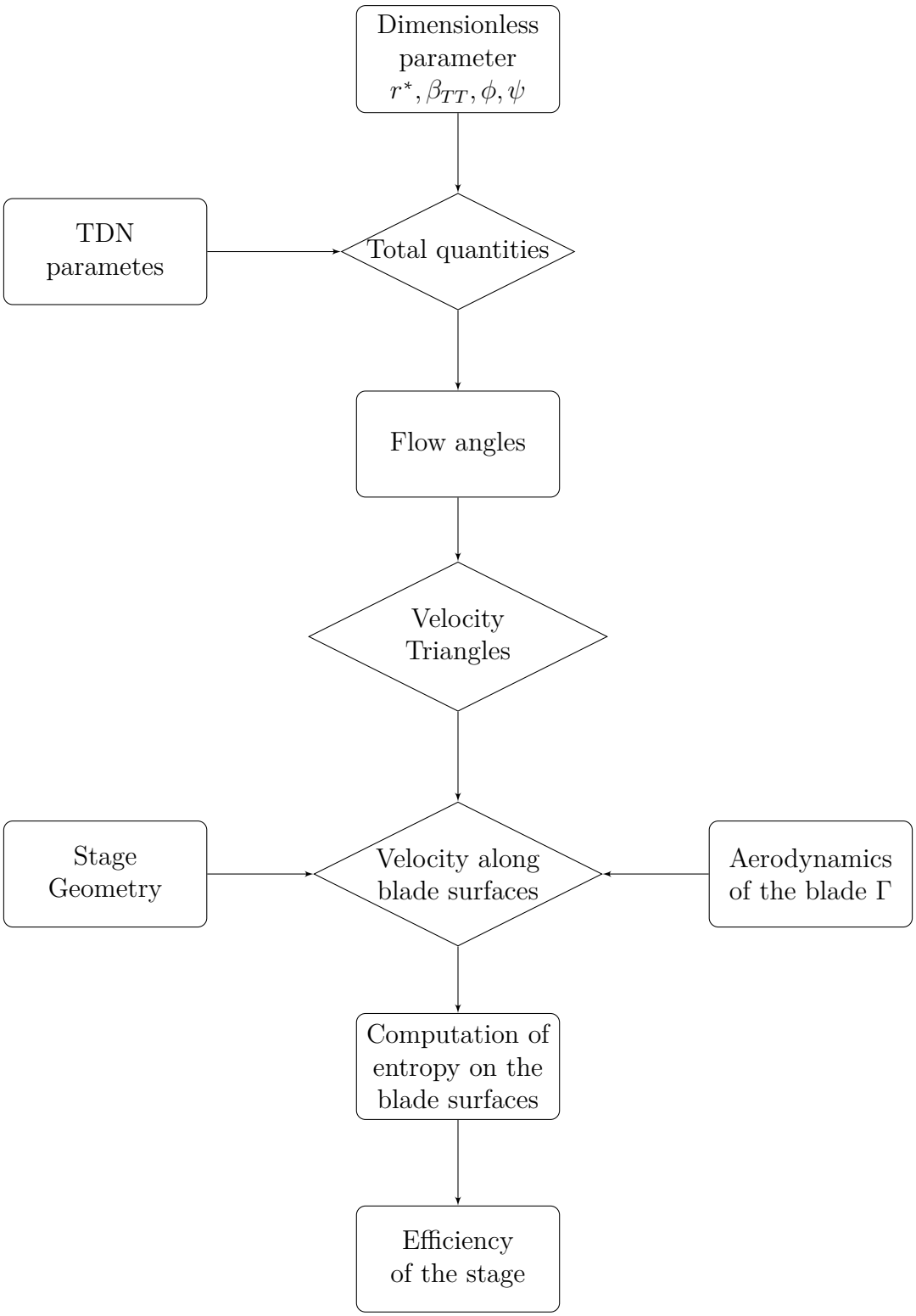

Figure 3.10: Computational process for boundary layer profile losses

Entropy along the blade

Following the formula presented by Denton:

$$\dot{S}_{gen} = \dot{S}_{PS} + \dot{S}_{SS} = \int_0^S \left(\frac{C_d(\varrho V^3)}{T} dx\right)_{PS} + \int_0^S \left(\frac{C_d(\varrho V^3)}{T} dx\right)_{SS} \tag{3.16}$$

Efficiency in terms of profile losses

Finally the efficiency is computed with the formula already presented in chapter 2:

$$\eta_t \approx \frac{h_{in} - h_{out}}{h_{in} - h_{out} + T_{out}\Delta s_{gen}} \tag{3.17}$$

Results for incompressible air:

For incompressible flow (Mach<0.3) all the densities are canceled out and the final form is strongly simplified:

$$\zeta_s = \frac{T\dot{S}}{\dot{m}0.5V_{ref}^2} = 2\sum \frac{S_0}{s\ cos\alpha_{ref}} \int_0^1 C_d \left(\frac{V_0}{V_{ref}}\right)^3 d\left(\frac{x}{S_0}\right) , \tag{3.18}$$

$$\Delta s = \Delta h_{is} 2\frac{V_{is}}{V_x} \sum \frac{S_0}{s} \int_0^1 \frac{C_d}{T} \left(\frac{V_0}{V_{ref}}\right)^3 d\left(\frac{x}{S_0}\right), \tag{3.19}$$

The results derived from Denton's model applied to our turbine stage at low speed flow i.e incompressible fig.3.11 match well with the shape of Smith chart. Also the magnitude is consistent. The best zone is inside the iso-line of 2 % and the best point presents a loss of one percent more or less. Since this is referred to the profile losses source and it represents roughly one third of the entire losses it is possible to conclude that the general losses (primary, endwall and tip leakage) are between the 3 and 4 percent which is reasonable for an optimized stage i.e built on Zweifel's criterion.

The next step is to add the compressibility effect starting from a perfect gas model: this choice is supported by the analytical availability of formulations for this thermodynamic model and also because in many fields perfect gas is enough for a preliminary stage

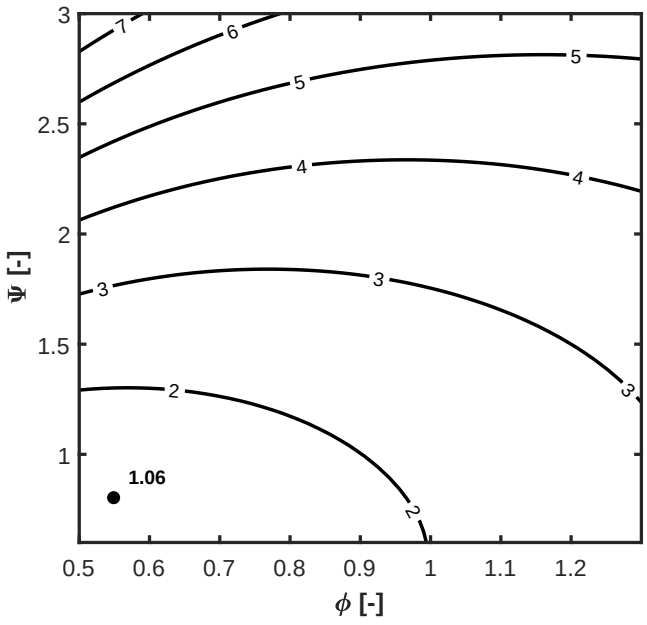

Figure 3.11: Physical-based model: Profile loss chart, incompressible formulation. 1.06 is the best working point since the losses are minimized.

studied [53, 32, 28]. The formulation, results of this thesis, is obtained starting from the isentropic relation for perfect gas https://www.grc.nasa.gov/www/k-12/airplane/isentrop.html

$$\dot{S} = \underbrace{\frac{P_T C_d S_0 MW}{R_u}}_{\text{common factor}} \Bigg[\underbrace{\frac{(\overline{V}+\Delta V)^3}{\left(T_T - \frac{(\overline{V}+\Delta V)^2}{2c_p}\right)^2 \left(1 + \frac{\gamma-1}{2} \frac{\overline{V}+\Delta V}{\sqrt{\gamma R_g (T_T - \frac{(\overline{V}+\Delta V)^2}{2c_p})}}\right)^{\frac{\gamma}{\gamma-1}}}}_{\text{Suction Side}} + \underbrace{\frac{(\overline{V}-\Delta V)^3}{\left(T_T - \frac{(\overline{V}-\Delta V)^2}{2c_p}\right)^2 \left(1 + \frac{\gamma-1}{2} \frac{\overline{V}-\Delta V}{\sqrt{\gamma R_g (T_T - \frac{(\overline{V}-\Delta V)^2}{2c_p})}}\right)^{\frac{\gamma}{\gamma-1}}}}_{\text{Pressure side}} \Bigg] \quad (3.20)$$

Moreover introducing the following classical relations from Mayer and the concept of

reduced thermodynamic quantities:

$$c_p = \frac{R_g}{\theta} \qquad T_T = T_c T_r \qquad P_T = P_c P_r \tag{3.21}$$

the problem is entirely defined in terms of dimensionless parameters where T_c and P_c are critical temperature and pressure and T_r and P_r are the reduced ones. It is very convenient to express these variables in these terms because they can be taken under certain zone i.e for ideal gas region the common assumption is $P_r < 0.1$ (look 1.5 (a)). Therefore for perfect gas the analysis is made with a reduced total pressure inlet less than this value. We have shown quantitatively what are the parameters which cause the entropy generation in profile losses:

- Total conditions, in particular total pressure has a linear impact on entropy rate (for rotor we will use the Rothalpy)
- Blade geometry: linear variation with S_0 (suction surface length = wetted surface)
- Nature of fluid: the terms related to the fluids are the molecular weight (MW), and index of complexity γ both present in the formulation 3.20
- Boundary layer state, contained in dissipation coefficient C_d

We can conclude that the classical Smith [28] chart is just a plane in a more complex 3-D space where the vertical axes is fluid properties.

$$\dot{S} = \text{entropy generation} = \dot{S}\Big(\underbrace{T_r, P_r}_{\text{TDN state}} , \quad \underbrace{S_0}_{\text{Blade geometry}} , \underbrace{T_c, P_c, MW, \gamma}_{\text{Fluid nature}}, \quad \underbrace{C_d}_{\text{BL state}} \Big) , \tag{3.22}$$

The results for this new formulation maintaining the same β_{TT} and inlet conditions are in fig.3.12

The effect of compressibility influences the results a lot. The comparison between the graph 3.11 and the incompressible one 3.11 shows clearly that the compressibility increase of one percentage the losses in the entire chart's space. Now it is possible defining two more studies:

1. effect of the stage pressure ratio
2. effect of the working fluid

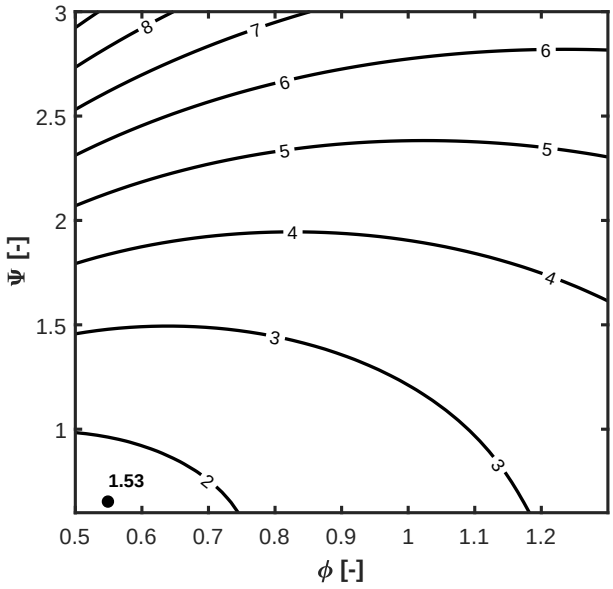

Figure 3.12: Physical-based model: Profile loss chart, compressible formulation

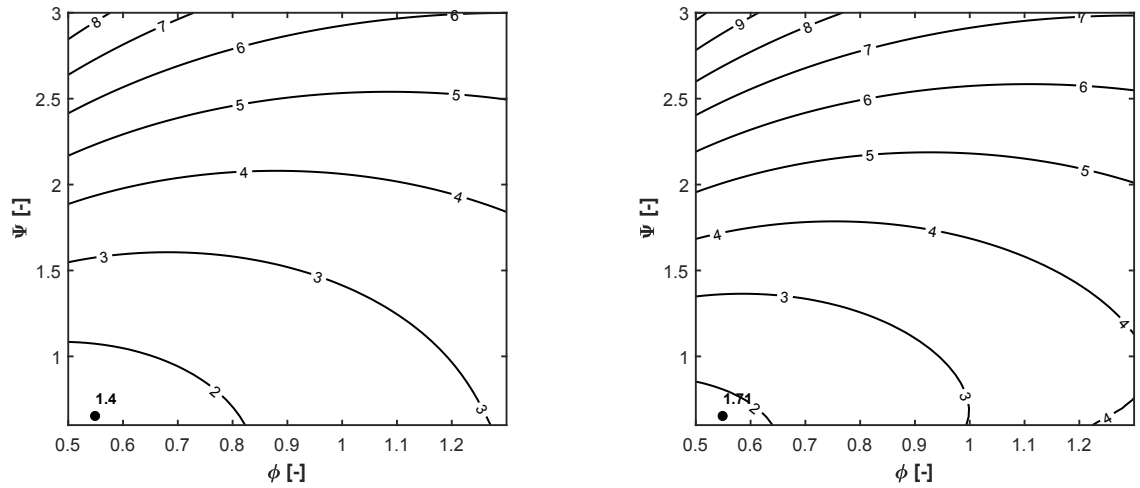

Figure 3.13: Effect of pressure ratio on profile losses: (a) β_{TT} = 1.5; (b) β_{TT} = 4.5. The optimum points also changes

Pressure ratio effects

In order to show the effect of β_{TT} the following chart fig. 3.13 are plotted. Naturally the limitations of β_{TT} is very important and if it is increased above a certain threshold many regions are not more computable since the velocities become so high that the efficiency falls down (~ 50 %) or worse: the thermodynamic energy amount is not enough to be converted in kinetic one in particular at low ψ. As we can guess the pressure ratio must be limited in order to moderate the losses in particular in the optimal zone at low load

coefficient. It is interesting the highly sensitive behavior of low zone in contrast to high load region. The pressure ratio has a general impact on the thermodynamic load of the entire stage. Naturally it is possible to find an optimum for the common turbine stage (in general quite higher than the compressor due to the smaller risk of flow separation).

Fluid influence

The next step is to verify the impact of the fluid on profile losses as stated from equation analysis eq. 3.22 reminding that we work in perfect gas region. To show the deviation due to the fluid, three main candidates are selected: Helium simple and light molecule, CO_2 medium complexity, used in new power technology and finally a siloxane very heavy and complex, very interesting for ORC technology.

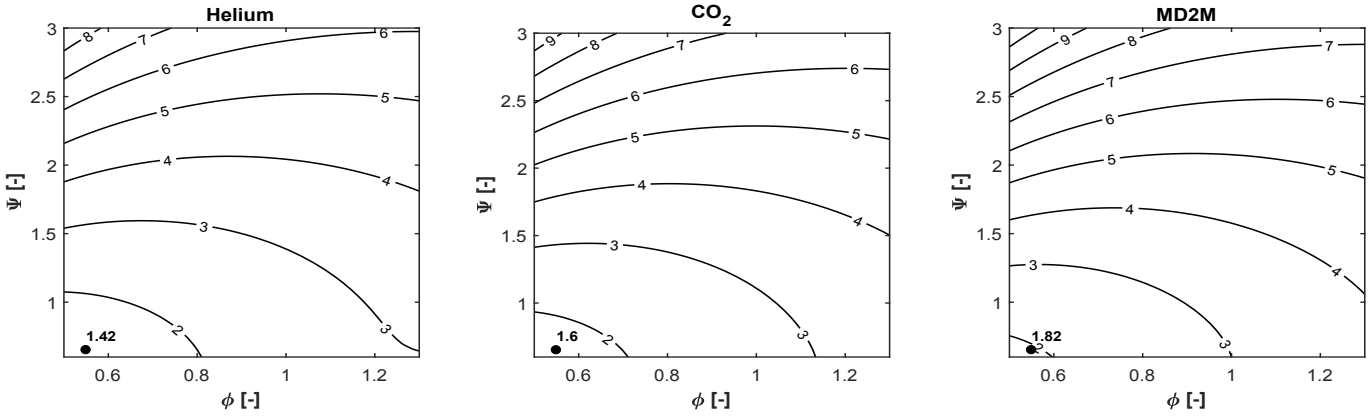

Figure 3.14: Impact of the molecular complexity on losses, for three different candidates: (a) Helium simple-light ; (b) CO_2 medium ; (c) MD2M complex heavy. With the respective optimum points.

It is clear how complexity impacts on the losses. The stage has the same conditions used for the air. The hypothesis of perfect gas is respected since the inlet reduced pressure (the highest one) is 0.05 for all fluids and all geometry parameters are based on the same assumption: Zweifel for axial solidity, camber line parabolic shape and same length of side surfaces $S_0 = 1.15b$ [52]. On this last point some clarification must be given: looking at the typical shape for ORC applications (fig. 3.2 (b)), the length of surfaces are higher than a classical reaction blade therefore for heavy complex fluids the losses could be higher than the one presented.
Helium (simple) not only shows general lower losses but also a more extended area under iso-line of 3 % this is because it is very difficult achieve high Mach number and high velocity for this fluid's category; therefore having contained speed along surface also the profile losses are slightly smaller.

Real gas effects

The last analysis is to check the capability of the physical-based model to estimate the real gas effects in a turbine stage. Now it is not possible using a set of explicit thermodynamic relations for density, moreover enthalpy and internal energy are no more functions only of temperature. The edge quantities which enter in the integral of entropy generation are:

$$\varrho_e = \varrho_e(h,s)_e \qquad\qquad T_e = T_e(h,s)_e \quad , \tag{3.23}$$

For a pure substance knowing two thermodynamic variables the state is completely defined. Since the free stream or edge of the boundary layer is generally considered isentropic, the inlet of the stage has the same specific entropy on both sides of the stator. Then the entropy generation of this cascade is added to the inlet value. Through relations:

$$s_{rotor} = s_{inlet} + \Delta s_{stator} : \text{ value used to compute rotor thermodynamic variables} \tag{3.24}$$

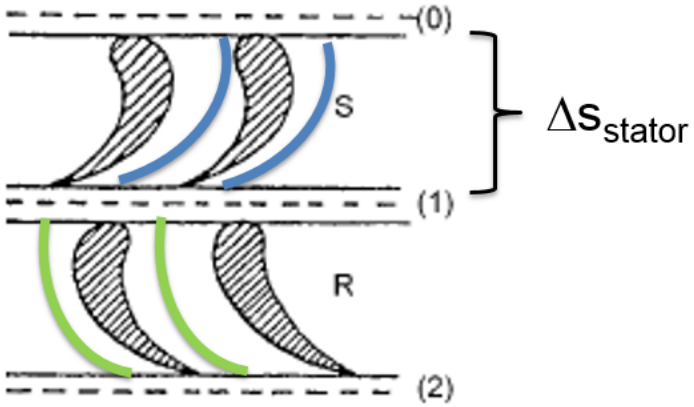

Figure 3.15: Cascade computation for real gas case. (—) represents the boundary layer edge for stator blade, and the (—) is the edge for the rotor. Δs_{stator} is the specific entropy produced by the stator to compute the properties in the rotor through a fluid library.

Once the method is set we must choose the thermodynamic region. Three different point i.e compressibility factors are chosen. In particular, fixing the reduced temperature and changing the reduced pressure it is possible to shift to a lower Z.

The results obtained with RefProp NIST library [6] integration in the code are in figure 3.16:

Since the limitation factor is the computational time due to the slowness of fluid library, now the total amount of points is reduced to 30x30.
There is an important manifestation in the charts 3.16: the non-ideality effects tend to increase the losses in general. This is intuitive since whatever non ideal phenomena tends

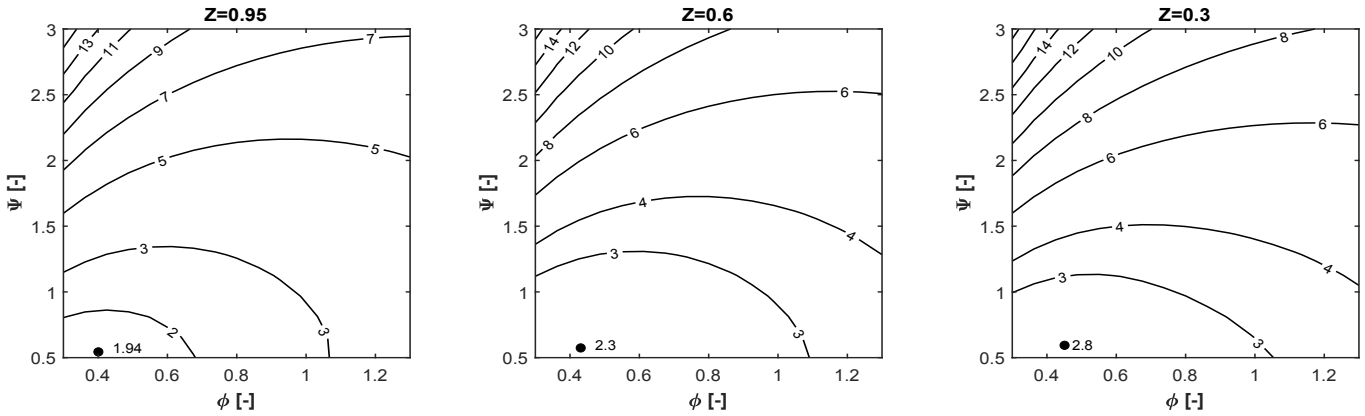

Figure 3.16: Effect of non-ideality on the profile losses chart on the same reduced isothermal $T_r = 1.1$: (a) Ideal gas region $P_r = 0.15$ and Z≈1 ; (b) Real gas effects $P_r = 0.9$ and Z=0.6 ; (c) Strong real gas effects $P_r = 1.5$ and Z=0.3

to decrease the efficiency of the process but more important looking at the equation of entropy computation along the blade

$$\dot{S} = \int_l \left(\frac{C_d(u_e^3 \varrho)}{T_e} \right)_{side} dx \tag{3.25}$$

The density tends to be higher for real gas since it is the meaning itself of compressibility factor:

$$Z = \frac{v}{v^0} = \frac{\varrho^0}{\varrho} \qquad \text{for low Z: higher } \varrho \tag{3.26}$$

The lower the Z, the higher is the ϱ so larger numerator of the integrand that means higher generation of entropy due to boundary layer. Therefore a stage which expands a real gas working fluid is intrinsically less efficient, at least in terms of profile losses, respect to ideal gas.
We can appreciate the capability of the physical based approach to understand the nature of certain phenomena because all the relations derive from fundamental laws.

Conclusion

In all this analysis the parameter which hold the boundary layer concepts, *dissipation coefficient* C_d is maintaining fixed to 0.002 as recommended by Denton ([2, 26] eq.16)

and other many authors [41, 57, 58] however this value is purely an approximation for incompressible boundary layer (air) for an airfoil with a Reynolds momentum thickness in a certain range (≈ 1000). This is summarized in the figure 3.17.

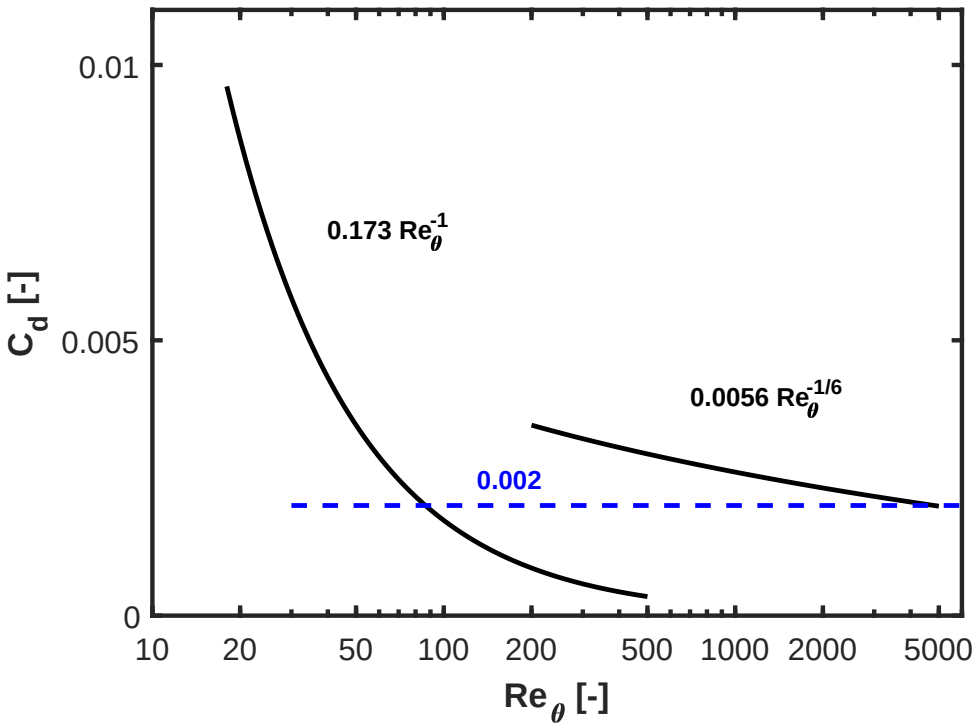

Figure 3.17: Dissipation coefficient as function of Reynolds number based on momentum thickness; laminar and turbulent trend. The blue dashed line (▪▪▪) is the value used in turbomachinery applications

The main characteristic of the trend in fig. 3.17 is the pseudo flat shape in the turbulent region, the most likely flow regime in turbine application. This peculiarity is very useful for a model since it is possible to estimate a common constant value suitable for computation (more precisely C_d can be extracted from all operator like integration).
Nevertheless this analysis is very rough and poor from physical point of view. Moreover the Mach number effect or fluid impact could be phenomena that change a lot the boundary layer state and results ergo the C_d itself. The analysis and the knowledge must be expanded, for this reason the following chapters represent the core of this thesis work respectively a complete study for laminar boundary layer (Chapter 4) and then turbulent (Chapter 5). The attention will be focused on the C_d however all the other typical coefficients are presented in order to understand the viscous flow behavior.

Chapter 4

Dissipation coefficient in Laminar boundary layer

The following results will be presented in increasing order of complexity. The first step is the verification of literature results, more precisely the trend of dissipation coefficient for the existing case: incompressible air with and without pressure gradient on an adiabatic flat plate. After this the compressibility effects (i.e increasing Mach number) computation will be performed. In the end the impact of gas reality will be investigated.

4.1 Dissipation coefficient: concepts and meanings

As already presented in the chart of physical based models the computation of C_d is possible only with a boundary layer code (2.7) because it is necessary to know many details of viscous fluid flow close to the wall. The first step is to introduce the definition of the dissipation coefficient:

$$C_d = \frac{T_{ref}\dot{S}_a}{(\varrho u^3)_e} \ , \tag{4.1}$$

Where the entropy computations are based on these formulations:

$$\dot{S}_a = \int_0^e \dot{S}_v dy \qquad\qquad \dot{S}_v = \frac{\tau}{T}\frac{\partial u_x}{\partial y} \tag{4.2}$$

Following the authors' statement, the reference temperature T_{ref} could be selected equal to the edge quantity for low speed, or recovery temperature (wall one) for high speed ([1] pag. 6 and also [36] eq. 5.4.12). However for the sake of consistency the best reference is the first option (edge temperature) since in the profile loss model is always used this one. C_d is not only the crucial parameter in the turbomachine physical-based losses but it is

something more: it represents the state of boundary layer, describes some flow phenomena (the order of magnitude indicates what is the flow regime) and it defines quantitatively the dissipation inside the layer itself. It can be view as destruction of kinetic energy or a generation of entropy. Some authors [59, 1] underline the superior aspects of this coefficient with respect to the classical friction coefficient c_f and the drag coefficient c_D. Drela is one of the firsts to use C_d for aerodynamic purposes [60] underlining three superior aspects of C_d with respect to c_f coefficient [59]:

- C_d captures all drag-producing loss mechanisms. In contrast, c_f does not allow to account for the pressure-drag contribution.
- C_d is a scalar quantity, so the orientation of the dy line element in the integral is immaterial. In contrast, c_f represents a force vector integral, and as it is written is strictly correct only for flat-plate surfaces aligned with the free stream flow.
- C_d is strictly positive, so there are no force cancellation problems which often occur with near field force integration. The best example is the phenomenon of separation characterized by changing in flow direction.

The equation 4.1 is the formulation in terms of common parameter however it must be expressed through the fundamental quantities 2.2 for boundary layer purposes.

- velocity ratio (f')
- f" shear parameter ($\frac{\partial f'}{\partial \eta}$)
- C Chapman -Rubesin parameter defined as $\frac{\mu \varrho}{\mu_e \varrho_e}$
- u_e velocity at the edge
- transformed coordinate η including N_x ($\sqrt{\frac{\mu_e \varrho_e x}{u_e}}$)

Here following the derivation typical of boundary layer environment:

1. derivation of entropy generation per unit volume

$$\dot{S}_v = \frac{\mu}{T}\left(\frac{\partial u}{\partial y}\right)^2 \qquad (\frac{\partial u}{\partial y})^2 = u_e^2(\frac{\partial f'}{\partial \eta})^2(\frac{\partial \eta}{\partial y})_x^2 \qquad (\frac{\partial \eta}{\partial y})_x = \sqrt{\frac{u_e}{\varrho_e \mu_e x}\varrho} \tag{4.3}$$

2. Integration in transformed domain ([39] eq.6.4):

$$\dot{S}_a = \int_0^y (\dot{S}_v) dy \qquad \frac{\partial \eta}{\sqrt{\frac{u_e}{\varrho_e \mu_e x}\varrho}} = \partial y, \tag{4.4}$$

3. Re-arranging the final expression for C_d reads:

$$C_d = \sqrt{\frac{\varrho_e \mu_e}{u_e x}} \int_o^\delta [\frac{T_e}{T} C(f")^2] d\eta, \tag{4.5}$$

Now, looking at the definition of Reynolds number based on momentum thickness:

$$Re_\theta = \frac{\varrho_e u_e \theta}{\mu_e} \tag{4.6}$$

Where θ In terms of boundary layer parameter [39]:

$$\theta = \sqrt{\frac{\mu_e x}{\varrho_e u_e}} \int_0^\delta f'(1 - f') d\eta \tag{4.7}$$

Therefore:

$$Re_\theta = \sqrt{\frac{\varrho_e x u_e}{\mu_e}} \int_0^\delta f'(1 - f') d\eta \tag{4.8}$$

We can recognize that the dissipation coefficient includes the inverse of several terms of the Re_θ and the temperature ratio is. This is a first proof of the inverse power law:

$$C_d \approx f(\frac{1}{Re_\theta}) \tag{4.9}$$

Moreover the temperature ration introduce the Mach effects and the nature of the fluid because the particle temperature T (inside the layer) is related to the BL edge through the next relation:

$$T = T_e f(Mach_e, \text{type of fluid}) \tag{4.10}$$

Where f($Mach_e$) is an implicit formulation which takes into account the dissipation of kinetic energy into thermal one inside the layer. Therefore the maximum temperature is the wall one. Since the Mach number depends by the velocity and the nature of fluids (i.e MW and complexity γ), we can extend the final formulation of dissipation coefficient to:

$$C_d = C_d\left(\frac{1}{Re_\theta}, Ma_e, \text{fluid nature}\right) \tag{4.11}$$

The two additional concept respect to skin friction are the integration on vertical span and the presence of temperature ratio which is definitely dependent by the fluid. Now we present the computational concept to calculate entropy inside the boundary layer (4.1).

The figure 4.1 shows the core of computation for dissipation coefficient: the $\dot{S}_v$ is computed for each node of the mesh then an integration is performed for each horizontal station ξ. The last step is the simple computation of the ratio between entropy multiplied for edge temperature over the kinetic specific power at the edge.

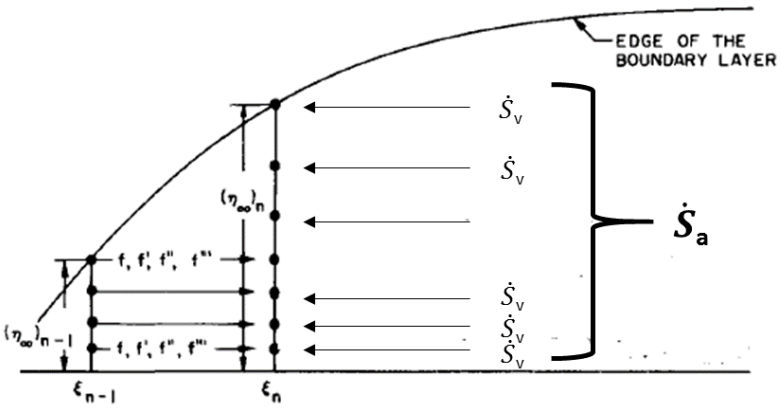

Figure 4.1: Entropy computation concept: $\dot{S}_v$ is entropy generation per unit volume and it is a particle properties therefore computed in the node; $\dot{S}_a$ is the result of the integration along vertical span.

4.2 Incompressible, zero pressure gradient

The results are in figure 4.2: the verification of our code with respect to the power law

$$C_d = 0.173 Re_\theta^{-1} \tag{4.12}$$

The stations used for the computation in the code are 16 in this case however the perfect matching happens for a larger number of points. The flow is at low speed therefore no appreciable temperature increasing happens inside the layer. C_d can be described through the inverse of the Reynolds number based on momentum thickness. The physical concept is: the increase in momentum inertia, θu_e, with respect to the viscous forces ν_e means a reduction of dissipation due to the latter. Therefore working at high Re_θ, remaining in laminar regime, will produce lower dissipation and in the end lower boundary layer losses. An important question is how the temperature and pressure of the edge impact on the dissipation coefficient: 4.3.

They are clear three outcomes looking at the fig. 4.3: the increase of temperature in the free stream flow tends to shift the curve at low Re_θ, in contrast at high pressure the Reynolds based on momentum thickness is higher. In all case the law is perfectly respected. Therefore there are no deviation from the analytical formulation changing the free stream thermodynamics conditions. The figure 4.3(b) is obtained without transition. Higher pressure tends to makes happen the transition, indeed, looking at the definition of Reynolds:

$$Re_\theta = \frac{\theta u_e \varrho_e}{\mu_e} \ , \tag{4.13}$$

the edge properties are strictly related to the free stream, therefore increasing pressure

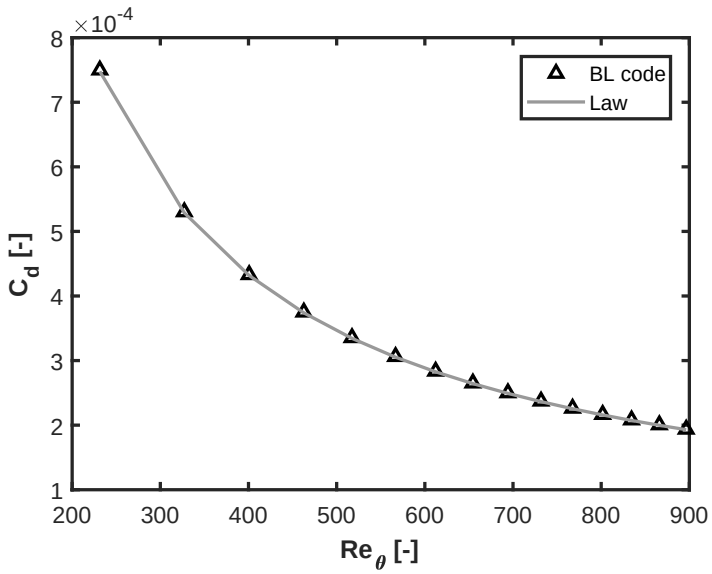

Figure 4.2: Dissipation coefficient in incompressible flow: verification with our code. Input: $Ma_e = 0.1$, $P_T = 1$ bar, T_T=298 K, constant properties. Adiabatic wall. With perfect gas model (air)

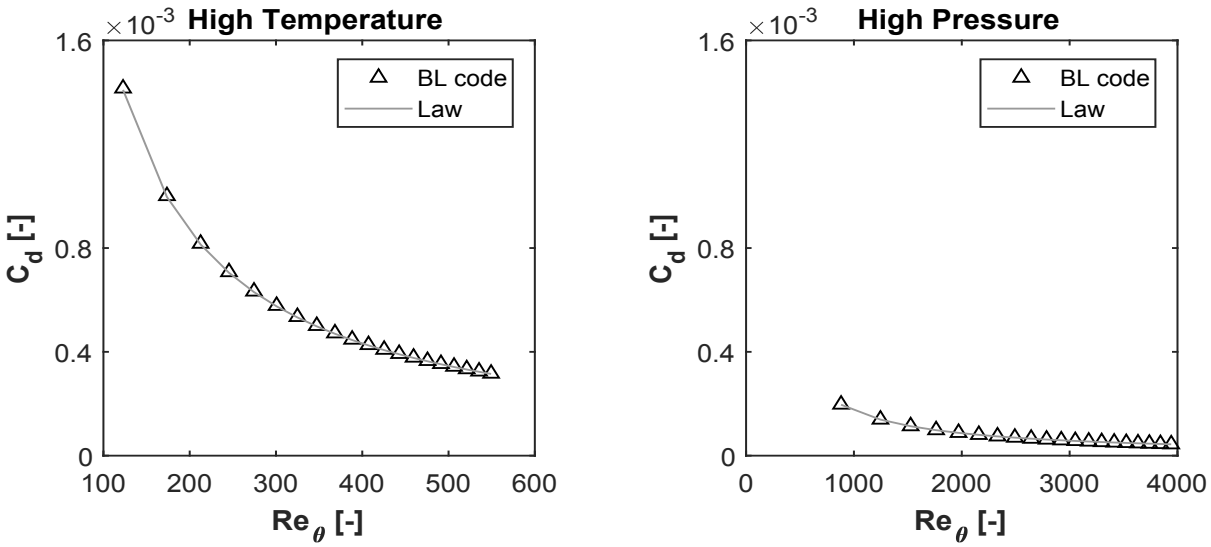

Figure 4.3: Influence of the free stream conditions: (a)Temperature (800 Kelvin) ; (b) High total pressure (30 bar). The law is the one already introduced $C_d = 0.173 Re_\theta^{-1}$

means higher density so larger numerator (higher Reynolds: more likely transition to turbulent regime); the opposite tendency happens for temperature increasing.
This little study suggests an interesting aspect in terms of application: since the best zone

to work, in order to decreasing dissipation, is the last part of laminar curve, it should be convenient retard the transition to turbulent regime. To achieve this goal a good "trick" is increasing the temperature since:

$$Re = \frac{xU_e\varrho_e}{\mu_e} \tag{4.14}$$

Increasing T means decreasing density and increasing the viscosity (it is simple to see also by Sutherland's law [61]).
For what concern the ratio of temperature inside boundary layer: it remains on the unity (no increase inside the layer) in fact:

$$T = T_e(1 + \frac{\gamma - 1}{2} r Ma^2) \qquad \text{with} \qquad r \approx \sqrt{Pr} \tag{4.15}$$

Finally in the figure 4.4 there are the distribution of: the shape factor (constant at 2.59 on each flat plate station) and the two most important flow parameters, the f' velocity ratio and f" the shear parameter. Both (a) and (b) 4.4 serve to validate our code since 2.59 is the Blasius result and the other is perfectly overlapped.

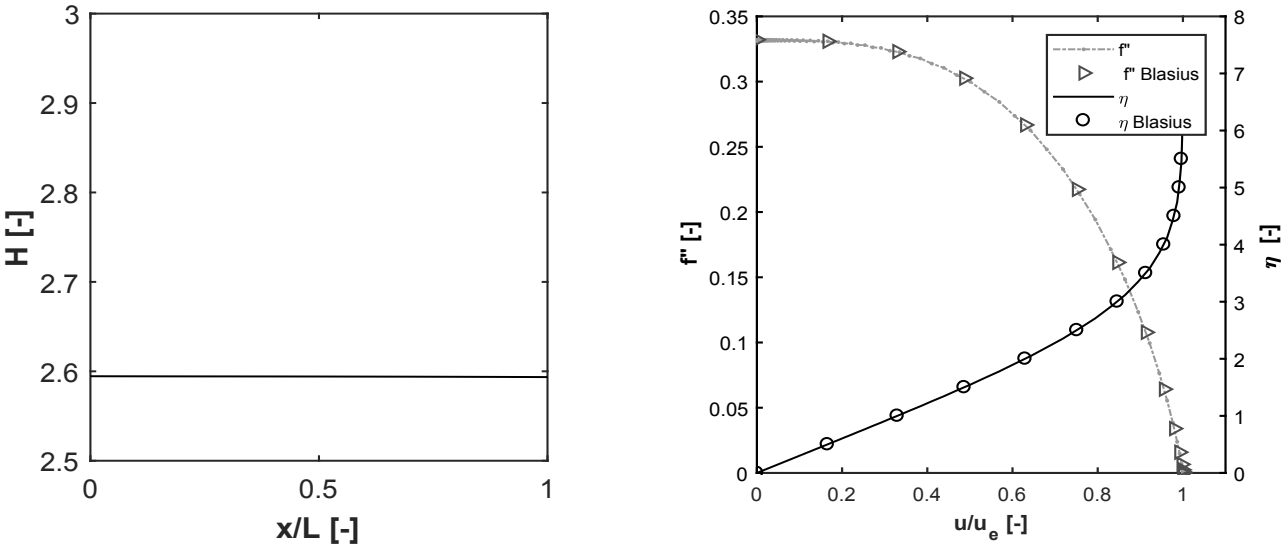

Figure 4.4: : (a) Boundary layer shape factor H perfectly matches the Blasius value 2.59 ; (b) Transformed coordinate η right axis and the shear parameter f" on left axis, also in this case perfect verification through Blasius profile.

4.2.1 Pressure gradient effects on laminar Cd

The concept of acceleration is a characteristic of the flow independently by the fluid nature. The classical boundary theory has investigated for a long time the pressure gradient effects [62, 63]. In this part only the results of acceleration will be presented however the concepts are general.
Looking at the set of the integral equation of boundary layer 2.34, eq. 2.35 it is possible to obtain a general formulation which takes into account the effect of pressure gradient along the edge. The original formulation of this approach was proposed by Von Karmàn [42] introducing the acceleration factor named Λ (Von Karmàn-Pohlausen parameter). The definition is:

$$\Lambda = \frac{\delta^2}{\nu}\frac{du_e}{dx} \tag{4.16}$$

Which depends by the pressure gradient (directly related to $\frac{du_e}{dx}$), kinematic viscosity ν and the thickness of boundary layer (δ). Denton, in his paper ([2] eq.(18)), uses this concept to fit a polynomial relation for dissipation coefficient in order to include pressure gradient (it is possible only in laminar regime):

$$C_d = (0.1746 + 0.0029\Lambda + 0.000076\Lambda^2)Re_\theta^{-1} \ , \tag{4.17}$$

It is clear how much the Pohlausen-Von Karmàn parameter affects the dissipation inside the laminar boundary layer since:

$$-12 < \Lambda < 12 \tag{4.18}$$

The deceleration is in the negative region, otherwise an acceleration characterizes the positive one. Therefore analyzing the equation 4.17 it is evident the more dissipative nature of an accelerated flow (i.e favorable pressure gradient) for a laminar boundary layer.
This concept is confirmed also by a physical explanation: an acceleration on the edge, fixing the thickness of boundary layer, means a strong increase in the velocity gradient $\frac{\partial u}{\partial y}$ (and so the shear stress itself) whose square terms is one of the factors (and causes) of entropy generation in viscous flow.

Two main concepts appear from the comparison in figure 4.5: the code is able to compute the pressure gradient phenomena, the accelerated flows are more dissipative, as already stated, with respect to the 0-pressure gradient.
This analysis gives us two outcomes:

- Denton fit is a little bit smaller than our curve
- his formulation does not collapse on the zero pressure gradient form since it contains 0.1746 and not 0.173 for a Λ=0

A different polynomial form is extracted from our code:

$$C_d = (0.173 + 0.0029\Lambda + 0.00056\Lambda^2)Re_\theta^{-1} \ , \tag{4.19}$$

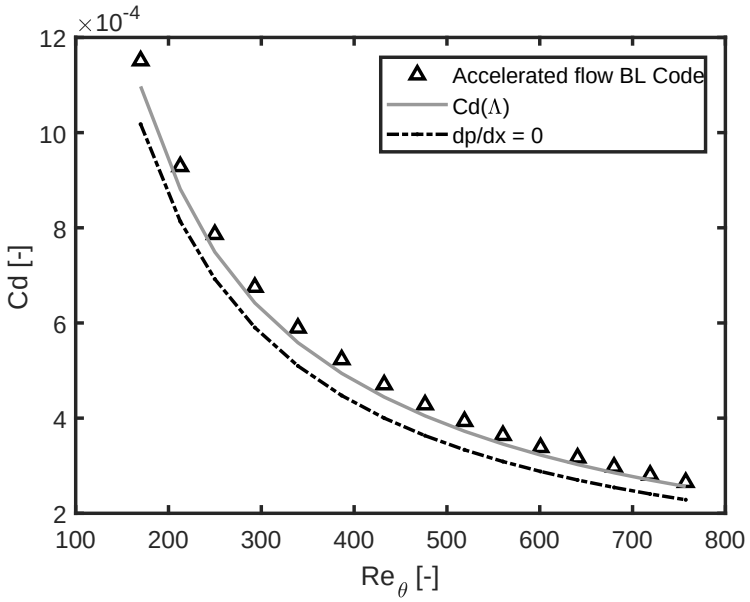

Figure 4.5: Effect of acceleration on dissipation coefficient at low speed (0.1 < Mach < 0.5). Adiabatic wall

To conclude this section it remains only to clarify and to show in quantitative way the causes about the the higher dissipation. Looking at the figure 4.6 the shear parameter f" (i.e shear stress) is larger due to the higher velocity gradient. This is the principal cause of increasing of entropy generation (see equation 4.3); it is quite intuitive from geometrical point of view that the entropy generation per unit area $\dot{S}_a$ is the underlying area under the shear parameter (f" curves) profile. Looking at fig.4.6 and comparing the Blasius case with the accelerated flow f": the area of the latter is much bigger so the entropy generated (i.e C_d). Also the velocity profile is consistent with this concept: flatter profile for accelerated so $\frac{\partial u}{\partial y}$ is higher.

Other information regarding the defect of inertia are given by the shape parameter H: we can appreciate that it is smaller than 0-pressure gradient values (2.59) this means that the defect of momentum θ is higher with respect to the mass defect:

$$H = \frac{\delta^*}{\theta} \tag{4.20}$$

Therefore accelerated flows, in laminar regime, are worse in terms of both energy and momentum losses. The implications on aerodynamic blade concept is very important: a good aerodynamic design should avoid great increase of velocity in the first part the suction surface (here the flow is laminar) because C_d could increase of more than 10 % therefore the final profile losses will increase too.

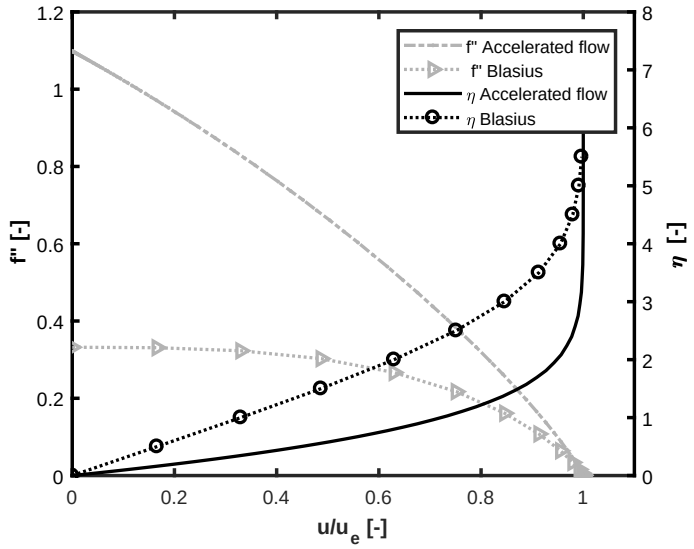

Figure 4.6: Effect of acceleration on velocity profile and shear parameter. Great discrepancy with respect to Blasius theory. Adiabatic wall, air in perfect gas model. Velocity profile at the edge: from $Ma_e = 0.1$ to $Ma_e = 0.5$.

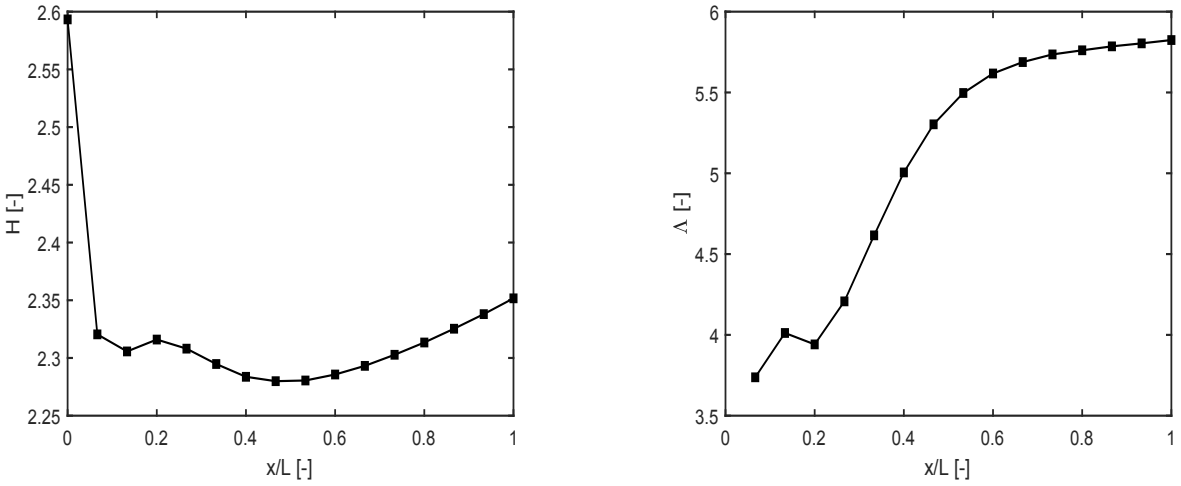

Figure 4.7: Effect of the acceleration on typical BL parameters: (a) Shape factor influenced by acceleration ; (b) Von Karman-Pohlausen parameter along flat plate

4.3 Compressible, high speed flows

The effects of Mach number on boundary layers is one of the most investigated phenomena in fluid mechanics. For the laminar regime, the pioneering works were made by Luigi Crocco [64] and then the fundamental work by Van Driest [65] where a laminar boundary layer study is performed until Mach=20. This approach serves to extract physical conclusion from the study, therefore this section will follow it. In our case the investigation

will take into account flows until Mach number equal to 2 (turbomachinery application).

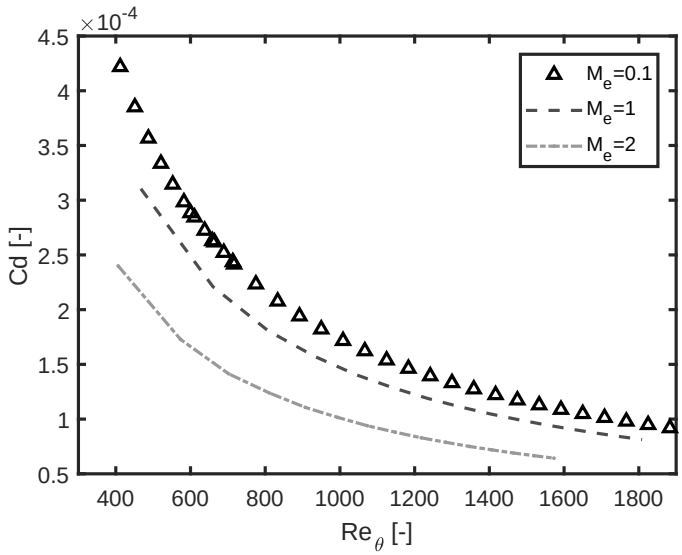

Figure 4.8: Effect of compressibility through high speed flow on C_d. Transition deactivated, laminar regime. Adiabatic wall, air perfect gas

It is evident, from fig. 4.8 the high decrease in terms of dissipation coefficient in the entire range of Reynolds based on momentum thickness. A power law is still valid but there is a visible shift down with the Mach (~ 30 % less at Ma=2). The behavior in the first sight could appear counter intuitive however this response to high speed effects in not unique since it is well known in aerodynamic field that also the friction coefficient c_f has an important decrease with Mach number [36, 66]. More precisely see fig.19.1 Anderson [55].
These coefficients are dimensionless quantities therefore their behavior at high Mach numbers does not deal with an absolute decrease of inertia defect (c_f) or entropy production (C_d) but it is just a comparison between the losses with respect to the free stream/edge values.
Two very important effects in compressible laminar boundary layer are the heating of the viscous flow inside the layer and the change in the boundary layer shape factor fig. 4.9

These two last phenomena represented in the 4.9 are full of physical meanings. For adiabatic flat plate in all flow regimes (i.e laminar and turbulent) the universal phenomena is the conversion of kinetic energy in thermal energy through viscous friction. This increase in temperature can achieve very high values (~ 70 % at Mach=2) and it is the cause of the density decrease inside the viscous layer (for a ideal gas is inversely proportional):

$$\frac{T}{T_e} \approx \frac{1}{\frac{\varrho}{\varrho_e}} \ , \tag{4.21}$$

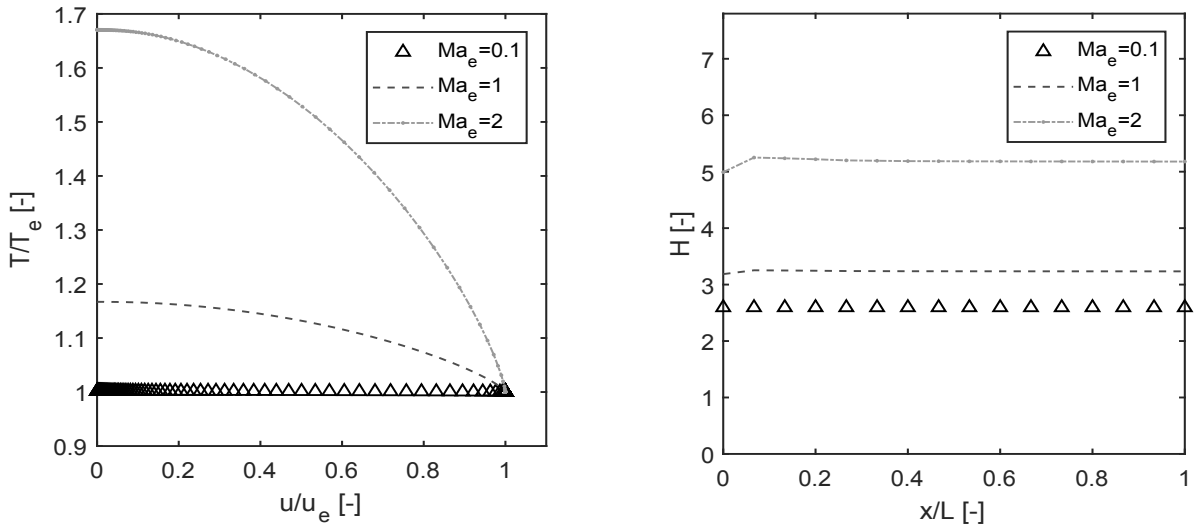

Figure 4.9: Mach number effects for laminar boundary layer (a) Temperature profile inside boundary layer; (b) Shape factor on the entire plate.

The decrease in density close to the wall is a peculiar effect due to the viscous nature of the flow, for this reason the shape factor (fig.4.9(b)) increases a lot in the supersonic regime:

$$H = \frac{\delta^*}{\theta} = \frac{\text{displacement thickness}}{\text{momentum thickness}} \tag{4.22}$$

As we can see the great increase in H is due to the strong change in displacement thickness with respect to the momentum thickness. In other words, in supersonic flows the defect of mass flow rate, due to viscous phenomena, compared with inviscid case (δ^*) is higher with respect to the defect in momentum (θ). Many works are made to show this phenomena both with experiment and DNS (Direct Numerical Simulation) the latter case is studied in the paper [67]. As final thesis we can state that high speed flow phenomena impact on temperature distribution inside the boundary layer region, in density and all transport properties. Also the velocity profile is influenced 4.10: it starts to deviate from the Blasius trend.

There are several opposite effects on the dissipation coefficient:

- the first one is positive in the sense that the velocity profile is less steep with high Mach numbers so the gradient $\frac{\partial u}{\partial y}$ is lower than incompressible: it is present as square quantity in the generation of entropy generation per unit volume 4.3
- the second one is negative: an increase in thickness of boundary layer and in dynamic viscosity too since $\mu \approx T$

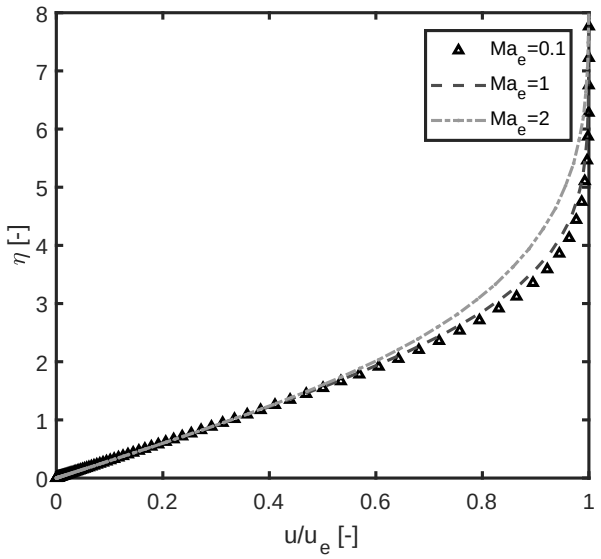

Figure 4.10: Effect of compressibility through high speed flow on laminar velocity profile, deviation from Blasius trend. Air ideal gas. Adiabatic wall

- Finally the temperature ratio is the determinant factor. It is included in the integral computation 4.5 and it determines a huge decrease of the coefficient

Putting together all these aspects the results is a general decrease of C_d. The general aspects related to air have been presented. This section finishes with some important questions: what is the impact of fluid on the laminar boundary layer? In particular: can the high speed flow regime for different fluids, with respect to air, present the same behavior? What is the trend of ORC fluids?
In the next chapter an answer will be given to all this question, again for the laminar regime.

4.4 Effect of working fluid on dissipation coefficient

The purpose of this part is to set a general study with the goal to determine what are the major causes of difference in dissipation coefficient. This approach is necessary since the C_d is never challenged and it is composed by many factors, therefore only changing variables one by one fixing all the other can allow to estimate quantitatively which is the most important factor/s. Because the fundamental dimensionless group is the Prandtl number in terms of transport fluid properties the analysis is performed in three main steps respectively the three variables of the group:

$$Pr = \frac{\mu c_p}{\lambda}$$

- **Step 0**: change of fluids, different complexity γ and molecular weight (MW). Viscosity (μ) and thermal conductivity (λ) fixed equal to the reference of air i.e 1.718 10^{-5} Pa s and 0.0257 W/mK.
- **Step 1**: change of fluid type and dynamic viscosity μ. Thermal conductivity is fixed 0.0257 W/mK (air reference).
- **Step 2**: change in all the three quantities; ideal gas with variable properties.

It is important at this point the choice of the fluids. The candidates are selected in order to show the differences: air as reference, Helium simple light, Xenon (heavy light), CO_2 medium complexity and very interesting fluid in energy application; MM and MD2M for the class of complex heavy fluids (siloxanes). The utilization of this classes helps to distinguish between complexity and weight, looking at the behavior of Helium and Xenon (same γ =1.67 but very different MW). [1] The entire set of results are presented in the figure 4.11.

[1]During the research work many other fluids (R134, R1233ZD for refrigerant, iso-penthane, steam) have been investigate between the range however because they do not add anything to the final knowledge, for the sake of clarity only the ones mentioned are important.

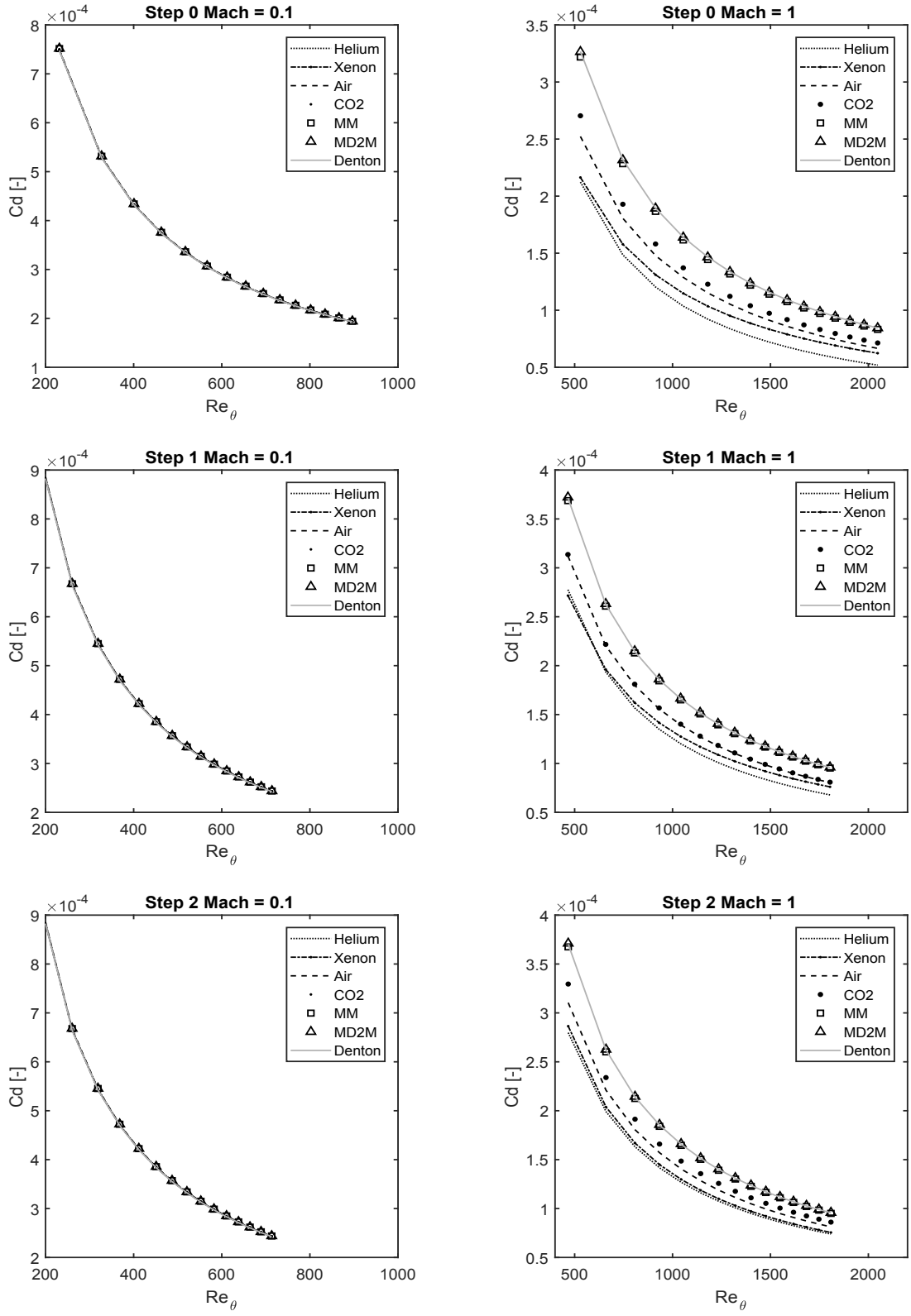

Figure 4.11: Sensitivity analysis for dissipation coefficient: (a) Step 0 low speed flow; (b) Step 0 high speed flow; (c) Step 1 low speed flow; (d) Step 0 high speed flow ; (e) Step 2 low speed flow ; (f) Step 2 low speed flow.

The physical conclusion is that the major parameter is the complexity γ rather than molecular weight, viscosity and thermal conductivity. Looking at the first row of fig. 4.11 it is evident that just the difference in molecular complexity determines a great discrepancy between several categories of fluids. More precisely the simple fluids (γ high) like helium and xenon have a shift towards lower value of C_d. The roles played by viscosity and thermal conductivity are negligible and they add only a correct general behavior in terms of transport properties and so Prandtl number. Moreover the molecular weight has no impact for sure since Helium and Xenon are characterized by the same trend even if they have very different weight (4 for Helium and 161 for Xenon). The fact that at low speed (left column of 4.11) all the steps show a collapse on the incompressible law for whatever fluid is interesting. Therefore the final conclusion is that the difference in fluid nature impacts on C_d only with high Mach number (for adiabatic case).

The behavior of siloxanes and in general of complex heavy fluids is to follow the incompressible formulation of dissipation coefficient also in sonic condition. Since the discrepancy appears at high speed, it is necessary to understand why it happens and what are the intrinsic behavior of simple and complex molecules at sonic or high Mach. Now we focus our attention on the physical trend of other quantities, in particular the temperature distribution inside the layer and the velocity profiles 4.12:

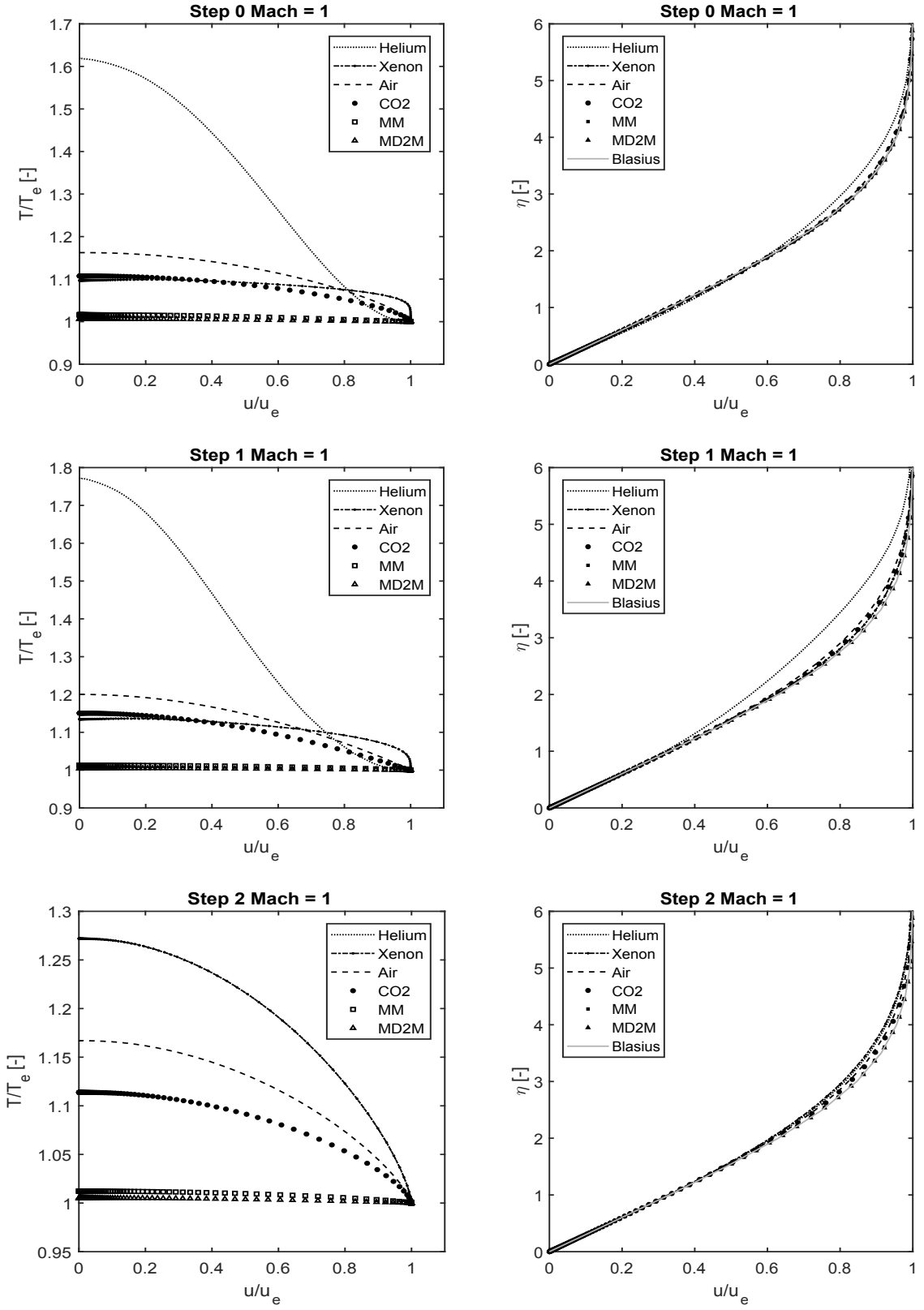

Figure 4.12: Sensitivity analysis for temperature and velocity profile: (a) Temperature profile Step 0; (b) Step 0 Velocity profile; (c) Temperature profile Step 1; (d) Step 1 Velocity profile; (e) Temperature profile Step 2; (f) Step 2 Velocity profile .

The main phenomena inside the laminar boundary layer has been explained: the nature of fluid manifests itself on a different temperature profiles inside the viscous region. For complex fluid at Mach=1 there is not any increase, in contrast for simple fluids, in all cases, the kinetic energy dissipated in thermal one is so high therefore the wall temperature can be much higher than the edge one (fig.(a) (c) (e) 4.12). This is the cause of the deviation from the incompressible Blasius velocity profile (Helium, Xenon in particular). Again complex fluids in contrast follow perfectly the incompressible velocity law like in the C_d case. Notice that the density is the inverse of temperature for an ideal gas and therefore the simple molecular fluid will show a strong reduction of it close to the wall, on the contrary the more complex the molecules the more constant is this parameter (no compressibility effect).

As last proof of this thesis another important index will be presented: shear parameter (the most "robust" parameter because it rarely shows deviation from the classical Blasius 0.332 at the wall) and the shape factor H only for the step 2 (correct ideal gas model) 4.13 at Mach=1.

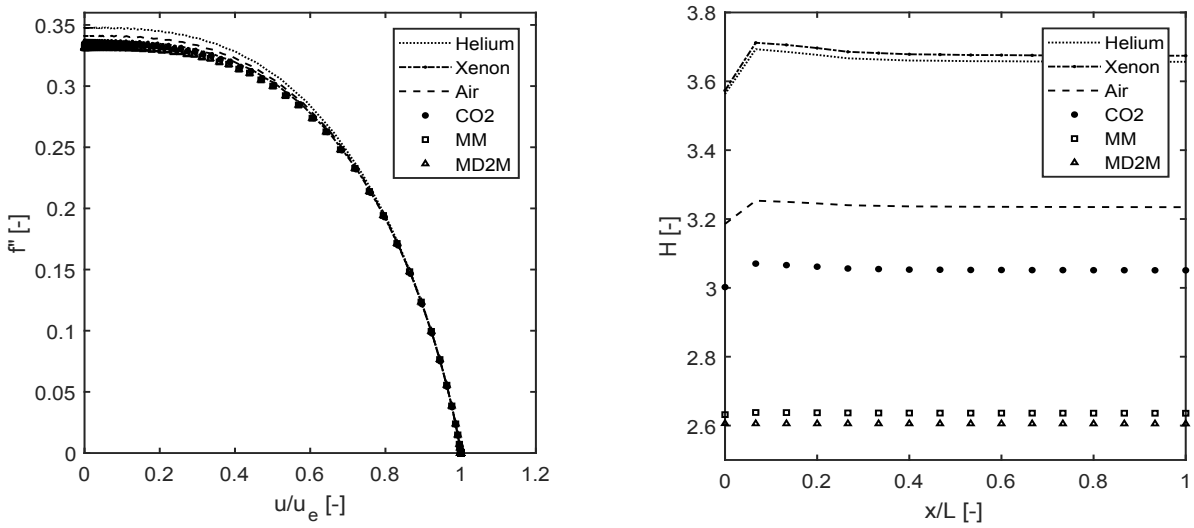

Figure 4.13: (a) Shear parameter f" for different fluids; (b) Shape factor of different fluids; ideal gas condition and Ma_e=1. Siloxanes remain on incompressible trend.

The study presented compares all class of fluids until a sonic condition (Mach 1) however the complex fluids shows a perfect incompressible behavior until Mach=2 fig. 4.14.

The concept of lack of compressibility effects shown by complex fluids have been studied by one author (Kluwick) whose paper was published during the period of this work; he arrived to the same conclusion [27, 68].
If we want go in deep to find the physical causes, the main reason why this discrepancy is given by the complexity of the fluid is contained in the energy equation (Navier-Stokes)

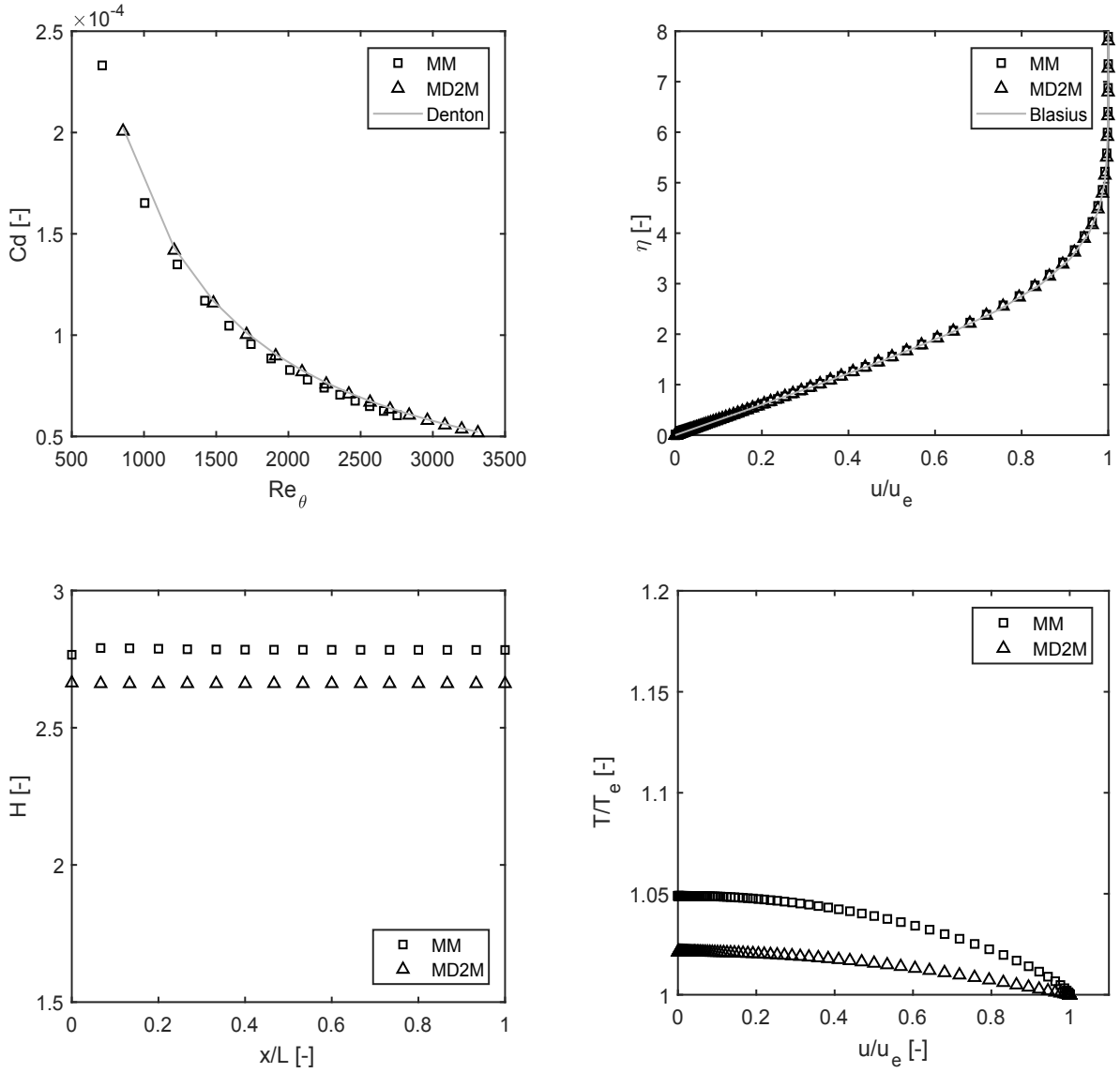

Figure 4.14: Siloxanes behavior at Mach 2: (a) Dissipation coefficient ; (b) Velocity profile; (c) Shape factor; (d) Temperature profile inside the boundary layer

for boundary layers [37, 66]. First the dimensionless analysis is performed:

$$x^* = \frac{x}{l} \qquad \overline{y} = y^*\sqrt{Re} \qquad y^* = \frac{y}{l} \qquad u^* = \frac{u}{u_{ref}} \qquad \theta = \frac{T - T_\infty}{\Delta T} \tag{4.23}$$

$$u^*\frac{\partial\theta}{\partial x^*} + v^*\frac{\partial\theta}{\partial\overline{y}} = \frac{1}{Pr}\frac{\partial^2\theta}{\partial\overline{y}^2} + Ec \underbrace{\left(\frac{\partial u^*}{\partial\overline{y}}\right)^2}_{\text{dissipation function}} , \tag{4.24}$$

Our attention is focused on the Ec dimensionless group related to the so called dissipation function: the Eckert-number. It is defined as:

$$Ec = \frac{u^2}{c_p \Delta T} \qquad \text{for perfect gas it becomes :} \qquad Ec = (\gamma - 1) Ma^2 \ , \tag{4.25}$$

in words: the Eckert number is a measure of how the viscous dissipation affects the flow increasing its temperature. Since it grows in proportion with the square of velocity, in low speed application is neglected while it is crucial in high speed study (supersonic aerodynamics, i.e air)due to the great dissipation converted in thermal energy. Nevertheless for siloxanes (i.e complex heavy fluids), and in general complex fluids, it is always very close to 0 no matter what is the Mach number because γ is close to one (look eq. 4.25). The smaller the γ the smaller is the increase of temperature due to viscous friction inside the flow. Therefore for close-to-zero Ec number, in adiabatic boundary layer, the compressibility effects are negligible also at high speed since temperature and consequently transport fluid properties is almost the same of the edge (4.14 (d)).

4.5 Effect of flow non-ideality on dissipation coefficient

In order to study the real gas effect, we have to decide the comparison parameter. The compressibility factor is the natural one since by definition it represents the deviation from ideal gas condition. We will investigate only complex fluid since the final task of this thesis work is about the ORC applications.[2]. Therefore MM will be observed in three different Z as shown in fig.4.15.

The three points represent respectively: ideal gas zone, moderate effect of non ideality, strong non ideality. The following results for dissipation coefficient are shown in charts 4.16. It is clear which is the role of non the ideality effect: negligible.

The reason is that the C_d is characterized by ratio of the properties inside the layer over the edge ones therefore even if we work in this zone there is not any discrepancy. Both low speed and high speed do not present any deviation from incompressible law.

It has been shown clearly how real gas effect does not add anything new to the behavior of complex fluids. In particular the decrease in Z counteracts the compressibility effects since the increase of specific heat given by reality of the gas increases the tendency of the fluid to store energy: indeed the temperature increase inside is much smaller. In the figure (a) 4.17 the case $Z = 0.3$ has a wall's temperature ($\sim 2\,\%$) higher than edge one,

[2]For sure it is not the field of this present work investigating real gas effect of simple molecule (Helium, Xenon and air). Air in real condition happens only in strong hypersonic regime (space application) in that case the complex phenomena such as molecular dissociation or plasma flow start. This topic is totally outside the horizons of this work.

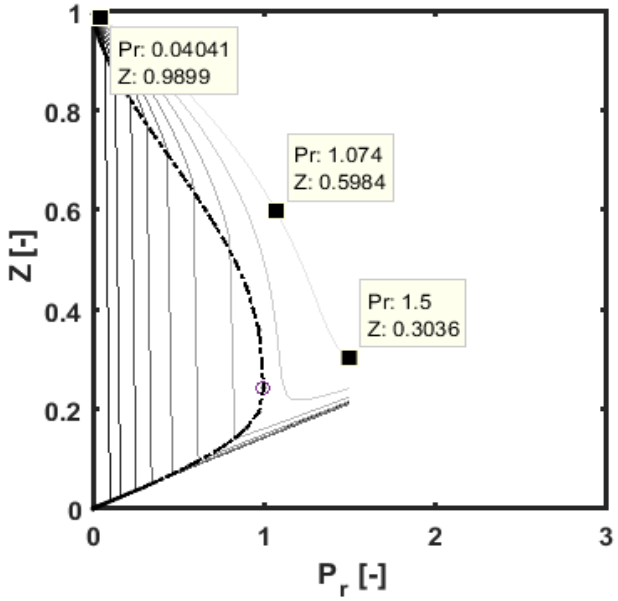

Figure 4.15: Thermodynamic working points for real gas effects analysis

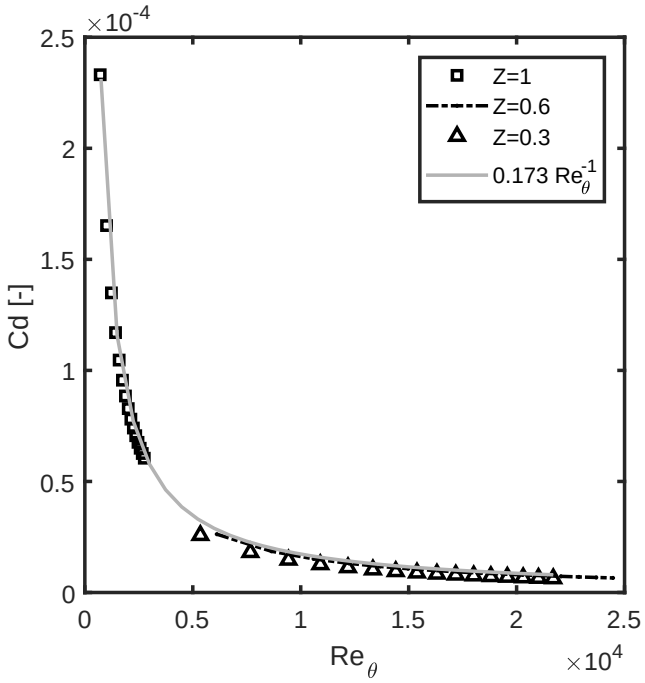

Figure 4.16: Real gas effect on C_d at Mach=2: there is not any deviation for complex fluid. Library used: RefProp [6]

in contrast the ideal gas ($Z = 1$) is more than the double. The general conclusion is that in laminar boundary layer complex heavy molecules follows the incompressible behavior also at strong supersonic regime and real gas zone. Siloxanes belong to this group.
From this point of view the ORC turbine theory could benefit from this concept since the mean-line-design in terms of physical based approach is the one already proposed by

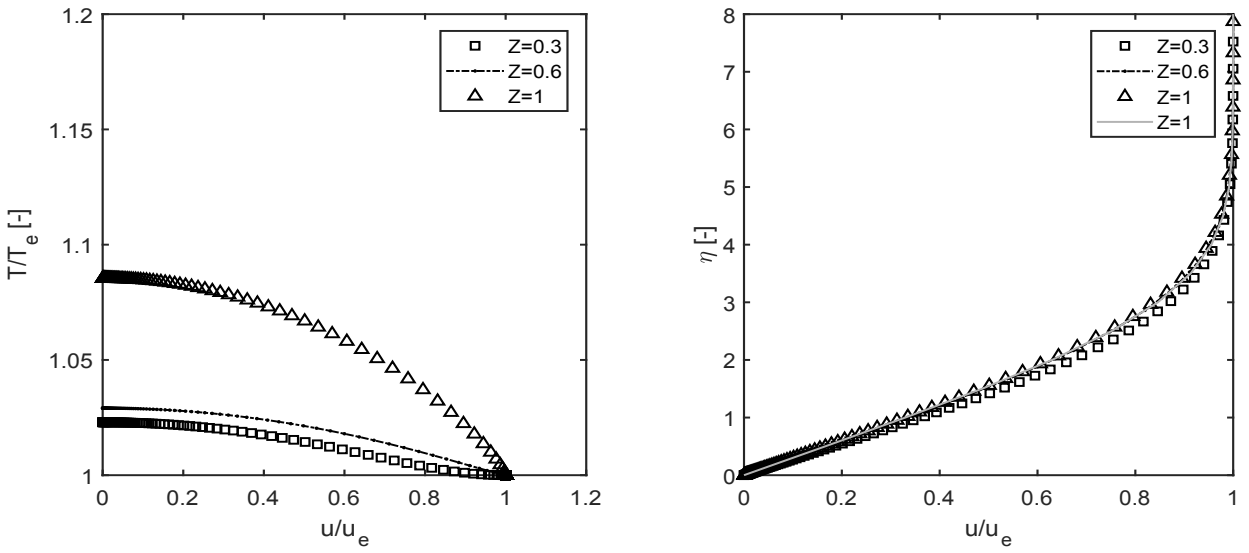

Figure 4.17: Real gas effect inside supersonic BL for MM: (a) Temperature profile the denser gas shows lowest heating; (b) Velocity profile: perfect overlapped to Blasius profile

Denton without any change each computation step.
To conclude this chapter as last case is shown also to test our knowledge: working in the B-Z-T (Bethe Zel'dovich Thompson) region we can check if the dissipation coefficient shows some "exotic" behaviour as this gas-dynamic region is. The study made is inspired by Kluwick investigation [27]: a classical decelerated flow also known as Howart boundary layer profile,

$$u_e = u_\infty \left(1 - \frac{x}{L}\right) , \tag{4.26}$$

If we are able to enter into the B-Z-T region the phenomena related to shock waves due to explosion of Mach number could happen even if we decelerate the flow. The charts 4.18 represent the phenomena described.

The possibility to work at low Γ influences also the boundary layer behavior: the separation is delayed with respect to common fluids like air. However the dissipation coefficient remains the same for incompressible flows depending only by Λ.

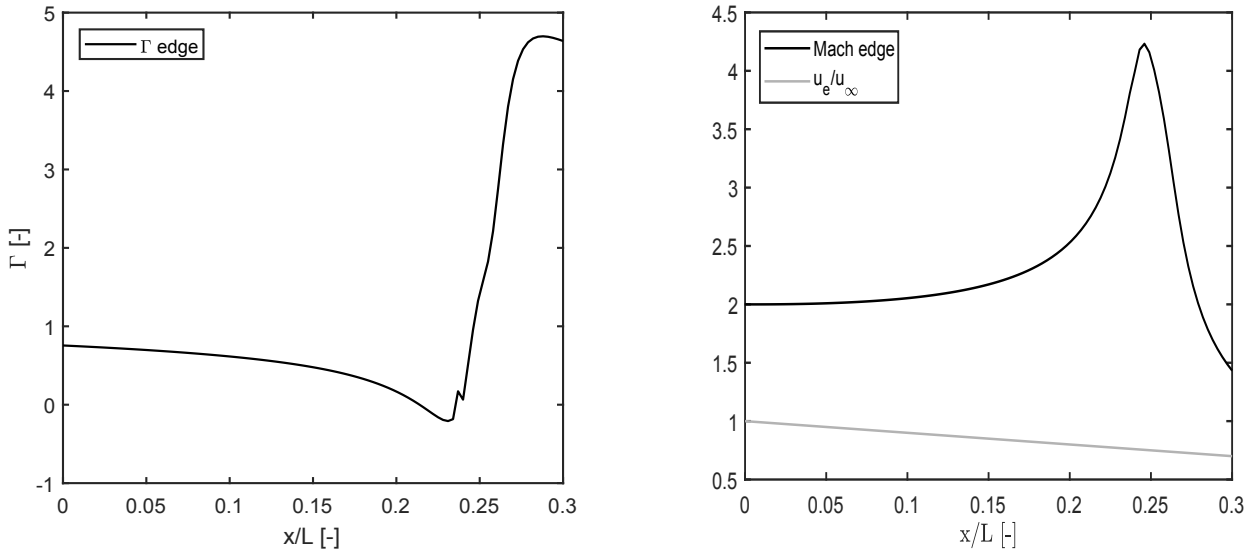

Figure 4.18: B-Z-T zone and (a) Fundamental derivative of gas-dynamic smaller than zero ; (b) Explosion of Mach number despite the decelerated flow.

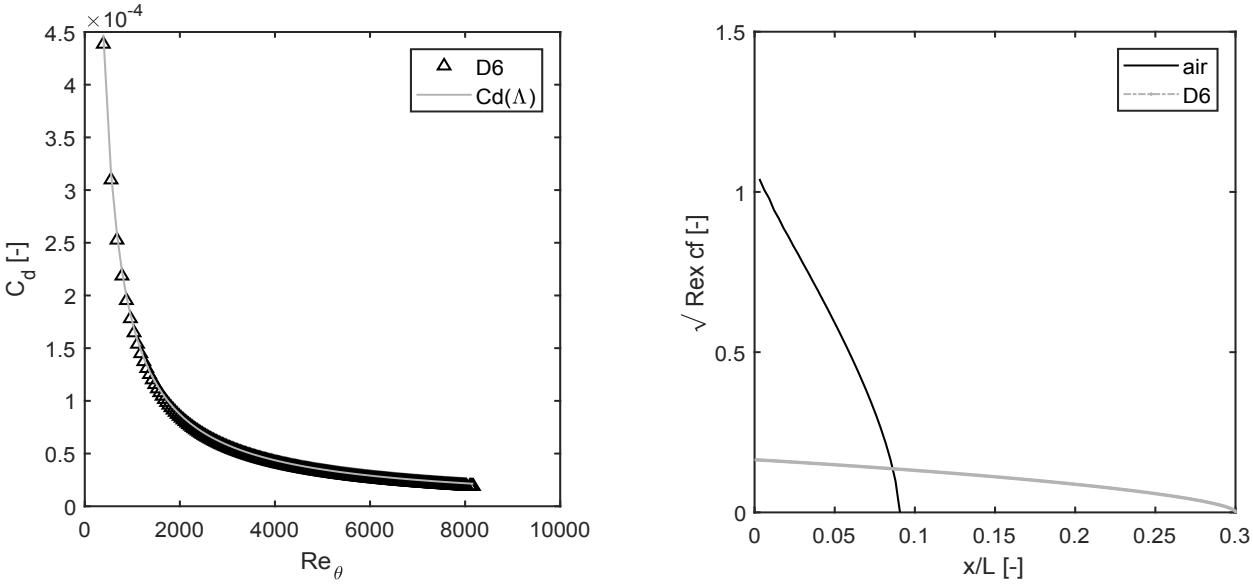

Figure 4.19: (a) Dissipation coefficient for deceleration in B-Z-T; (b) Skin friction. Delay of separation point thanks to increase of Mach number.

Chapter 5

Dissipation coefficient in Turbulent Boundary layer

The classical approach to manage turbulence phenomena in boundary layer was based on a very general and simplified vision without any turbulence transport equations; therefore the so called 0-equation model have been used. Also our code is based on classical boundary layer theory[1]. The integration of Cebeci-Smith model was the most natural and easy way to complete the code. The relations used have been presented in chapter 2 (2.2.2).

5.1 Incompressible

The incompressible study revolves around to the verification of the C_d law:

$$C_d = 0.0056 Re_\theta{}^{-\frac{1}{6}} , \tag{5.1}$$

This is the one discussed by Denton in his papers [26, 26] and originally proposed by Rotta [69] and described by Schlichting [41]. The other formulation proposed, again a power law, is very similar and it was by Walz [70].

$$C_d = 0.0052 Re_\theta{}^{-\frac{1}{6}} , \tag{5.2}$$

The difference is very small and it does not add anything o the physical concept. The chart 5.1 contains the verification for incompressible air.

[1]The authors (Clutter, Smith and Cebeci) were involved also in the building of a 0-equation model.

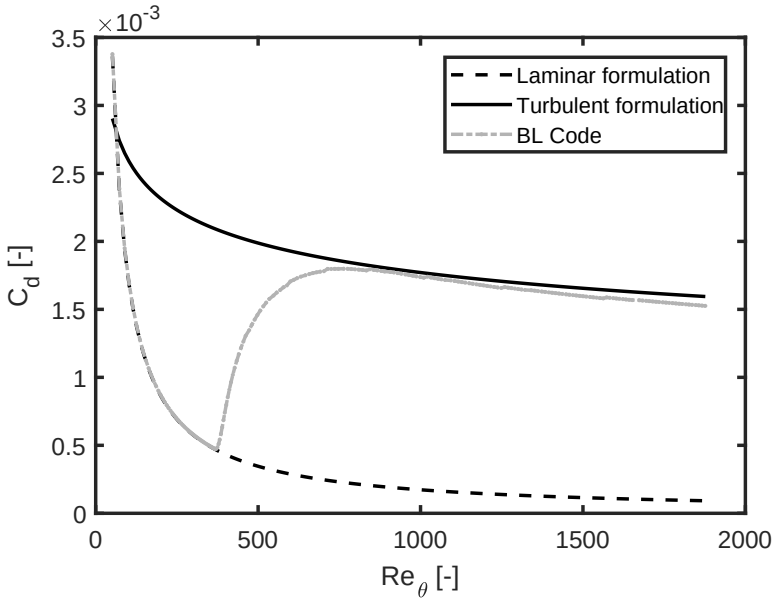

Figure 5.1: Verification of the incompressible dissipation coefficient with our code. Transition happens in the typical range quotes by Denton. Input: $Ma_e = 0.1$, ideal gas conditions, constant properties. Adiabatic wall

Apart from the verification (well performance of the code) the important aspect is the intrinsic more dissipative nature of the turbulent flow close to the wall. The specific dissipation (C_d) is 4 times higher than the final part of laminar regime, this aspect indicates that the best zone for application would be in the laminar region, i.e the one close to transition, being carefully to avoid it. The reason why turbulent is more dissipative respect to laminar flow in boundary layer is due mainly two physical behavior:

1. flatter velocity profile close to the wall $\frac{\partial u}{\partial y}$, therefore higher gradient and so shear stress.
2. presence of supplementary viscosity effect due to the turbulence structure on the entire spectrum, resumed in a mean term: the eddy viscosity μ_τ. This parameter is very strong in the outer layer where turbulent phenomena are predominant.

In order to clarify all these concepts, these quantities described abobve are presented in the following plots 5.2 and for velocity 5.3(c).

The figure (a) 5.2 is the law of the wall and the scaled quantities derive from the Van

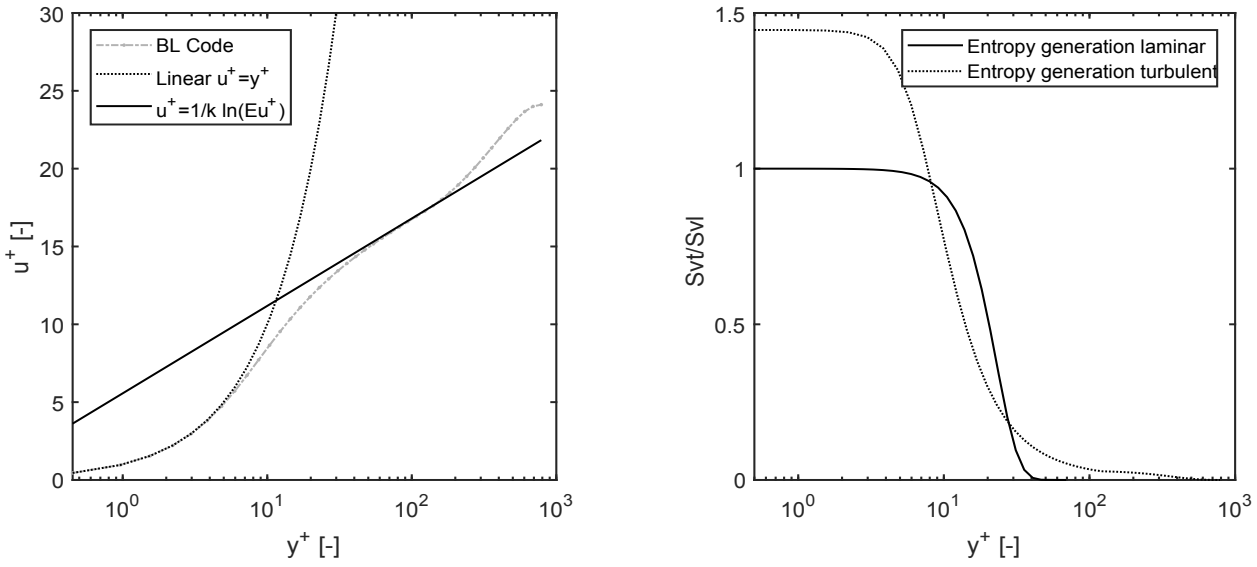

Figure 5.2: Features of turbulent boundary layer: (a) Law of the wall through Van Driest transformation (source of verification); (b) Entropy generation per unit volume scaled with respect to laminar wall value

Driest transformation through the friction velocity u_τ (τ_w is the wall shear stress).

$$u^+ = \frac{u}{u_\tau} \qquad \text{where} \qquad u_\tau = \sqrt{\frac{\tau_w}{\varrho}} \qquad y^+ = \frac{y u_\tau}{\nu} \tag{5.3}$$

The y^+ has the form of a Reynolds number with the inertia do to shear stress with respect to viscous forces. The law of the wall fig.(a) 5.2 presents the universal behavior of turbulent boundary layer distinguishing different region with proper phenomena:

- viscous sublayer: included between $0 < y^+ < 5$ [44] characterized by laminar behavior since the viscous force are so strong with respect to the inertia ones. The molecular diffusive phenomena are predominant; the law is linear: $u^+ = y^+$
- buffer layer between $5 < y^+ < 30$ [44] in which both turbulent and laminar phenomena are equally important
- outer layer: from buffer to the free stream ($30 < y^+ < Re_\tau$) [3], predominance of turbulence structure; $u^+ = \frac{1}{\kappa} ln(Eu^+)$ and E=9.8 and κ universal Von Kàrman constant (0.41)

This distinction has a huge influences on the generation of entropy, indeed in fig.(b) 5.2 the trend inside layer is shown. The major source of entropy generation (destruction of kinetic energy) is in the laminar viscous sub layer and a little part of the buffer (until $y^+ \approx 10$);

the discrepancy with respect to a pure laminar flow is very high: ~ 50 % more than non turbulent flow 5.2. Other important characteristic of turbulent flow are represented by the eddy viscosity, turbulent Prandtl number and a different shape factor with respect to laminar case 5.3. Moreover the velocity profile is very different with respect to the laminar

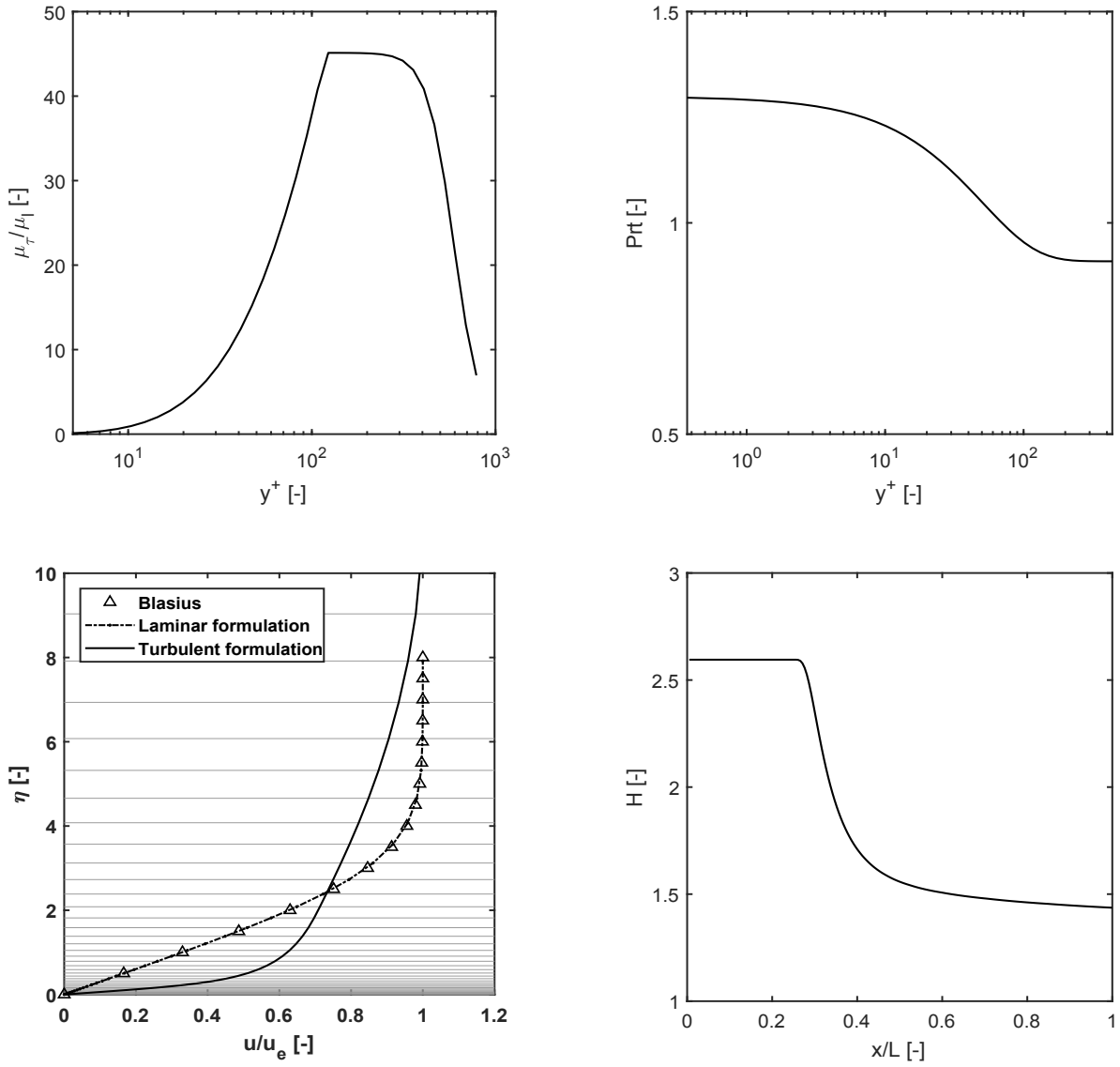

Figure 5.3: Typical properties of turbulent BL: (a) Eddy viscosity with respect of laminar $Re_\theta = 1000$; (b) Turbulent Prandtl number at $Re_\theta = 1000$; (c) Velocity profile of laminar compared with turbulent with the mesh presentation; (d) Shape factor along the plate laminar and transition to turbulent;

one, all this parameter are plotted in the figure 5.3. The eddy viscosity (a)5.3 is perfect consistent with the concept of the different layers: it is close to zero in the wall region (indeed the term laminar sub-layer), then it achieves a peak ($y^+ \approx 10^2$) and it continues with a smooth plateau in the outer layer (turbulence phenomena are predominant). The

turbulent Prandtl number is influenced by molecular properties in the laminar sub-layer being higher and then collapse to a typical value of 0.9 (used in all classical RANS model) 5.3(b). The Pr_t is defined as:

$$Pr_t = \frac{\nu_t}{\alpha_t} \qquad \text{with} \qquad -\overline{u_i' T'} = \alpha_t \frac{\partial T}{\partial x_i} \tag{5.4}$$

The figure c 5.3 represents the velocity profiles of laminar and turbulent. The typical flatter shape close to the wall of turbulent flow is one of the reason of higher shear stress (and so the higher dissipation). The laminar follow the Blasius theory (incompressible), the turbulent flow has higher thickness. The vertical gray lines represents the mesh of the BL code which is stretched close to the edge and very thin at the wall in order to describe the sub-layer phenomena. All profiles corresponds with $Re_\theta = 0$. It is known that the shape factor(d) 5.3 for classical turbulent boundary layer is lower with respect to the laminar Blasius value. The typical range reported in literature is 1.3 - 1.4 and it it is another confirmation of the validity of our results. In particular for a turbulent boundary layer we can state that the defect of momentum is higher with respect to the mass one (the concept of H itself).

5.1.1 Incompressible with pressure gradient

The effect of pressure gradient on dissipation coefficient it is very important since it is the most likely behavior in a turbomachinery application. The characteristics of this simulation are: air, perfect gas, low speed. The velocity profile chosen are:

- accelerating flow: $u_e = u_\infty(1 + 3\frac{x}{L})$,
- decelerating flow: $u_e = u_\infty(1 - 3\frac{x}{L})$

The figure 5.4 shows the results from our code.

As quoted by Denton the major dissipation happens for decelerating flow in the zone of separation. It is already known from aerodynamic point of view that separation is the worst possible scenario for an airfoil, however we conclude the same concept also from entropy point of view. The acceleration flow does not show great deviation with respect to the zero pressure gradient by the way is little smaller as stated by Denton [1]. Anyway it is sure that our turbulence model takes into account the effect of moderate pressure gradient eq. 2.45.
In order to understand the causes of different dissipative trend we are going to plot and to describe another important parameter such as the shear stress distribution (τ) inside the BL at the station characterized by $Re_\theta = 1000$. This plot can be considered also a source to validate our results in turbulence field (with respect to fig.4 [1]). The figure 5.5 underlines an interesting concept about the turbulent boundary layer: at the wall (laminar sub-layer) the smallest shear, and therefore the entropy irreversibilities, is for decelerating flow (laminar decelerating flow is less dissipative, it is consistent with 4.2.1) but in the

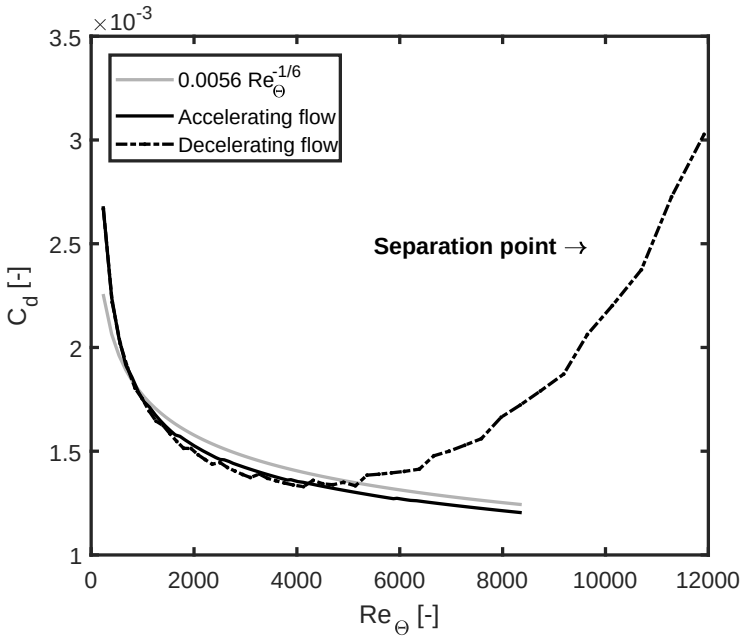

Figure 5.4: Turbulent incompressible boundary layer: the effects of pressure gradient on dissipation coefficient

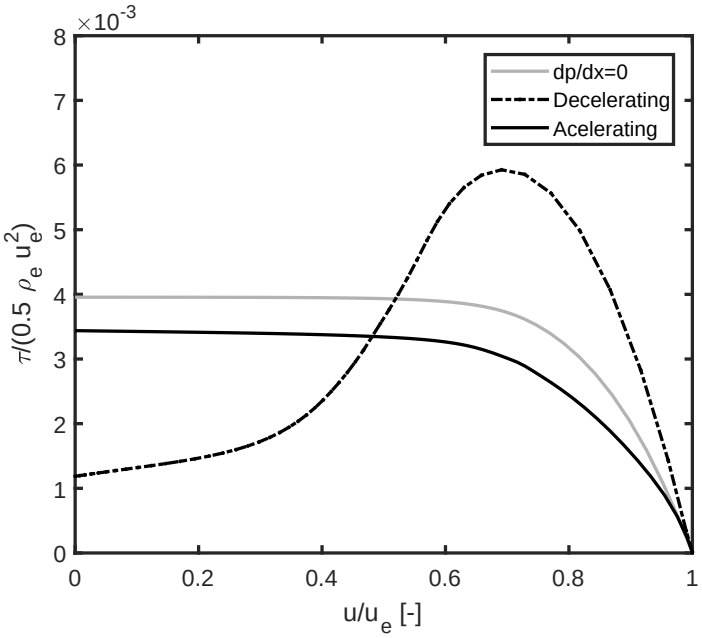

Figure 5.5: Effect of pressure gradient on turbulent boundary layer for Re_θ = 1000 5.5. The decelerated flow shows high shear stress in zone of separation. Accordance with Denton fig.3[2].

outer layer the turbulence phenomena make it the highest. This is the cause for which the dissipation is higher for this type of flow. In terms of shape factor (H) it happens the same behavior since the deceleration makes H higher therefore the momentum thickness is larger than displacement one.

5.2 Compressible, high speed flow

The effect of Mach number (supersonic flow) on the adiabatic turbulent boundary layer has been investigate by many authors [65, 72, 73, 74], but, as always, no results for dissipation coefficient have been presented until now. In particular all these research studies have a common thesis: the Van Driest transformation (universal log wall) has a general validity also in supersonic flow. The general law behind this concept is the *Morkovin's hypothesis* which stated that for "moderate" Mach numbers (until Ma=5) the essential dynamics of these shear flows will follow the incompressible pattern. This concept makes possible a scaling velocity for turbulent quantity (fluctuations and turbulent kinetic energy). Therefore high-speed turbulent boundary layers can be computed using the same model as at low speeds by assuming that the density fluctuations are weak ([75] and Bradshaw (1974)). Because the density fluctuations (ϱ') are dependent by the statistical velocities we can write:

$$\varrho' = \varrho'(Ma') \quad \text{where} \quad Ma' = \frac{u'}{\sqrt{\left(\frac{\partial p'}{\partial \varrho'}\right)_s}} \tag{5.5}$$

But the quantities u', p' are negligible also at supersonic regime, in other words even if the Mach average is high the Mach due to fluctuation velocity is small because $u' << \overline{u}$. This physical concept is applicable until Mach 5 therefore is perfectly respected for our purpose.
The first step is to check if our tool (BL code) works well in high speed flow. To verificate this we will use two references:

1. the law of the wall (it must work until Mach 5) and the lack of deviation for turbulent Prandtl number despite the high Mach number.
2. DNS data from a work made by the Fluid Mechanics department of TU Delft. In particular this research group introduces a new factor of scaling suitable fo turbulent phenomena with high variable fluid properties close to the wall.

Our results fig.(a) 5.6 respect the first point. Moreover the thermal phenomena caused by the heating due to supersonic regime are governed (analogy concept) by the turbulent Prandtl number. As quoted by literature this parameters is not affected by increase in Mach. Results presented 5.6(b) are quite similar to the ones of Rotta and Meier ([75] fig.5.1).

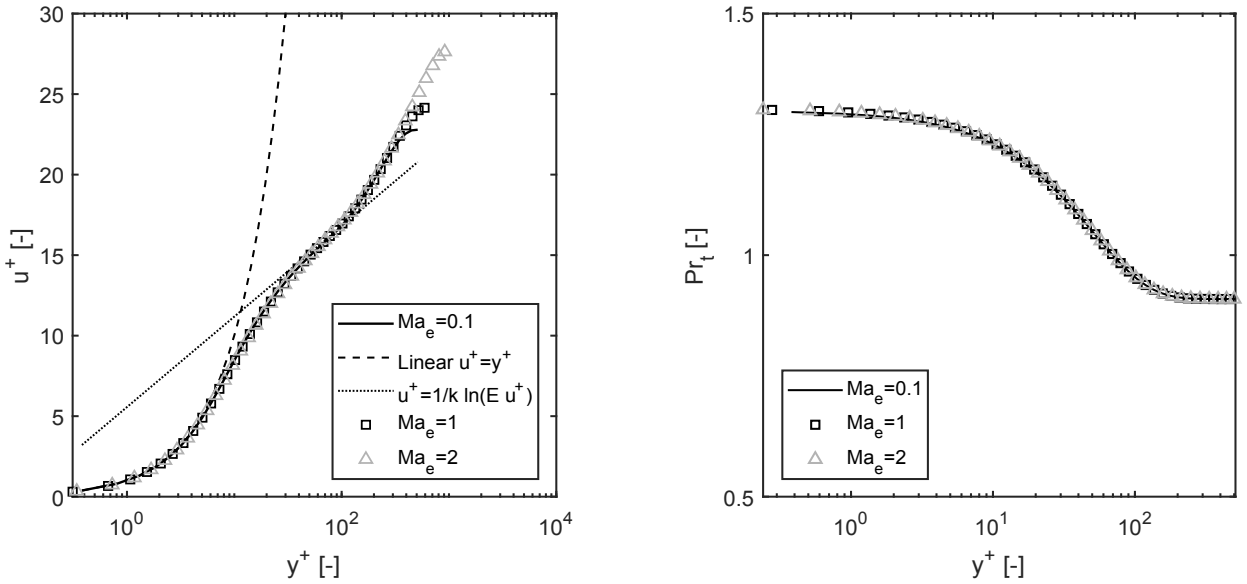

Figure 5.6: Supersonic turbulent boundary layer effects of compressibility do not affect the trends: (a) Law of the wall ;(b Turbulent Prandtl number)

For the second verification we will use the semi-local Re_τ^* and y^* [3] defined as:

$$Re_\tau^* = Re_\tau \sqrt{\frac{\overline{\varrho}}{\overline{\varrho}_w}} \Big/ \frac{\overline{\mu}}{\overline{\mu}_w} \qquad\qquad y^* = \frac{y}{\delta} Re_\tau^* \tag{5.6}$$

These new dimensionless groups catch the strong variable property phenomena and represents the collapse in near wall region 5.7.

All these plots serves to consolidate our knowledge about such complex field and in particular to set up the background to investigate the dissipation coefficient, first for air and then for complex fluids.

In the figure 5.8 it is shown that the Mach number increase affects the C_d, shifting the trends to smaller values. The several curves at high Mach number are allocated between the two incompressible laws, therefore at high speed the C_d decreases. Again it is important to know the physical causes of this great discrepancy even larger than in laminar regime. For sure the increase in temperature determines the shifting already seen in section 4.3, but now there is also the impact on the eddy viscosity μ_τ (see fig. 5.9),

Therefore, for air in ideal gas model, in turbulence there are a two effects: one on physical properties, the increasing in temperature and variation of thermo-physical properties, and

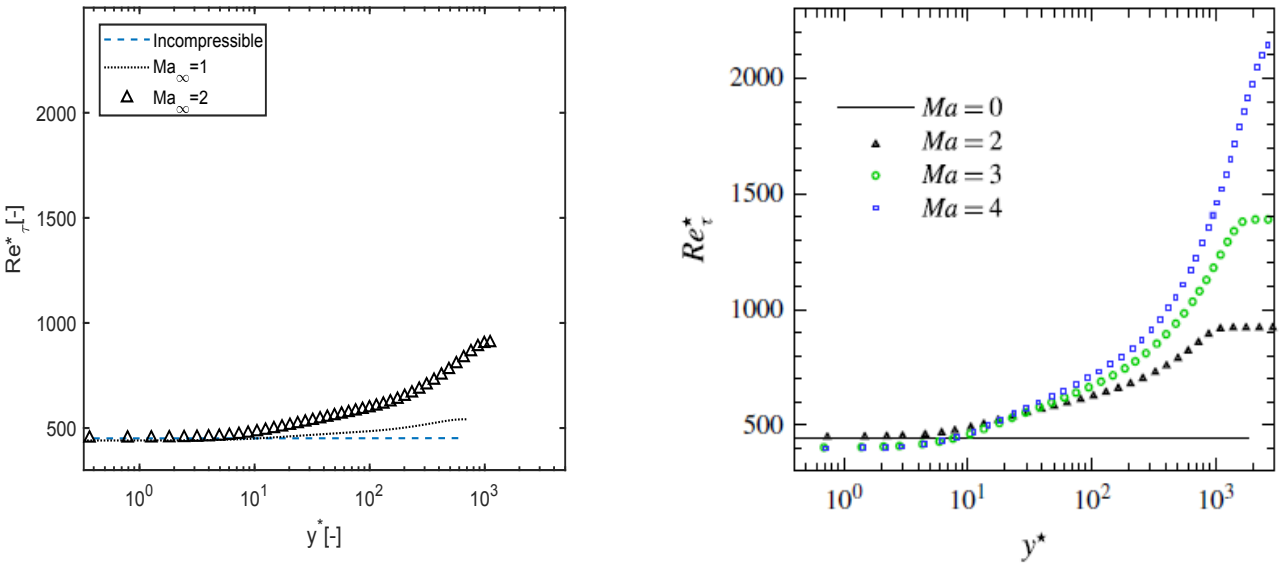

Figure 5.7: Verification of BL code with DNS data on scaled quantities: (a)BL code (our results); (b) DNS data [3]. Comparison made at Re_τ=400

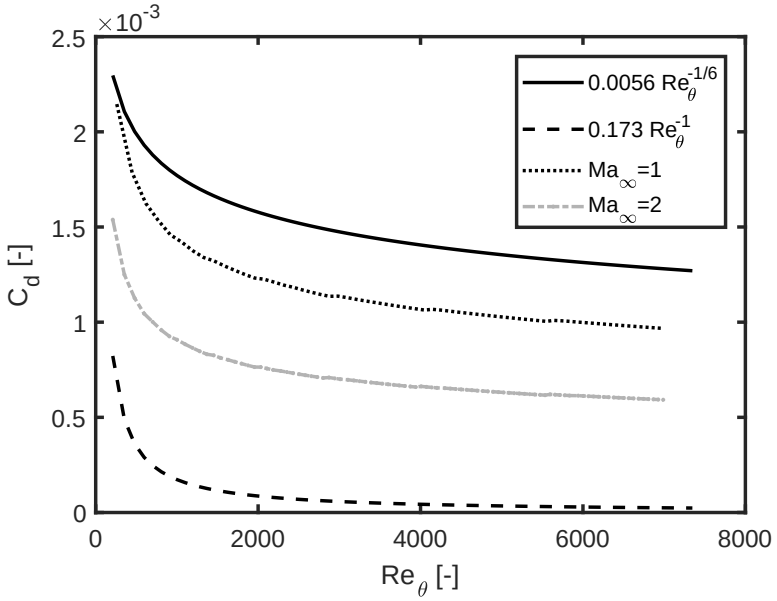

Figure 5.8: Dissipation coefficient for supersonic flow, on adiabatic flat plate. Effect of compressibility

the second one is on the flow i.e the decrease of dynamic eddy viscosity. Indeed:

$$\mu_\tau = \varrho \nu_\tau \ , \tag{5.7}$$

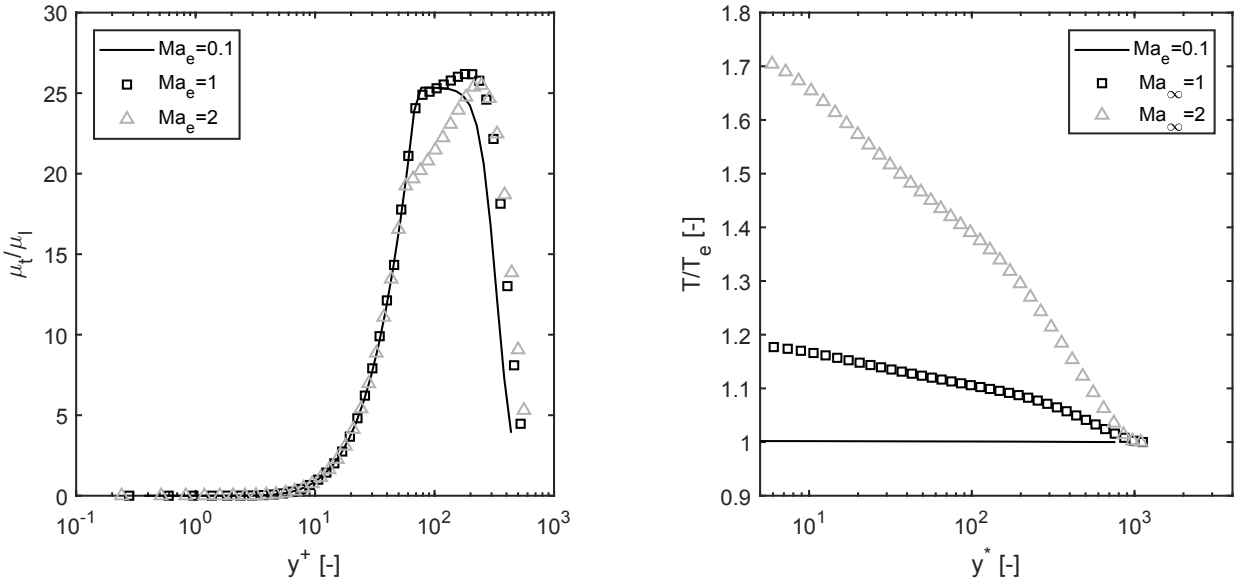

Figure 5.9: Effects of Mach on turbulent characteristics ($Re_\theta = 1000$): (a) Eddy viscosity ;(b) Temperature ratio

since the dynamic eddy viscosity contains the density (which decrease a lot for simple-medium fluid molecules (as shown in chapter 4 4.4). The deviation is in the outer layer (b)5.9 where turbulent phenomena are preponderant.

5.3 Turbulent dissipation coefficient for ORC fluids

Because of the structure of the turbulence model, it should not be wise using this instrument to investigate other fluids than air in particular for strange cases like close-to-critical phenomena. Moreover it is a limitation of RANS turbulence model the fact that they contain constant terms, fitted for particular conditions. Nevertheless the absence of changes in fluid transport properties inside the boundary layer coupled with Morkovin's hypothesis are the theoretical background to investigate ORC fluids. For the other classes like simple fluids or CO_2 finer tools are necessary (Appendix E, [76]) [2] As expected the ORC fluids maintain their value perfectly on the incompressible law 5.10. Another very important concept is that dissipation coefficient in turbulent regime tends to became an auto-function with respect to Re_θ and therefore we return to the preliminary applicative concept used by Denton in "Loss Mechanisms for turbomachines": constant value. The complex fluids tend to have very large momentum thickness Reynolds and no effect of Mach number ergo the functional dimensionless formulation becomes:

$$C_d \neq C_d(Re_\theta, Ma) \ , \tag{5.8}$$

[2] the author of this thesis has had the possibility to join to the conference held by Dr.Soshi Kawai at the Process and Energy department of TU Delft on this topic: DNS and modeling for trans-critical turbulent boundary layer. This experience has suggested the impossibility to investigate critical BL with a simple turbulence model.

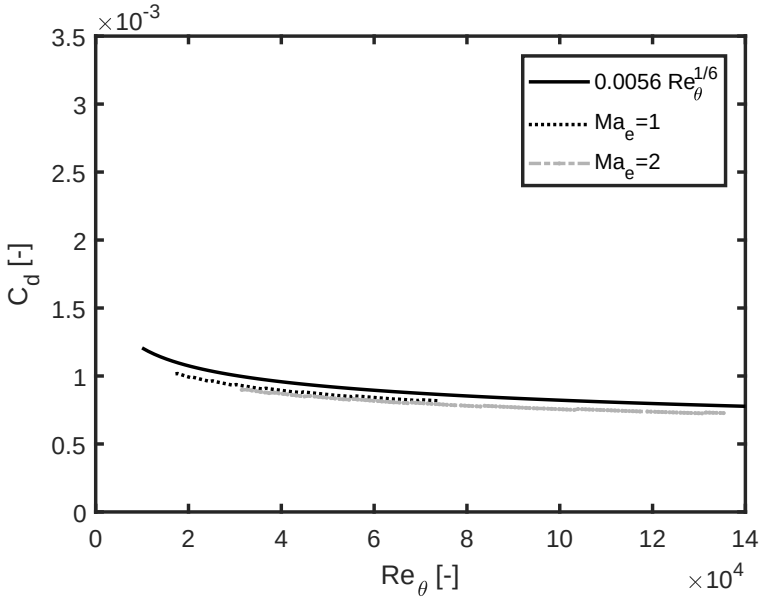

Figure 5.10: Dissipation coefficient for complex fluids in ideal gas region. No deviation also in case of turbulent boundary layer with respect to the incompressible law.

Therefore for incompressible and whatever regime for complex fluids (ORC) the C_d has a flat distribution with respect to Re_θ at high values of this last one term ($> 10^4$) so it is very insensitive to the BL states [69, 77, 41] in contrast to skin friction which manifests great discrepancy in whatever range. If the range of application is in extremely high Re_θ the limit is no more 0.002 (upper limit) used by Denton but quite smaller 0.015 or something less lower.

To complete this chapter we present also the real gas effect on the MD2M siloxane 5.11

The results do not present anything strange or new: the C_d follow the incompressible law, there is not any change in temperature distribution inside the layer (as in laminar regime) and also the compressibility factor (very low 0.25) remains constant too. The fluid transport properties do not change.

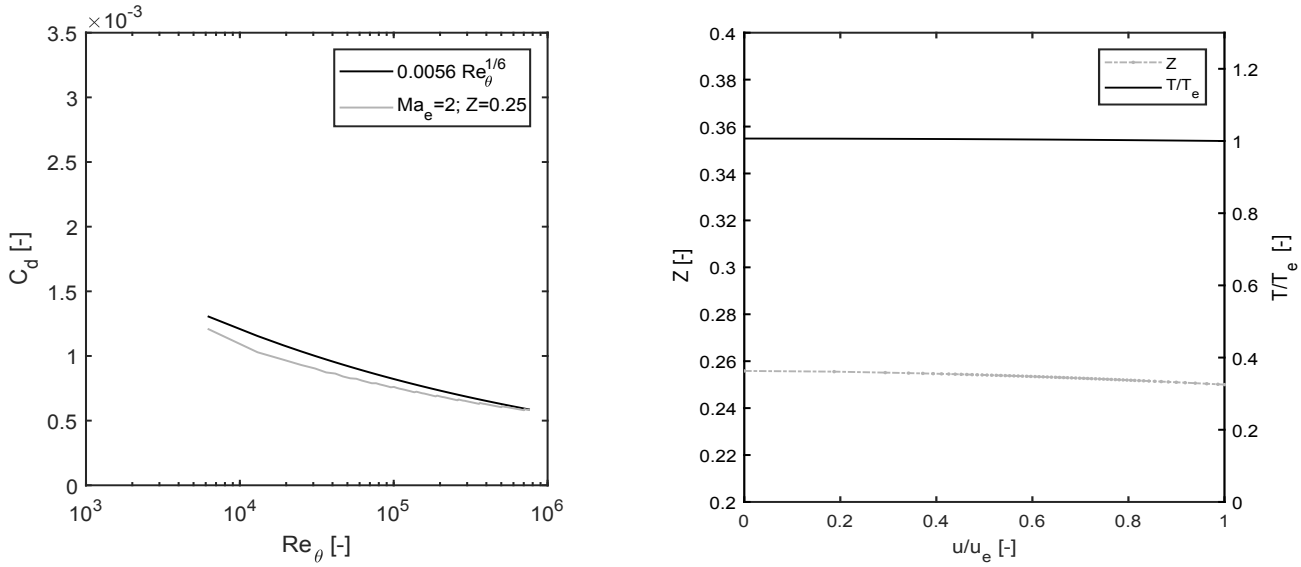

Figure 5.11: Real gas effects in turbulent boundary layer: (a) Dissipation coefficient; (b) Compressibility factor Z and temperature distribution

Conclusion

We have set a general study of C_d and in general of the boundary layer phenomena for different fluids. In the following chapter two applicative study will be challenged using the these results.

Chapter 6

Applications

The aim of this chapter is the estimation of the accuracy of th results given by our BL code, the ones gives by Denton model through the comparison with respect a CFD code (SU2 [29]).

6.1 Code settings

The SU2 (Stanford University Unstructured) code is an open source software https://su2code.github.io/ developed for aerospace analysis and optimization. It is composed by many modules written in C++. The software contains two turbulence model: Spalart-Allmaras, and SST Menter (AppendixD). the latter will be used.

In figure 6.1 the geometry of the blade and the mesh is presented (a); in particular the discretization adopts a triangular-type elements, very suitable for aerodynamic problem which can involve shock wave phenomena. Moreover the unstructured nature of this mesh allows to increase the element density close to the wall with two very packed zones, the most difficult to analyze due to the complex phenomena involved (mixing losses, recirculation, wakes): the stagnation point and the trailing edge. In fig.6.1(b) the pressure distribution is shown. There is a small pike close to x = 0.2 in suction side due to the high streamline curvature of the geometry.
The general presentation of SU2 environment has been discussed now we are ready to investigate the different cases.

In terms of investigation we will use three different instruments:

1. SU2 direct results
2. Denton profile loss model

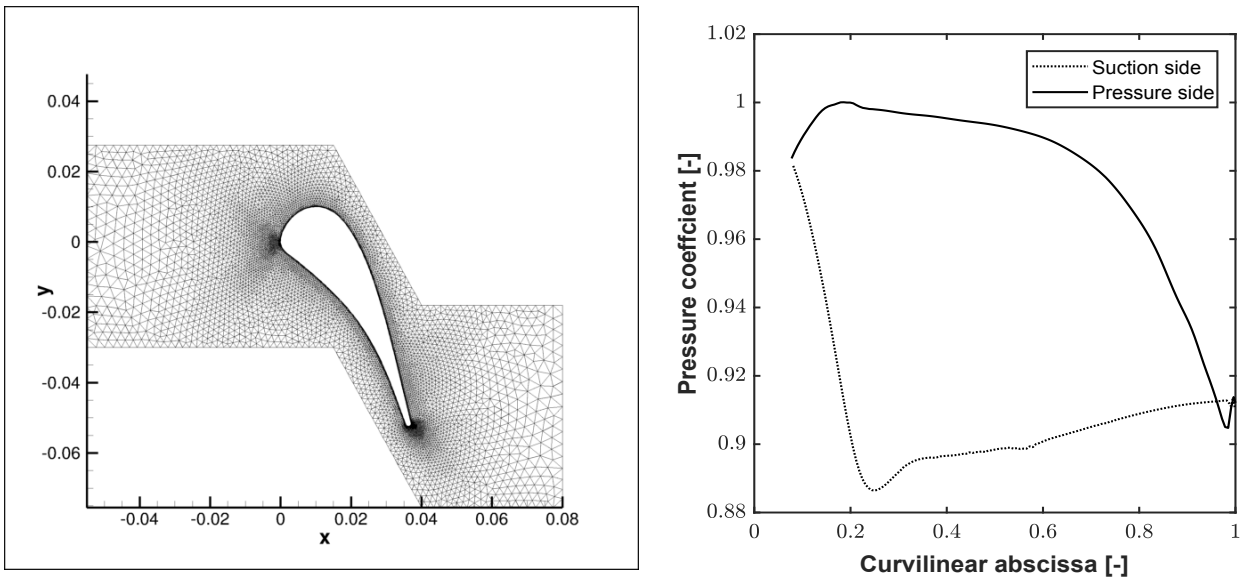

Figure 6.1: General features of from LS89 simulation: (a) Mash domain ; (b) Pressure distribution along the blade for low speed case, small oscillation at the end due to mixing phenomena at the trailing edge

SU2 Settings	**Choice**
Physical Problem	Navier Stokes
Turbulence model	SST Menter
Math problem	Direct
Boundary condition	Inlet total
Mixing process	Algebraic
Numerical Method for Spatial Gradients	Weighted least square
Turbulent Numerical Method	Scalar Upwind
Convective Spatial Numerical Order	2° order
Turbulent Spatial Numerical Order	2° order
Courant Friedrichs Lewy number	40
Number of iterations	1001

Table 6.1: Settings of the SU2 code

3. BL code with the pressure profile (from SU2 post processing file) at the edge as input

The point 1) is based on the entropy results of the SU2 given by post processing phase:

$$\zeta_s = \frac{T_2(S_{in} - S_{out})}{H_{Tout} - H_{out}} \tag{6.1}$$

The entropy S_{in} and S_{out} are present in the file "Turbomachinery" output for post-processing and the dimensions are [J/K] instead enthalpy is [J]. Because they are quantities related to section distant from the blade, they take into account the trailing edge loss due to mixing out of the wake.

For what concern the point 2) it is used the low speed formulation for a blade cascade eq.(46) [2] of Denton model.

$$\zeta_s = \frac{T_{out}(S_{in} - S_{out})}{0.5\dot{m}\overline{V}^2} = C_d\left(2\frac{\overline{V}}{\Delta V} + 6\frac{\Delta V}{\overline{V}}\right) \tag{6.2}$$

Reminding the definition of average velocity $\overline{V}$ and the discrepancy ΔV derived from circulation and the conservation tangential momentum equations 3.12 and 3.10.

And finally the 3) point is the most complex: since the BL code is only for layer flows in proximity of the wall, we split the problem in two simulation, one for suction side and one for pressure side, excluding the trailing edge and the stagnation point. Then the summation is made to compute the entire boundary layer losses. So the general equation

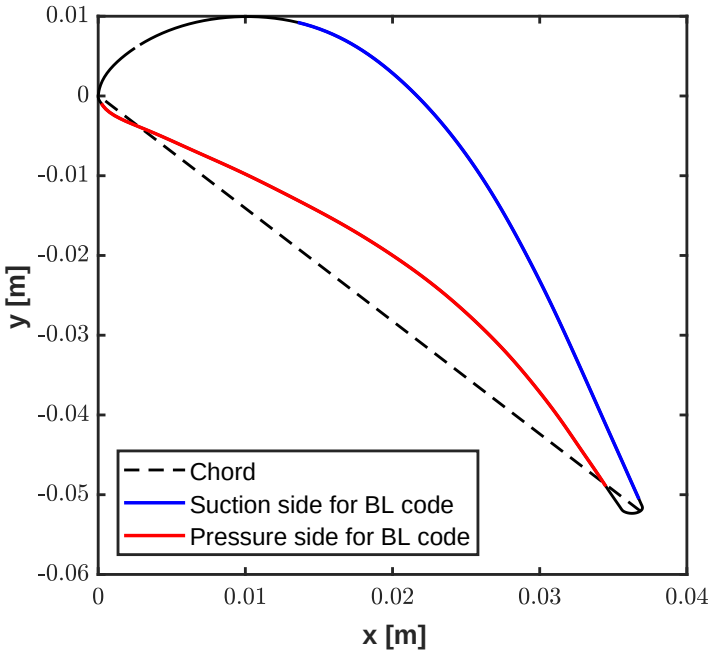

Figure 6.2: Main features of the geometry extracted for boundary layer code computation: exclusion of stagnation point, too high curvature and the trailing edge.

is:

$$\dot{S}_{gen} = \sum_{BL} C_s \int_0^1 \left(\frac{C_d(\varrho V^3)}{T} \right)_e \frac{dx}{L} \ , \tag{6.3}$$

and then:

$$\zeta_s = \frac{T_{out} \dot{S}_{gen}}{\dot{m} V_{out}^2} \tag{6.4}$$

The integration is very simple inside the code itself having the right distribution of C_d, ϱ_e, Te, V_e^3 and it is performed on the dimensionless length, after this we multiply for the surface, which is estimated using the classical finite difference method for curvilinear abscissa:

$$S(j) = S(j-1) + \sqrt{(x(j) - x(j-1))^2 + (y(j) - y(j-1))^2}; \ 2 < \text{j} < \text{end} \tag{6.5}$$

6.2 Results

In this section the results for subsonic and transonic case will be presented.

6.2.1 Subsonic case

The thermodynamic input are reported in table 6.2.

Input for SU2 and BL code	Value	Dimension
Ma_∞	0.1	[-]
$P_{T\infty}$	202650	Pa
$T_{T\infty}$	500	K
ϱ_∞	1.41	kg/m^3
MW	28.97	kg/kmol
γ	1.4	[-]
Prandtl	1 (constant)	[-]
μ	constant=1.7 10^{-5}	Pa s
Model	Perfect gas	[-]

Table 6.2: Thermodynamic and fluid properties of the free stream inlet for subsonic and transonic case

As we can see the free stream flow is incompressible since the Mach is very low. The inputs are selected carefully in order to reproduce the same conditions used for the construction

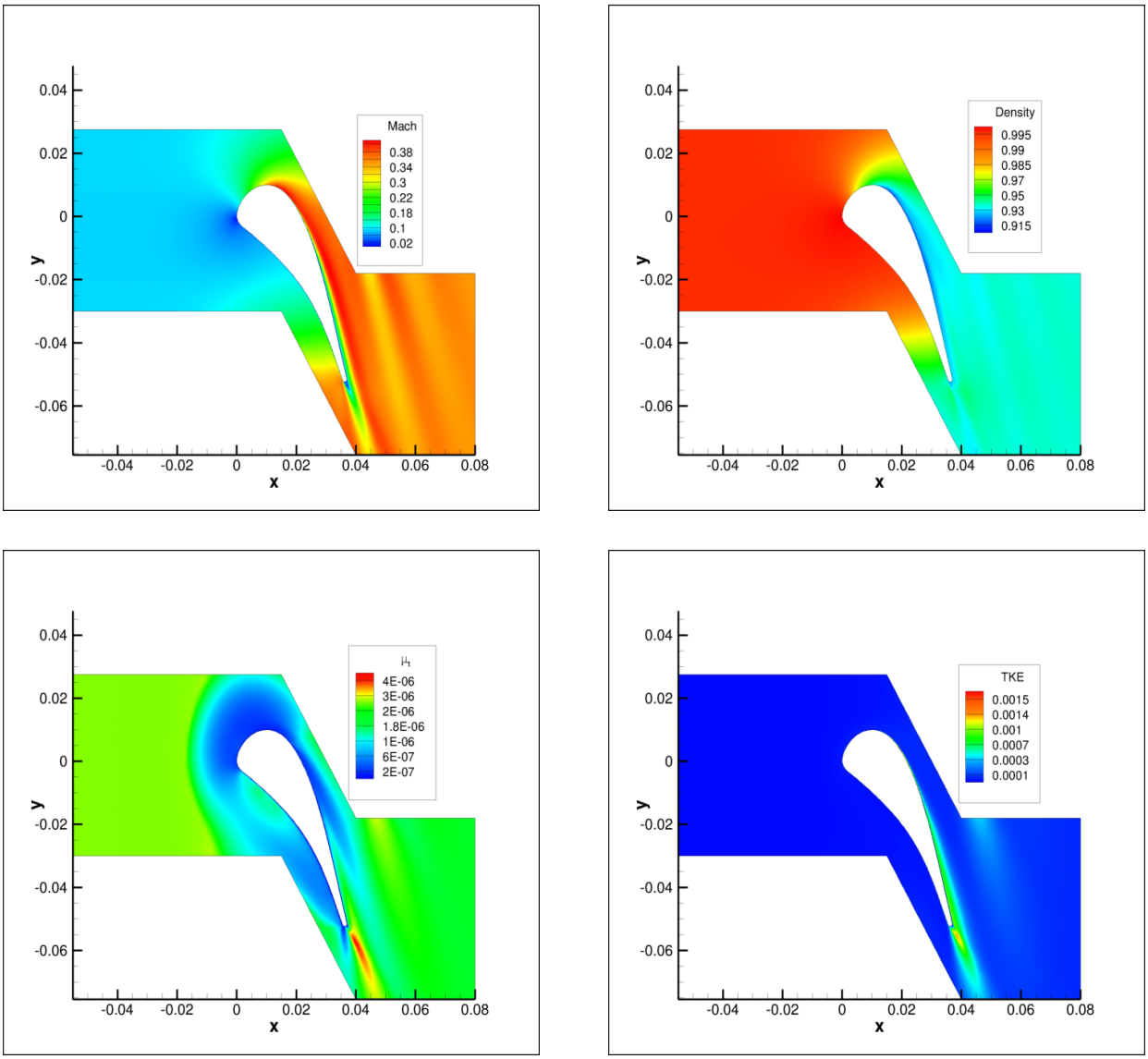

Figure 6.3: Contour results from SU2 and TecPlot: (a) Mach field, the maximum in under 0.4 ; (b) Density very low discrepancy: good assumption $\varrho \approx$ const; (c) Eddy viscosity: huge increase in the trailing zone therefore high source of losses; (d) Turbulent Kinetic Energy: final part of suction and trailing edge increase.

of the Smith chart (typical inlet condition of a low pressure turbine stage) 3. The post-processing of SU2 simulations serves as input for the other two methods.

The ensemble of figure 6.3 shows several interesting and useful concepts: the Mach number do not vary a lot, the maximum values is under 0.4 so we can assume the incompressible flow also looking the figure (b) since the density decrease only of 7 %. The last two figure deal with turbulence concept: (c) 6.3 shows the μ_τ eddy viscosity: is present in the entire field with the peak in the trailing edge: this type of losses belongs to other group so

we must avoid to include in our computation. The TKE (turbulent kinetic energy) is consistent with the last one quantity: it presents an explosion after the trailing edge. Because the turbulence happens from the domain's inlet, we start with turbulent flow also in our BL code.

BL code results

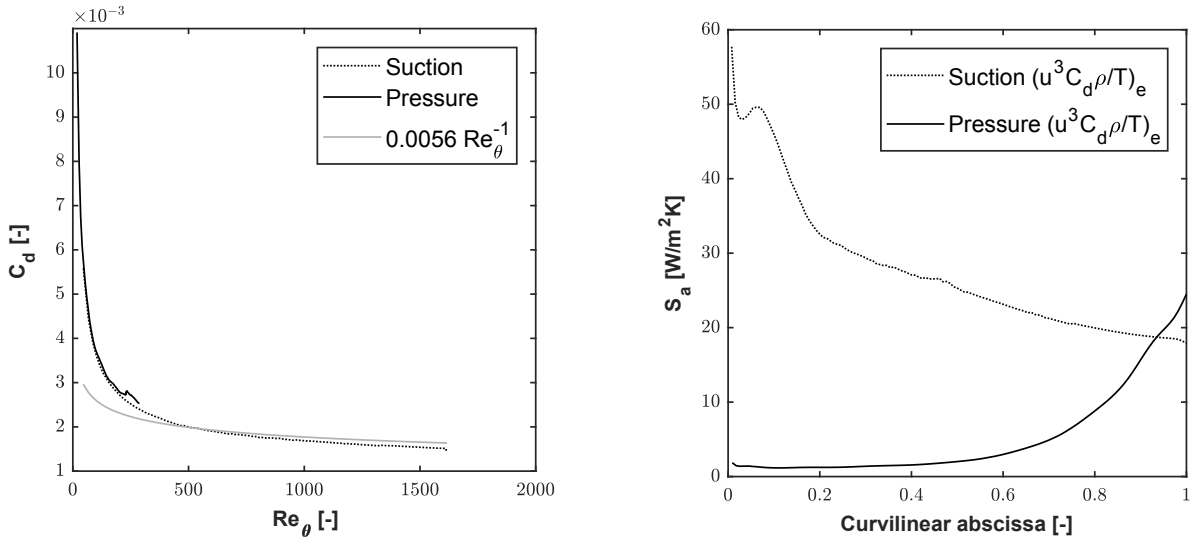

Figure 6.4: Subsonic blade: (a) Dissipation coefficient distribution on suction and pressure side; (b) Integrand computation on both blade's side for subsonic case. The suction, as quoted by Denton, is the major cause of losses due to higher velocity.

The results of BL code are summarized in two charts 6.4. The (a) is the behavior of dissipation coefficient along both surfaces, i.e suction and pressure side, and it is higher in the previous station and then it matches the power law. The plot (b) 6.4 deals with the entropy generation on suction and pressure. As quoted by Denton the major source is the suction side having higher speed. In the next three table 6.3 there are contained the factors for the loss coefficient for the three groups. And the final loss coefficients for

S_{in} [J/K]	0
S_{out} [J/K]	0.84
T_{out} [K]	492
H_{out} [J]	489854
H_{Tout} [J]	502237

$\overline{V}$ [m/s]	67.08
ΔV [m/s]	53.20
C_d	0.002

T_{out} [K]	492
(Suction) S [W/Km]	2.37
(Pressure) S[W/Km]	0.45
V_{out} [m/s]	156
Surface [m]	0.087

Table 6.3: Results of the three model to compute losses for LS89 blade (subsonic). (a) SU2; (b) Denton model; (c) BL code

the three models are in 6.4:

	SU2	DENTON	BL CODE
ζ_s	3.3 %	5.2 %	3.0 %

Table 6.4: Final results for subsonic LS89

It is necessary to spend some words to comment these results. The boundary layer code presents the lower losses since all the phenomena related to high streamline curvature, trailing edge mixing losses and stagnation point are discarded in principle (look fig. 6.2); the 1/5 of the surface is not take into account therefore, considering this facts, the losses perfectly match the SU2 results also because this latter contains the mixing losses. The Denton model gives the major losses. Even if the results could seem greater than the preliminary chart for incompressible case, 3.11 we must consider two fact:

- our study is made only on stator blade
- the geometry is not optimized

The second point deals with the length surface, pitch' s choice and the stagger angle which are already set by SU2 file mesh. Therefore is not an optimized geometry with respect to the flow angle.

6.2.2 Transonic case

The second and last study of this chapter is transonic blade case. It is important to verify what is the ability of the two model (Denton, BL code) to estimate this more complex situation. It is a nice test also for the C_d obtained in right way with boundary layer code (chapter 5) since, as we have presented in section 5.2 the Mach number and acceleration play an important role for air in terms of dissipation. The pressure ratio now is much higher and this impacts on the great acceleration along the profile. The Mach overcomes the sonic condition and the decrease in density is very strong now: no more incompressible behavior fig. 6.5.

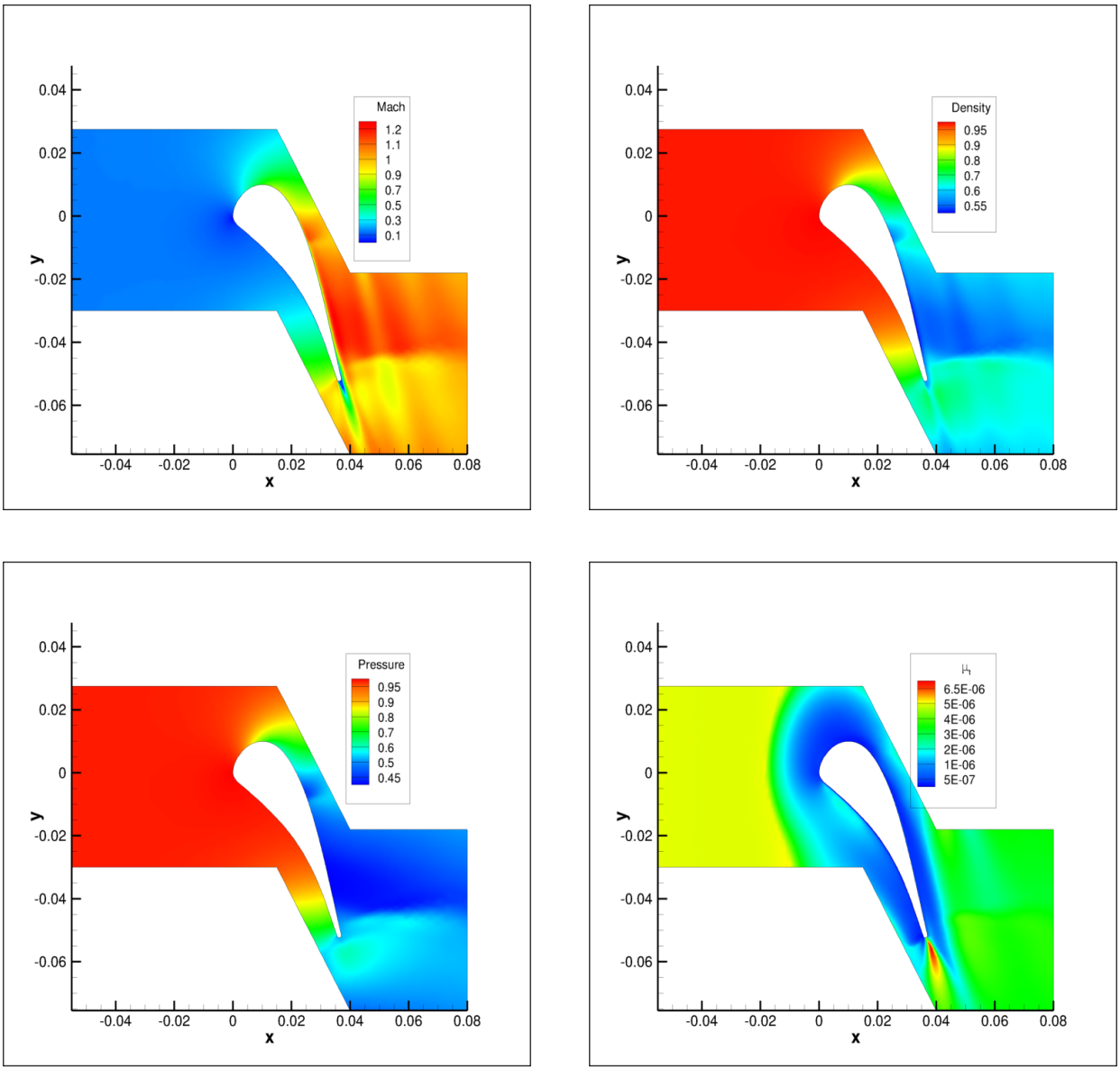

Figure 6.5: Contour results from SU2 and TecPlot for transonic blade: (a) Mach field, supersonic conditions are achieved ; (b) Density, strong decrease; (c) Pressure; (d) Eddy viscosity: huge increase in the trailing zone therefore high source of losses;

The approach to obtain the results is the same as before. There are different thermodynamic results from the SU2 program which means different input variables for the BL code and the Denton model. In the next three table are contained the results for the three groups 6.5.

S_{in} [J/K]	0
S_{out} [J/K]	6.31
T_{out} [K]	413.2
H_{out} [J]	415716.14
H_{Tout} [J]	502237

$\overline{V}$ [m/s]	147
ΔV [m/s]	142.5
C_d	0.002

T_{out} [K]	413.2
(Suction) S [W/Km]	20.7
(Pressure) S[W/Km]	19.3
V_{out} [m/s]	419.94
Surface [m]	0.087

Table 6.5: Results of the three model to compute losses for LS89 blade (transonic). (a) SU2; (b) ; Denton model(c) BL code;

BL code results for transonic blade

A before we point out the results given by our tool 6.6 The figure (a) 6.6 is consistent

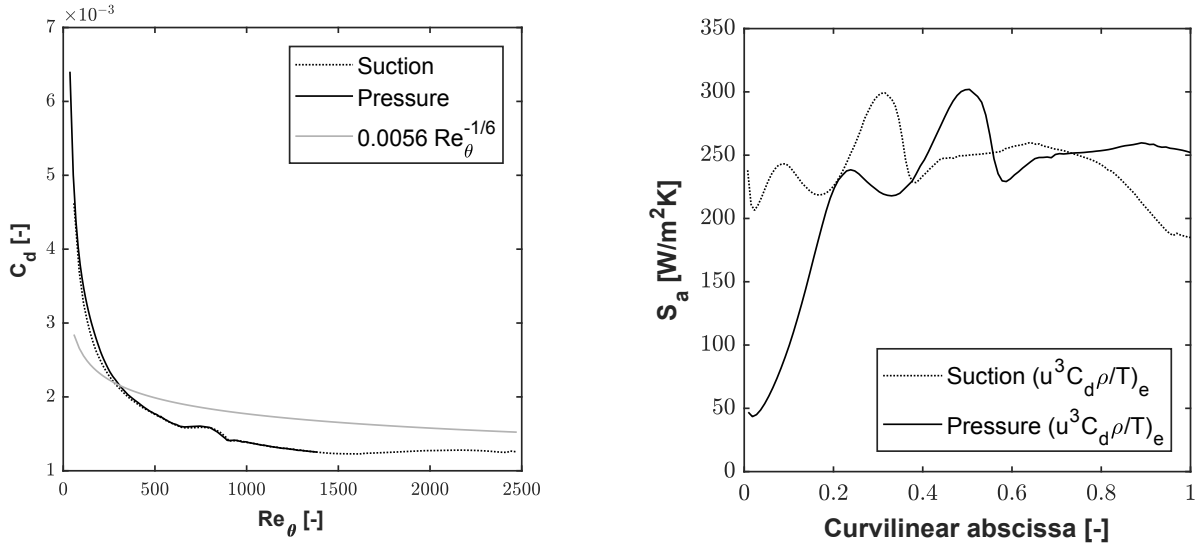

Figure 6.6: Features of transonic case for BL code calculation : (a) Dissipation coefficient; (b) Entropy generation on both sides.

with the results of section 4.3. Moreover on the transonic blade surfaces are coupled two effects: the pressure gradient and the compressibility ones and they both contribute in a reduction of C_d. Despite the C_d behavior the entropy generation per unit area is higher than supersonic case and the most important aspect is the similar values for both pressure and suction side. Now they contribute equally to the final losses. The final results are the following:

	SU2	**DENTON**	**BL CODE**
ζ_s	3.01 %	5.75 %	3.29 %

Table 6.6: Final results for transonic LS89

Final remarks

Denton model tends in general to overestimate the losses of the profile losses for two main reason: the velocity used to scale the entropy generation is the mean $\overline{V}$ which is in general lower for the exit one so it is a matter of definition. The second reason is substantial: the dissipation coefficient is fixed to 0.002 which is simply the upper limit, using the right one the losses decrease a little bit in particular at high speed flows.
The BL code captures very precisely the boundary state and it is the most sensitive to the changes. The results remain very close to the incompressible since even if the velocities are higher, the compressibility effect on C_d counteracts the negative effects due to higher velocities. The Denton model moreover requires the two velocity $\overline{V}$ and ΔV which derives from a simplified aerodynamic profile and they need the utilization of the conservation of momentum in tangential direction (based on a low speed formulation). As we can see in the central table 6.5 while the velocity on suction side is very high on the pressure side is very small (only 3m/s) which is very different with respect to the real profile given by SU2 and BL code. In fact looking at the entropy generation contribution 6.6(a) the aerodynamic profile change a little bit with the compressible effects (a) and above all the contribution of suction and pressure sides are equally. Therefore they have the same impact on the losses in contrast with low speed case.
Our code is in between of the other two tools and it is a positive aspects. We have to remember that the trailing edge phenomena are not included and a part of the surface's blade is excluded therefore quite higher results could exit from BL code in contrast to SU2 which take into account also this phenomenon.

Chapter 7

Conclusions and Recommendations

In this final part the main conclusion of this thesis work are summarized and further development/studies are proposed.

7.1 Conclusions

The main findings of this work are consequences of the research points: 1) what is the trend of the C_d for incompressible and compressible flows?; 2) What is the non-ideality effect on C_d for complex fluids (ORC)?; 3) What is the accuracy of our results with respect a common CFD code?
The following conclusion can be drawn:

1. With respect to incompressible and compressible studies:
    - The dissipation coefficient's trend can be represented by a power law of the type $0.173Re_\theta^{-1}$ at low speed (Ma < 0.3) for whatever fluid in laminar regime. Only the pressure gradient has a strong impact on it: accelerated flows are more dissipative.
    - For turbulent regime our analysis was more confined due to the complexity of the turbulence. However the incompressible formulation follow perfectly the fitting relation $C_d = 0.0056Re_\theta^{-1/6}$. Turbulent flow are intrinsically more dissipative than laminar: C_d 3-4 times higher. In this regime the deceleration close to separation point is the most dissipative scenario since the turbulent phenomena in outer layer increase a lot the shear stress so the entropy production.
    - Compressibility effects appears only for certain classes of fluids: simple and medium complexity. These fluids show a strong decrease of C_d with Mach number, more than 30 % at $Ma_e = 2$, and in general high change in transport fluid properties close to the wall; in contrast complex-heavy molecules such as siloxanes remain perfectly on all incompressible trends, i.e C_d, velocity profile

inside BL, shape factor and no deviation of thermo-physical properties inside the boundary layer. This concept is valid both for laminar and turbulent regime. The latter shows even more deviation (for air) because the Mach affects physical fluid properties and the eddy viscosity too.

2. non ideality effects are totally negligible for complex fluids. C_d shows no deviation from the incompressible law.

3. the results of profile boundary layer losses coupled with the correct C_d implemented in the Boundary layer code shows good agreement with the losses computed with SU2 (CFD). In this final point the general remarks are:

   In the chapter 6 for both the subsonic and transonic case the entropy coefficient (ζ_s) results are very close: BL code is in the order of 3 %, SU2 the same and quite higher for Denton formulation 5 %.

This thesis wanted establishing physical knowledge about the dissipation coefficient. Moreover in chapter 3 the applications of this parameter are shown in order to set up a profile losses chart for mean-line design. However the C_d is necessary not only for primary losses field but also for endwall (secondary) estimation, in other words it is necessary for whatever boundary layer phenomena computation in turbomachinery field (and whatever equipment which deals with fluid). Therefore this dimensionless group has a double function:

- from scientific point of view it is a source of boundary layer information; in particular it represents how dissipative is the layer and it is possible to estimate the fluid-dynamic regime (turbulent or laminar) knowing its order of magnitude.
- from applicative perspectives it is the base of physical based methods and in general calculation of losses in whatever boundary layer process

The physical-based profile loss model is able to describe all the phenomena in turbine stage such as the compressibility effects and the deviation from ideality gas state. The classical method (AM, DC, KO) fail in describing profile losses. The results of chapter 3 are:

- higher pressure ratio β_{TT} affects negatively the stage since the losses increase on the entire Smith's plane.
- the simple fluid are better in terms of boundary layer losses; the complex heavy show higher losses.
- the real gas nature, expressed by Z also tends to decrease the efficiency of the stage in terms of profile losses.

The loss formulation proposed by Denton are still valid and we can tell that the physical based approach in terms of profile losses is the best one for siloxanes or inversely the complex fluids are the most suitable category for Denton model since the parameters inside the boundary layers are almost constant.

7.2 Recommendations

Many works/efforts must be made in the future to extend the formulation of dissipation coefficient until a general understanding is achieved. It is important to divide the future development in three main categories:

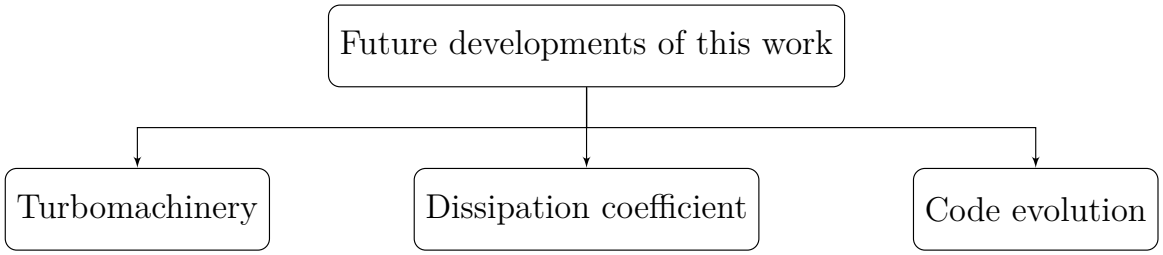

Figure 7.1: Three main categories of development of this work: applicative, physical and numerical

Turbomachinery

The first group of 7.1 "Turbomachinery" includes all the applicative concepts related to the loss models: new C_d for profile and endwall losses. In terms of profile losses a more realistic velocity distribution is in fig.7.2.

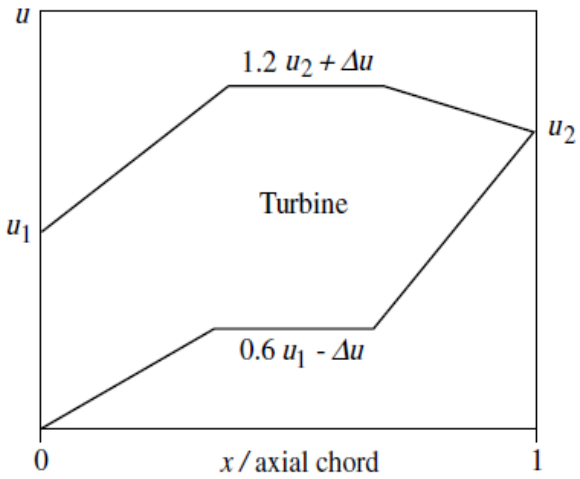

Figure 7.2: Realistic turbine velocity distributions along the blade [36, 26].

The acceleration affects the losses, probably there will be a general increase in all region of the Smith's charts due to acceleration flow across both suction and pressure side of the blade. Moreover this shape is derived from the common pressure distribution and it is very useful and convenient since it connects directly the velocity triangles with suction and pressure side velocities without the necessity to use a further relation (momentum

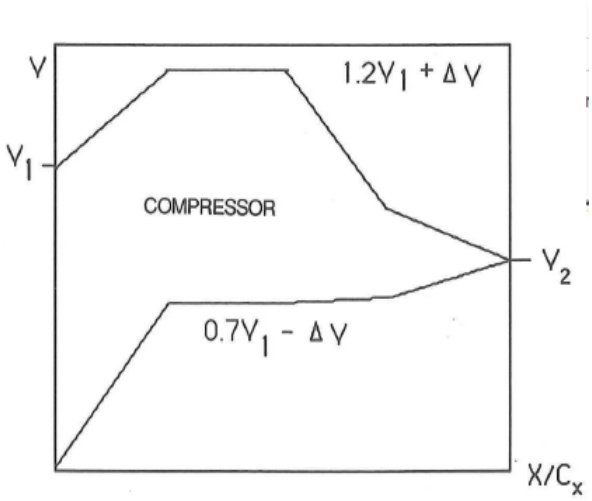

Figure 7.3: Realistic compressor velocity distributions along the blade. [36, 26].

conservation in tangential direction).
Other study that can be performed is for other type of turbomachines: the compressor.

The velocity distribution proposed by Denton is presented 7.3.

Dissipation coefficient

The major improvements can be done in this field. In particular:

- heat transfer process in boundary layer are very important. The impact on C_d should be crucial as mentioned in chapter 2 2.27. More precisely the cooling or heating phenomena can respectively decrease or increase the generation of entropy of particle and in the end the C_d. Moreover the non-adiabatic situations are directly correlated with the so called "control of boundary layer", a study field which investigates the fluid mechanics regime function of the heat exchange.
- the unsteadiness characteristics also change a lot the distribution of C_d on the chart. The group of Denton himself published a paper on this [52, 4]. In the figure 7.4 it is reported.

  The great deviation is in turbulent region since the stochastic behavior appears. In laminar part the concentration of experimental results is very good therefore the theoretical analysis has a good response.

Code enhancement

In terms of numerical development, the boundary layer code present margin of improvements:

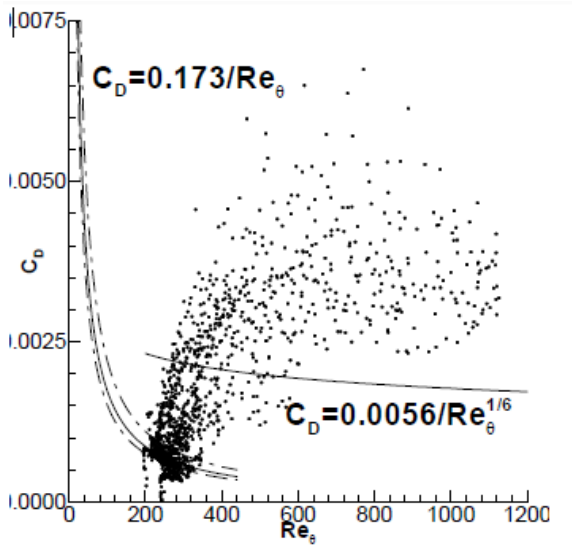

Figure 7.4: Experimental results (points) of dissipation coefficient in unsteady phenomena. [4] from Whittle Lab.

- transition model between laminar and turbulent improvement regime because Wazzan model is accurate for subsonic flat plate boundary layer.
- the original structure is based on the Clutter-Smith equations [39, 50] which are suitable for axial-symmetric body with not elevated streamline curvature.
- turbulence model can be extended to 1-equation to 2-equation following the last work of Cebeci [51, 79]. This study could be quite difficult since the core structure of Keller box matrix must be changed from 5x5 to 6x6 (for example Spalart-Allmaras) or 7x7 (k-ε or k-ω)

Appendix A

The critical phenomena in boundary layers

In thermodynamics, a critical point (or critical state) is the end point of a phase equilibrium curve. The most prominent example is the liquid-vapor critical point, the end point of the pressure-temperature curve that designates conditions under which a liquid and its vapor can coexist. At higher temperatures, the gas cannot be liquefied by pressure alone. At the critical point, defined by a critical temperature Tc and a critical pressure pc, phase boundaries vanish.
In ORC turbine application there is the possibility to work in non-ideal gas zone but never in critical point. The example of this statement we will cite the following work [16]. However for othe new technology such as super critical CO_2 turbine (or compressor) the critical point it is under the attention of the designer. In this state some assumption made for this work could collapse due to the extremely high explosion of transport properties (and therefore the Prandtl number) and the form of reological expression of the newtonian shear stress must be taken in its most general formulation [37]:

$$\tau_{ij} = \mu(\frac{\partial u_i}{\partial x_j} + \frac{\partial u_j}{\partial x_i}) + \lambda\frac{\partial u_k}{\partial x_k} - \delta_{ij}p \tag{A.1}$$

To clarify everithing: μ is the dynamic viscosity and it is associated by the cross partial derivatives in tensorial notation due to the shear stress (deformation part). This is the common part used in whatever application. The rest is the bulk viscosity λ which multiply the divergence of the velocity in physical terms the dilatation/contraction of the particle without any changes in form.[1] The last part is present only for the diagonal terms of the

[1] this is a general concept of continuum mechanics so it is present also in solid field: the bulk viscosity is the so called Lamè constant and the general form is:

$$K = \lambda + 2/3\mu$$

in elasticity theory μ is the shear modulus and K is the so called bulk modulus

tensor since it contains the delta of Kronecker with the respective properties.

The thermodinac concept are shown in figure A.1. The charts represents the close-critical point for CO_2 more precisely at 80 bar. About the reference temperature are computed at the same pressure and 300 K (ambient). Then each values is scaled with the respect its reference: the explosion in particular of specific heat describes the peculiar behaviour of this zone.

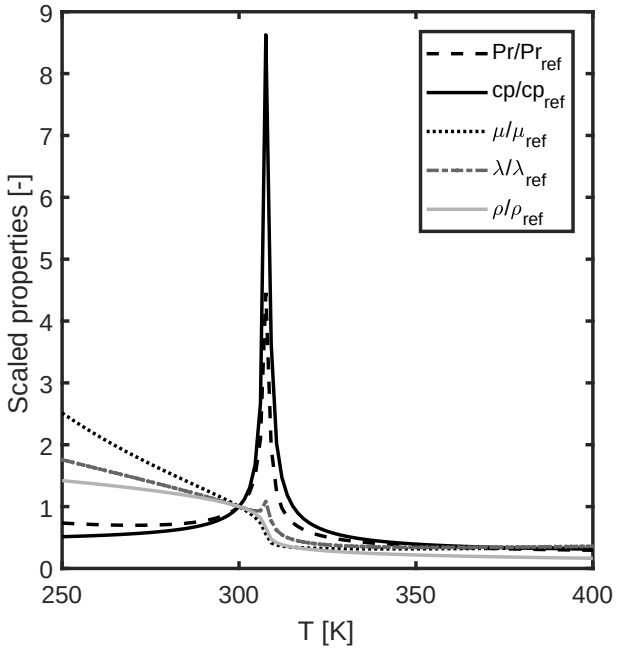

Figure A.1: Trend of the fluid transport properties close to crtical point scaled by the reference values (80 bar and 300 K): Pr (Prandtl number), cp (specific heat), μ dynamic viscosity, λ thermal conductivity and ϱ density

In terms of dissipation coefficient, our standard formulation does not show any deviation with respect to ideal gas zone. The fact is that to show the impact of trans critical passages we must set the critical point inside the layer and not on the edge or in free stream flow: this is quite complex exercise. To explain this sentence we must think in terms of ratio: dissipation coefficient (and in general all the boundary layer parameters) is expressed in terms of:

$$\frac{\text{inside quantities}}{\text{edge quantities}}\,, \tag{A.2}$$

therefore fixing the pressure along vertical coordinate ($\frac{\partial P}{\partial y} \approx 0$) only temperature can change the thermodynamic state: therefore in adiabatic flat plate the subsonic case is not affected by any change (P,T are constant inside the layer) supersonic case as shown in this thesis are affected only for medium- simple molecules but simple like helum xenon

has crtitical point outside common insudtrial purposes. In the end water or CO_2 could be interesting candidate but with heat transfer phenomena in order to put the critical point inside the layer.

Appendix B

Structure of the BL code and its general utilization

As always told the Matlab code [45] is the instrument through which all the results have been posible. Int this appendix the most important frafments are presented. Moreover a brief series of instruction will be given for a ideal user.
In chapter 2 a general scheme and overview is given. The basic script (running script) is the file BLAYER which call all the functions, structures, and computations.

```
[style       = Matlab-editor,
basicstyle = \mlttfamily,]
%% The program BLAYER is segmented into three principal parts; the subroutines INPUT,
% PRECAL, TURBLN. These, in turn, call several other subroutines.

clear all
clc
close all

tic % start timing

%% Case
INPUT_case_FlatPlateforcomputation
%INPUT_case_FlatPlate;
% INPUT_case1400_old;
% INPUT_NACA0012_old; %This reads in and prints the input data and checks for errors.
% INPUT_NOZZLE_CURVEDWALL_old; INPUT_NOZZLE_CURVEDWALL_INP2;

%% Precalculation of parameters that remain constant during calculations
[propsE,SgP,BLC]=PRECAL_old(OPT,KVPM,KSMTH,KSPLN,BWG);

%% Solving the laminar and turbulent BL equations using Keller's Box method []
and calculating the BL characteristics/parameters
[solTURB,solgTURB,FPropsTURB,BLTURB]=TURBLN_Rich_adapted_1(propsE,BLC,OPT,tr); %NO_Rich

toc % end timing
```

It is only a "push botton file" which allows the running. An estimation of time is present through the command tic-toc this is very important to estimate the time cconsuming for complex case like high number of cells and real gas study.
The user must insert the input of the boundary layer in the $Input_file$ [45]. In particular a large range of options are avaible: first the thermodynamic study of fluid is set through the command OPTION:

- **OPTION 1** : the incomprresible perfect gas. Valid only for very low Mach flow without heat transfer. There is not any variation of fluid properties (c_p, λ, μ) moreover the Pradntl number is set equal to one everywhere. The energy equation does not take into account the diffusivity phenomena.
- **OPTION 2** : perfect compressible gas. In particular the thermodynamic definition is calorimetric perfect, in other words the specic heat is constant but the other properties are variables. In the optyc of viscosity and thermal conductivity, we can select the invocation of flui-libraries or the faster Southerland law. Naturally the Prandtl is variable and the energy equation is strictly coupled with the momentum.
- **OPTION 3** : the most general environment since it happens the coupling between the code od the fluidlibraries FLUIDPROP [6]. There are seven libraries avaible but for this work only the NIST database has been utilized. In this way all the propertu in the thermodynamic could be investigate.

The second choice is about the flow input, a large number of possibilities is avaible. The string is characterized by name KVP:

- **KVPM 1** The distribution of pressure at the edge is given as input. This case is formulated for studies characterized by pressure ratio knowledge across the airfoil/-plate. Only checked and debugged in this work.
- **KVPM 2** The input is the velocity profile along the edge. This is a typical choice for a boundary layer analysis. This selection has been used for incompressible preliminary studies and for verification and validation of the code with respect to standard case like Götler, Blasisu, Howarth, Cohen Reshotko : for more detail see [38]
- **KVPM 3** : The most suitable approach in terms of turbomachines studies and aerodynamic application since the Mach number distribution at the edge is given as input. All the studies presented in this report have been made through this appoach in order to del with dimensionless quantities.

The following step is the construction of the flat plate geometry: X coordinate varies between 0 and n (a good choice is setting a unitary length) with whatever number of station, this selection will impact on the time required by the code to compute the boundary layer phenomena.
Once we have selected what type of profile input will be utilized, it is required the computation of free stream total quantities. For a stationary adiabatic system the Total enthalpy will be constant in eulerian flow (edge and free stream). In particular Total temperarure and pressure must be insert. It is possible inserting also static ones. In the end the energy boundary conditions must be insert in order to close the problem in term of trensport equation (Navier -Stokes). The universl typologies of boundary condition are three [71, 80] but in this code the Robin mixed closure is not present. Therefore the possible thermal settings are:

- **BWG 0** : Temperature of the wall is the boundary condition. It is possible to select whatever wall temperature distribution (naturally is a vectorial form with the same length of X plate coordinate). A particuar case is constant temperature so an isothermal study is created. From mathematical point of view this represents the Dirichlet condition, first species.
- **BWG 1** : Heat flux at the wall. It is the other From mathematical point of view this represents the Neumann condition, second species derivative is explicitated.

To conclude, the last option is about transition:

- **tr 0** : the flow approaches leading edge in laminar regime. If Reynolds at the edge will overcomes the transitional threshold the turbulent code will be activated.
- **tr 1** : It is an imposition for which the flow regime is turbulent from the beginning.

Certain conditions are added in the last version of the code in order to treat the numerical problem related to stagnation point (for aerfoil studies) since it is a mathematical singularity in the which affects stability.
Here the input file is plotted:

```
%     Input                %

%% Subroutine INPUT (reads and prints) provides all input data. It also checks for errors in the
% input.
global PTZ TTZ UPMACH X Y PRES UE ME TWAL QWAL MM R GAM
global FPid
%% CASE
%-----------------------------------------------------%
% Define Case
%-----------------------------------------------------%
% Case is integer indicating case being used
% Case 1400 ..........................................1
% NACA0012 ...........................................2
% NOZZLE CURVED WALL .................................3
% NOZZLE FLAT WALL ...................................4
% Case Flat plate Denton(preliminary).................5
CASE=6;
%% INPUT
%-----------------------------------------------------%
% Define the fluid and the thermodynamic model
%-----------------------------------------------------%
% OPT = integer from 1 to 3 indicating how fluid properties are computed
%       1 incompressible air,
%       2 ideal air but compressible + (Cinf,C=1,Pr=1),
%       3 real gas properties;
OPT=3;
if OPT==1 || OPT==2
% General Parameters
% MM = Molecular Mass
%Type ideal fluids
%FLUID            MM              GAMMA
%Air                 28,97                1,399695205
%Argon   Ar          40              1,666614015
%IsobutaneC4H10 58                   1,094114121
%CarboxideCO2    44,01           1,288419786
%(R-22)          86,47           1,173726211
```

```
%Ethane C2H6     30                  1,188406112
%EthylenC2H4     28                  1,240814787
%Helium He           4               1,666528829
%n-HeptaneC7H16 100                  1,05298383
%n-HexaneC6H14   86                  1,061939516
%HydrogenH2      2                   1,405268392
% Krypton Kr     84                  1,666805685
% Methane CH4    16                  1,303529913
% Neon  Ne           20              1,666315103
% n-PentaneC5    72                  1,074402471
% Propane C3H8   44                1,127351474
% PropyleneC3H6 42                   1,148171964
% Steam H2O          18              1,328824878
% TetrachlCCI4   153,82            1,110883597
% (R-134a)           102,03              1,108371197
% (R-143a)           84,04               1,119167125
% Xenon Xe           131             1,666677893
% Toluene To     92,14             1,05572909
% MM             162,379           1,027641833
% MDM            296,533           1,013531784
% MD2M           310,687           1,012313436

MM=28.97; % choice of fluid
FPid.MM=MM;  %%% [kg/kmol]
% R = specific gas constant, [kJ/mol/K]
%FPid.R=0.2881966;
FPid.R = 8.314472/MM; %[kJ/kg/K]
% GAM = specific heat ratio, gamma
FPid.GAM=1.4;%Cp/Cv; %%% [-]
%FPid.Pr=1.0; %%% [-] Pr= mu*cp/k=nu/alpha
FPid.Pr=1; %ideal fluid
FPid.ksu=110.3333; %%% [K], reference temperature for using Sutherland's Law
elseif OPT==3
Init_FluidProp
%  Choose the fluid and the thermodynamic model
Model = 'REFPROP';
% number of substances in the mixture; set 1 for pure fluid
nCmp  = 1;
% name of the pure fluid or of substances in the mixture;
Cmp   = 'D6';
% molar fractions of substances in the mixture; set [1 0] for pure fluid
Cnc   = [1 0];
% Define the thermodynamic model in Fluidprop
ErrorMsg = invoke(FP,'SetFluid_M',Model,nCmp,Cmp,Cnc);
end
%-----------------------------------------------------%
% Geometry
%-----------------------------------------------------%
%---------This data should be read from a txt file
% X = array of X-coordinates of input stations, ft; m (see figs. 4 and 5)
%%% X=0.3048*[0 0.025 0.0625 0.125 0.25 0.375 0.5 0.75 1 1.25 1.3 1.35 1.4 1.45 1.5...
%%%     1.55 1.6 1.65 1.7 1.75 2 2.25 2.5 2.75 3.0 3.25 3.5 3.75 4 4.25 4.5...
%%%     4.75 5];
%X=1:0.05:2;   %%% [m]
X=0:0.05:0.5;
% Y = array of Y-coordinates of input stations, ft; m (see figs. 4 and 5)
%%% Y=0.3048*[0 0.05765 0.0947 0.13075 0.17775 0.21 0.23415 0.26725 0.28685 0.29705...
%%%     0.2981 0.2989 0.2996 0.29995 0.3001 0.2995 0.2996 0.299 0.29825 0.29735...
%%%     0.29105 0.27905 0.2647 0.2476 0.22815 0.20685 0.1832 0.15805 0.13115 ...
%%%     0.10275 0.0724 0.04035 0.0063];
Y = zeros(1,length(X));   %%% [m]
%-----------------------------------------------------%
% Free stream data (total conditions are mandatory)
%-----------------------------------------------------%
% KVPM = integer from 1 to 5 indicating which form of surface flow distribution is
%        given as input:
%        Pressure ..... 1
%        Free-stream velocity ..... 2
%        Free-stream Mach number ..... 3
```

```
KVPM=2;
% KSMTH = integer (0, 1, 2, . . . ) indicating number of times distribution of freestream
% velocity is to be smoothed prior to computation of surface gradients
KSMTH=0;
% PTZ = inlet or upstream relative total pressure (station O), [N/m2]
PTZ=; % [Pa]
Pstatic_in=;
Tstatic_in=;
% TTZ = inlet or upstream relative total temperature (station 0), T'_0, [K]
TTZ=639; %%% Guess, check in Coles; Old value: 600/1.8; % [K] %%% what to do with this?
% UPMACH = inlet or upstream Mach number relative to surface, M_0
UPMACH=2; Change by iteration (running model and check value)! see also PRECAL [-]
% PRES = array of static pressure P at X-Y input stations, [ N/m2]
PRES=ones(1,length(X)); %%% [Pa]
%PRES = linspace (a,b,length(X));
% UE = array of free-stream velocities ue relative to surface at X-Y input stations,
% [m/sec]
%---------This data should be read from a txt file

UE = UI.*(1-X);    %%% [m/s] Howarth decelerating profile
% C=c;
% m=d;
%UE = C*X.^m; % similar profile solution =solution (eta) constant profile along X
%UE=linspace(20,20,length(X)); %non similar case
% ME = array of free-stream Mach numbers M_e relative to surface at X-Y input
% stations

ME=linspace(a,b,length(X));
%-----------------------------------------------------%
% Temperature or Heat Flux at wall
%-----------------------------------------------------%
%TWAL = array of static wall temperatures at X-Y input stations,  [K] (If TWAL is
% unknown and surface is nearly isothermal, the value of TTZ may be used
% for TWAL.)
%QWAL = array of static wall temperatures at X-Y input stations.
% However, the free stream flow is always adiabatic.
% Note that if QWAL is imposed as B.C. and it different from zero
% it is necessary to know Twall to estimate gw'
% TWAL=600/1.8*ones(length(X),1); %%% [K]
QWAL=zeros(length(X),1); %%% [W/m2] = [J/m2/s], heat Flux
% BWG integer (0 or 1) indicating Boundary condition of the energy equation:
%          Temperature Distribution ..... 0
%          Heat Flux ..... 1
BWG=1;
%-----------------------------------------------------%
% Calculation options
%-----------------------------------------------------%
% Laminar and/or Turbulent Calculation options
%-----------------------------------------------------%
% tr = integer (0 or 1) laminar-transition-turbulent calculation or fully turbulent calculation:
%          Start with Laminar (transition has not yet occurred) ..... 0
%          Fully Turbulent (transition has already occurred) ..... 1
tr=0;\\
```

Once the input are set, the next step is developing all the quantities for the edge. For incompressible and in general perfect gas the isentropic ideal gas relations are used. For the general real study the FluidProp is used: for a pure substance only two thermodynamic variables are needed to define complitely the state. The algorithm depends by the input flow used (KVPM). The file is called PRECAL and is the base to compute all the fluid-properties in boundary layer.

```
function [propsE,SgP,BLC]=PRECAL_old(OPT,KVPM,KSMTH,KSPLN,BWG)
%% Subroutine PRECAL performs all the calculations required prior to the solution of
% the boundary-layer differential equations. All the variables it computes remain constant
% for the remainder of the program.
global FP FPid
```

```
global PTZ TTZ UPMACH X Y PRES UE ME TWAL QWAL MM R GAM
%% Thermodynamic properties at station 0
% TSZ static temperature at station 0
% RHTZ (Total) Density
Tref=0;%K - used only for cases OPT==1 & OPT==2
% The influence of Tref is only on the absolute value of g and gw',
% but it does not influence the boundary layer quantities
% Computational time grows as Tref ?
%COMPUTATION OF INLET QUANTITIES
if OPT==1
MM=FPid.MM; %[kg/kmol]
R=FPid.R*1000; %%% [J/kg/K]
GAM=FPid.GAM;  %%% [-]
CpId=R*GAM/(GAM-1); %%% [J/kg/K]
TSZ=TTZ/(1+(GAM-1)/2*UPMACH^2); %%% [K];  (unknown -> iterate))
RHTZ=PTZ/R/TTZ; %%% [kg/m3]; FIRST CHANGE WITH RESPECT OPT==2
hTZ=CpId*(TTZ-Tref)/1000; %%% [kJ/kg]
hSZ=CpId*(TSZ-Tref)/1000; %%% [kJ/kg], Changed TTZ to TSZ
PSZ=(TTZ/TSZ)^(GAM/(1-GAM))*PTZ; %%% [Pa]
RHSZ=PSZ/R/TSZ;

elseif  OPT==2
R=FPid.R*1000; %%% [J/kg/K]
ksu=FPid.ksu;  %%% [K]
GAM=FPid.GAM;  %%% [-]
CpId=R*GAM/(GAM-1); %%% [J/kg/K]
TSZ=TTZ/(1+(GAM-1)/2*UPMACH^2); %%% [K];400 (unknown -> iterate))
RHTZ=PTZ/R/TTZ; %%% [kg/m3]; (can this formula be applied to both total and static conditions?)
hTZ=CpId*(TTZ-Tref)/1000; %%% [kJ/kg]
hSZ=CpId*(TSZ-Tref)/1000; %%% [kJ/kg], Changed TTZ to TSZ
PSZ=(TTZ/TSZ)^(GAM/(1-GAM))*PTZ; %%% [Pa] OK CONTROLLATO
elseif OPT==3  %%%% NOT CHECKED!!! %%%%
hTZ=FP.Enthalpy('PT',PTZ/10^5,TTZ-273.15);% total enthalpy at station 0, [kJ/Kg]
sZ=FP.Entropy('PT',PTZ/10^5,TTZ-273.15);% entropy at station 0, [kJ/Kg/K]
PSZ=PTZ;%Pa
Pnew=0;
while abs(Pnew-PSZ)>1e-3
Pnew=PSZ;
[cZ,ErrorMsg] = invoke(FP,'SoundSpeed','Ps',Pnew/10^5,sZ);% speed of sound at station 0
hSZ=hTZ-(cZ*UPMACH)^2/2/1000;
PSZ=FP.Pressure('hs',hSZ,sZ)*10^5; % static enthalpy at station 0
end
TSZ=FP.Temperature('hs',hSZ,sZ)+273.15; % static T at station 0
RHTZ=FP.Density('PT',PTZ/10^5,TTZ-273.15);%
%
%
%
elseif KVPM==3 %input: Free-stream Mach number
if OPT==1
TSE=TTZ./(1+ME.^2/2*(GAM-1)); %OK THE COMPRESSIBLE EQUATION ARE VALID ALSO FOR INCOMPRESSIBLE
AE=sqrt(GAM*R*TSE); %DEFINITION OF MACH NUMBER
PRES=(TTZ./TSE).^(GAM/(1-GAM))*PTZ; %ISOENTROPIC RELATION
hSE=TSE*CpId/1000; % (ERROR CORRECTED)
elseif OPT==2
TSE=TTZ./(1+ME.^2/2*(GAM-1));
AE=sqrt(GAM*R*TSE);
PRES=(TTZ./TSE).^(GAM/(1-GAM))*PTZ;
hSE=TSE*CpId/1000;
elseif OPT==3
for i=1:length(PRES)
Pnew=0;
PRES(i)=PTZ;
while abs(Pnew-PRES(i))>1e-3
Pnew=PRES(i);
[AE(i),ErrorMsg] = invoke(FP,'SoundSpeed','Ps',Pnew/10^5,sZ);% speed of sound at station 0
hSE(i)=hTZ-(AE(i)*ME(i))^2/2/1000;
PRES(i)=FP.Pressure('hs',hSE(i),sZ)*10^5; % static enthalpy at station 0
end
TSE(i)=FP.Temperature('Ph',PRES(i)/10^5,hSE(i))+273.15;
end
```

```
end
UE=ME.*AE;
POPTZ=PRES./PTZ;
end
%
%
%
%
elseif OPT==3 %%% NOT CHECKED %%%
for i=1:length(PRES)
propsE.rhoE(i)=FP.Density('Ph',PRES(i)/10^5,hSE(i));
propsE.muE(i)=FP.Viscosity('Ph',PRES(i)/10^5,hSE(i));
propsE.rhoE(i)=FP.Density('Ph',PRES(i)/10^5,hSE(i));
propsE.SOSE(i)=FP.SoundSpeed('Ph',PRES(i)/10^5,hSE(i));
propsE.GAMMAE(i)=FP.Gamma('Ph',PRES(i)/10^5,hSE(i));
end
end
```

The other files presented in this Appendix are the FluidProperties and the Output:

```
function props=FluidProperties2(FP,solEE,sol,UE,HE,PE,it,eta,propsE,opt,ii)
% enthalpy J/kg Cp J/kg.K
global gw0
% he=HE-UE^2/2;
he=propsE.hSE(ii)*1000;
Lmax=length(eta);
f1=sol.uj;

if it==1
for i=1:Lmax
g(i)=gw0+(1-gw0)/eta(end)*eta(i);%da cambiare
end
else
g=solEE.gj;%% da cambiare
end
h=g*HE-(f1*UE).^2/2;

if opt==1 || opt==2 %Ideal and compressible fluid
ksu=110.3333;
MM=28.97;
R=8.314472/MM;%kJ/kg.K
GAM=1.4;
cp= R*GAM/(GAM-1)*1000;%J/kg.K
Tref=0;
Te=he/cp+Tref; %ok consistet with precal
T=h/cp+Tref;
%lambda=(he/cp+ksu)/(h(1)/cp+ksu)*sqrt(h(1)/he);%%mu_w/mu_e
end

for i=1:Lmax
if opt==1 %incompressible fluid
props.C(i)=1;
props.rhoR(i)=1; %constant: is the density ratio
props.Pr(i)=1;% constant
elseif opt==2 %Ideal but compressible
props.rhoR(i) =T(i)/Te;  %rho_e/rho Cebeci 1974 7.3.11
props.mu(i)=FP.Viscosity('PT',PE/10^5,T(i)-273.15);%h(i)/1000); %
props.C(i)=props.mu(i)./(props.rhoR(i).*propsE.muE(ii));
props.mu_ratio(i)=props.mu(i)./propsE.muE(ii);
props.lambdacond(i) =FP.ThermCond('PT',PE/10^5,T(i)-273.15);%h(i)/1000);
props.Pr(i)=cp*props.mu(i)./props.lambdacond(i); %along 11 station vertical
elseif opt==3 %Real gas
props.rhoR(i) =propsE.rhoE(ii)/FP.Density('Ph',PE/10^5,h(i)/1000);
muR =FP.Viscosity('Ph',PE/10^5,h(i)/1000)/propsE.muE(ii);
props.C(i)=muR/props.rhoR(i);
lambdacond = FP.ThermCond('Ph',PE/10^5,h(i)/1000);
CpS=FP.HeatCapP('Ph',PE/10^5,h(i)/1000);%kJ/kg
Pr=CpS*1000*FP.Viscosity('Ph',PE/10^5,h(i)/1000)/lambdacond;
```

```
props.Pr(i)=Pr;
end
end
props.eta=eta;
props.h=h;
props.Eckert_inside=((f1*UE).^2)./(cp.*Te);% the perfect model is fixed everywhere (in Precal)
props.Eckert_inside2=((f1*UE).^2)./(cp.*T(1));
z=()./();
end
```

The fluid properties file is very important since it allows to compute whatever properties for whatever model (ideal gas or real gas) inside the boundary layer. The approach has a general validity since all fluid transport properties (ψ) is computed on the follwing basis:

$$\psi = \psi(P_e, h) \; ; \tag{B.1}$$

Notice that the first input is the pressure (constant along the boundary layer) and the second one is enthalpy: this functional relation is general and it does not require any simplification. Therefore each node inside the layer has all this properties defined and also the Prandtl number.

The final script presented is the Output file which contains the implementarion of the boundary layer parameters (also C_d).

```
function BL=BL_OUTPUT_adapted(propsE,S,solfin,solfing,FProps,ii,opt,P,gw)
% not compatible with LAMNAR

% fluid properties (copied from EDDY.m)
% props.rhoR= rho_e/rho %%% (c) Cebeci (1974) formula 7.3.11a
rho=1./(FProps.rhoR/propsE.rhoE(ii)); %%% [kg/m3]
% props.C= rho*mu/(rho_e*mu_e) %%% [-]
mu=FProps.C./rho*propsE.rhoE(ii)*propsE.muE(ii); %%% [kg/m/s]
nuk=mu./rho; %%% [m2/s]

HE=propsE.HSE(ii)*1000; %%% [J/kg], total enthalpy
Nx=sqrt(propsE.muE(ii)*propsE.rhoE(ii)*S(ii)/propsE.UE(ii)); %
 [kg/m2] Clutter transformation 6.4

% y coordinate
BL.y=Nx*cumtrapz(solfin.x,interp1(FProps.eta,FProps.rhoR,solfin.x))/propsE.rhoE(ii);

% [m] equation 6.104
BL.nu=nuk;
%%% NEWLY ADDED %%% NOT NEEDED FOR CASE NACA0012
if P<=0 || gw <= 1
for i=1:length(solfin.uj) %%% actually most of the time only end-1 value is changed
if solfin.uj(i)>1.000001
solfin.uj(i) = 1;
end
end
end
%%% NEWLY ADDED %%%%%%%%%%%%%%%%

% BL thickness
[mm,am]=max(solfin.uj);
etainf=solfin.x(end);
etaref=[0:0.001:etainf];
solref.uj=interp1(solfin.x,solfin.uj,etaref);
% rhoR=interp1(solfin.x,FProps.rhoR,etaref);
% y=Nx*cumtrapz(etaref,rhoR)/propsE.rhoE(ii); %%% [m], ADDED for 2nd plot
```

```
if mm<1.000001 %%% comment this, and spikes in BL thickness will disappear
vfref=find(solref.uj>=0.99);
BL.deltaeta=etaref(vfref(1));
BL.delta=Nx*trapz(etaref(1:vfref(1)),interp1(FProps.eta,FProps.rhoR,etaref(1:vfref(1))))/

propsE.rhoE(ii);
else          %%%
[mmref,amref]=max(solref.uj);        %%%
indref=[amref:length(etaref)];       %%%
thresref=min((0.9+0.1*mmref),1.01); %%%%%
vfref=find(solref.uj(amref:end)<=thresref); %%%
BL.deltaeta=etaref(indref(vfref(1)));%%%

end           %%%

% thermal BL thickness
vft=find(abs(FProps.h-propsE.hSE(ii)*1000)<=20);
cond2=0;
ite=0;
if length(vft)>1
while cond2==0;
cond=(vft(end-ite)-1~=vft(end-ite-1));
if cond==1
break
end
cond2=(ite==length(vft)-2);
ite=ite+1;
pos=length(vft)-ite;
end
elseif length(vft)==1
pos=1;
else
disp('probably it is necessary to increase etamax')
diff=min(abs(FProps.h-propsE.hSE(ii)*1000));
pos=1;
vft=length(FProps.h);
end

% displacement thickness
BL.delta_ast_ad=trapz(etaref,(interp1(FProps.eta,FProps.rhoR,etaref)-solref.uj)); %
BL.delta_ast=Nx/propsE.rhoE(ii)*BL.delta_ast_ad; %
BL.delta_ast_ad_test=trapz(etaref,(1 - solref.uj./interp1(FProps.eta,FProps.rhoR,etaref))); % test
BL.delta_ast_test=Nx/propsE.rhoE(ii)*BL.delta_ast_ad_test; % test
BL.delta_ast_k_ad=trapz(etaref,(1-solref.uj)./

(interp1(FProps.eta,propsE.rhoE(ii)./FProps.rhoR,etaref))); %%% [m3/kg], kinematic
BL.delta_ast_k=Nx*BL.delta_ast_k_ad; %%% [m], , (page eq. 6.102 in Clutter)

BL.theta_ad=trapz(etaref,solref.uj.*(1-solref.uj)); %%% [m3/kg]
BL.theta=Nx/propsE.rhoE(ii)*BL.theta_ad; %%% [m]
BL.theta_ad_test=trapz(etaref,1./interp1(FProps.eta,FProps.rhoR,etaref)
.*solref.uj.*(1-solref.uj)); %%% test
BL.theta_test=Nx/propsE.rhoE(ii)*BL.theta_ad_test; %%% test
BL.theta_k_ad=trapz(etaref,solref.uj.*(1-solref.uj)./
(interp1(FProps.eta,propsE.rhoE(ii)./FProps.rhoR,etaref)));% [m3/kg], eq. 6.109 in Clutter
BL.theta_k=Nx*BL.theta_k_ad; %%% [m], kinetic
% momentum thickness Reynolds number
BL.R_theta=propsE.UE(ii)/nuk(end)*BL.theta; %%% [-],  (01-07-2017)
BL.R_kin_displ=propsE.UE(ii)/nuk(end)*BL.theta_k;
% form factor, H
BL.H=BL.delta_ast_ad/BL.theta_ad;
BL.H2=BL.theta_k_ad/BL.theta_ad;
% wall shear stress
BL.tau=1/Nx*FProps.C(1)*propsE.rhoE(ii)*propsE.muE(ii)*propsE.UE(ii)*solfin.vj(1);
% skin friction coefficient
BL.cf=2*BL.tau/propsE.UE(ii)^2*(FProps.rhoR(1)/propsE.rhoE(ii));
% heat transfer (approximation)
BL.q=-1/Nx/FProps.Pr(1)*FProps.C(1)*propsE.rhoE(ii)*propsE.muE(ii)*
*HE*solfing.Gj(1); %%% [J/m2/s] = [W/m2], heat flux -> heat transferred
% pressure gradient coefficient (2 definition found in literature)
```

```
BL.lamb = P*propsE.UE(ii)./S(ii)/propsE.muE(ii)*propsE.rhoE(ii).*BL.delta.^2;
BL.la = P*propsE.UE(ii)./S(ii)/propsE.muE(ii)*propsE.rhoE(ii).*BL.theta.^2;
% Temperature gradient at wall (to be added)
if opt==1 || opt==2
R=8.314472/28.97;%kJ/kg.K
GAM=1.4; %%air
cpwall=R*GAM/(GAM-1)*1000;%J/kg.K
elseif opt==3
cpwall=FProps.HeatCapP('Ph',propsE.PRES/10^5,FProps.h(1)/1000)*1000;%J/kg
end
BL.DTDY=HE*solfing.Gj(1)/Nx/FProps.rhoR(1)*propsE.rhoE(ii)/cpwall;
% Nusselt number (to be added)

%temperature for high Mach number
%BL.Recovery_check=./(TTZ-propsE.TSE(ii).);
BL.r=sqrt(propsE.Pr(ii)); %laminar
BL.Trf= propsE.TSE(ii).*(1+BL.r.*(propsE.gamma-1)/2*propsE.ME(ii).^2);

BL.Sv=FProps.C*propsE.UE(ii).^3/S(ii).*(solfin.vj).^2.*rho(ii)./(propsE.HSE(ii).
*1000/cpw- (propsE.UE(ii).*solfin.uj).^2/(2*cpwall)); %
BL.Sa=trapz(solfin.x,BL.Sv./rho(ii))*Nx;
BL.Cd=(propsE.TSE(ii))*BL.Sa/propsE.rhoE(ii)./propsE.UE(ii).^3; %per mach low
%BL.Cd=(BL.Trf*BL.Sa)/propsE.rhoE(ii)./propsE.UE(ii).^3; %high Mach
% %IMPLEMENTATION OF NON ADIABATIC CASE
% Sv=FProps.C*propsE.UE(ii).^3/S(ii).*(solfin.vj).^2.*rho(ii)./(propsE.TSE(ii))+

+BL.q; %  more general now
% BL.Sa=trapz(etaref,interp1(Sv,etaref));
% BL.Sa=trapz(solfin.x,Sv/rho(ii))*Nx;
% BL.Cd=(propsE.TSE(ii))*BL.Sa/propsE.rhoE(ii)./propsE.UE(ii).^3;
```

These are the main "pieces" of our code, to understand the general numerical structure (Keller-box method) matricial coefficient, Newton iteration method and turbulence model the reader must read the other thesis work [38]. In the same work the turbulence model and its the integration in the code.

Appendix C

On the nature of dissipation

The concept of dissipation is the fundamental physics phenomenon behind the results of this thesis work and the Cd (dissipation coefficient) is the parameter associated. All the fluid dynamics concept (in continuum mechanics) are contained in the Navier Stokes equations:

$$\frac{\partial \varrho}{\partial t} + \nabla \cdot (\varrho \vec{u}) = 0, \tag{C.1}$$

$$\varrho \frac{D\vec{U}}{Dt} = \varrho \vec{g} - \nabla p + \frac{\partial}{\partial x_j}[\mu(\frac{\partial u_i}{\partial x_j} + \frac{\partial u_i}{\partial x_j}) + \delta_{ij}\lambda \nabla \cdot (\vec{U})], \tag{C.2}$$

$$\varrho \frac{Dh}{Dt} = \frac{DP}{Dt} + \nabla \cdot (k \nabla (T)) + \vec{\Phi}. \tag{C.3}$$

This set of equation (respectively continuity, momentum and energy) are valid for Newtonian fluids, and whatever flow regime (in turbulent [44, 71] the istantaneous terms must be substitute). Moreover they contained the constitutive relation based on Newtonian assumption. The dissipative phenomena are contained in the dissipation function Φ characterized by a particular formulation derivated by Stokesian nature of fluids. In explicit general three dimensional formulation is:

$$\vec{\Phi} = \tau_{ij} \frac{\partial u_i}{\partial x_j}, \tag{C.4}$$

and in extended version cartesian 3-dimensional:

$$\vec{\Phi} = \mu[(2\frac{\partial u}{\partial x})^2 + 2(\frac{\partial v}{\partial y})^2 + 2(\frac{\partial w}{\partial z})^2 + (\frac{\partial u}{\partial y} + \frac{\partial v}{\partial x})^2 + (\frac{\partial w}{\partial y} + \frac{\partial v}{\partial z})^2 + (\frac{\partial u}{\partial z} + \frac{\partial w}{\partial x})^2] + \lambda(\frac{\partial u}{\partial x} + \frac{\partial v}{\partial y} + \frac{\partial w}{\partial z})^2,$$

(C.5)

where λ is the Lamè constant and the dynamic viscosity μ is always positive and is a macroscpic manifestation of molecular interaction. Looking C.5 the Φ term is positive always and is strictly correlated with the generation of entropy, therefore the dissipation coefficient is the dimensionless parameter related. In chapter 2 [37] speculates about the possibility to have negativity of this term: the unique solution is violating Stokes hypothesis:

$$\mu < 0 \qquad\qquad \lambda + \frac{2}{3} \geq 0,$$

Introducing at this point the *boundary layer hypothesis*, the set of equations changes and strong simplification are introduced:

$$(\frac{\partial w}{\partial z})^2 = 0 \qquad (\frac{\partial w}{\partial y} + \frac{\partial v}{\partial z})^2 = 0 \qquad (\frac{\partial u}{\partial z} + \frac{\partial w}{\partial x})^2 = 0 \qquad \lambda \approx 0 \tag{C.6}$$

The results is

$$\vec{\Phi} = 2\mu[(\frac{\partial u}{\partial x})^2 + (\frac{\partial v}{\partial y})^2] + ((\frac{\partial v}{\partial x}) + (\frac{\partial u}{\partial y}))^2 \tag{C.7}$$

Introducing, through magnitude analysis, the following simplifications

$$v << u \qquad\qquad \frac{\partial}{\partial x} << \frac{\partial}{\partial y} \tag{C.8}$$

The final result of the dissipation function for a Prandtl boundary layer:

$$\vec{\Phi} \approx \mu\tau_{xy}(\frac{\partial u}{\partial y}) = \mu(\frac{\partial u}{\partial y})^2 \tag{C.9}$$

This is the classical fluid dynamic vision of dissipation; in order to link this concept with the Denton formulation based on entropy approch (Appendix 1 [1]) this final expression must simply divided by static temperature of the flow particle

$$\dot{S}_v = \frac{\vec{\Phi}}{T} = \frac{\mu}{T}(\frac{\partial u}{\partial y})^2 \tag{C.10}$$

This connection introduces the entropy point of view so also the entropy transport equation is important. This formulation is achieved in different ways [1, 36, 57], naturally the result is the same. In particular the path followed by the first two is based on splitting the energy equation in two parts:

- kinetic energy equation
- enthalpy equation

Taking the second one and using the *Gibbs equation*, the final form is obtained:

$$\varrho \frac{Ds}{Dt} = \dot{Q} + \tau_{ij} \frac{\partial u_i}{\partial x_j} - \frac{\partial q}{\partial x_i}, \tag{C.11}$$

where $\dot{Q}$ is the source/sink term. Integrating and splitting the heat transfer term, using Gauss theorem:

$$\int_V \varrho \frac{Ds}{Dt} dV = \int_V \frac{\Phi}{T} dV + \int_V \frac{k}{T^2} (\frac{\partial T}{\partial x_i})^2 dV + \int_A \frac{k}{T} \frac{\partial T}{\partial x_i} \cdot \vec{n} dA \tag{C.12}$$

In two-dimensional, steady-state boundary layer field without energy generation in control volume, the expression becomes:

$$\varrho \frac{ds_x}{dx} = \tau_{xy} \frac{du_x}{dy} - \frac{dq}{dy} \tag{C.13}$$

Recalling that the convention about the sign of heat transfer: negative since is transferred to the on the ambient. This expression contains all the physical concept needed for the Cd coefficient: the only way to increase entropy are

- heat transfer to flow
- increase in entropy though irreversibilietis effect due to viscous friction, always present in whatever phenomena

The cooling phenomena reduce the entropy could decrease the increasing in entropy. Integrating this equation on the boundary layer domain (thickness) the *generation entropy per unit area* is then computed [1] eq.A17

$$\frac{d}{dx} \int_0^\delta (\varrho u_x (s - s_\delta)) dy = \int_0^\delta (\frac{\tau_{xy}}{T} \frac{du_x}{dy} - \frac{dq}{dy}) dy. \tag{C.14}$$

The purpose of this work was the adiabatic study of a boundary layer therefore the term dq is set equal to zero in all the simulations. As already showed this formulation is in the standard coordinates, no suitable for BL study.

C.1 Cd concept

The central coefficient of this work is C_d since all physical - based model depends by it. The definition, as alreast told, is:

The reference temperature could be selected equal to edge for low speed or recovery temperature (wall one) for high speed [1] pag.6 and also [36] eq. 5.4.12. However for the sake of consistency the best reference is edge one since in turbomachines application this condition is known and the boundary layer could be totally skip out. Cd is not only the crucial parameter in the turbomachines physical-based losses but it is something more: it represents the state of boundary layer, describes some flow phenomena (the order of magnitude indicates what is the flow regime) and defines quantitatively the dissipation inside the layer. It can be view also not a destruction of kinetic energy but as a generation of entropy. Some authors [59, 1] underline the superior aspects of this coefficient with respect to classical friction coefficient C_f and drag one C_D. As already mentioned in chapter 3 the superiority of dissipation coefficient.

The computation of C_d starts from the basic parameters of boundary layer:

- f" shear parameter
- C Chapman -Rubesin parameter
- u_e velocity at hte edge
- transformed coordinate η and N_x

Here following the derivation typical of boundary layer environment:

1. derivation of entropy generation per unit volume

$$\dot{S}_v = \frac{\mu}{T}(\frac{\partial u}{\partial y})^2 \qquad (\frac{\partial u}{\partial y})^2 = u_e^2(\frac{\partial f'}{\partial \eta})^2(\frac{\partial \eta}{\partial y})_x^2 \qquad (\frac{\partial \eta}{\partial y})_x = \sqrt{\frac{u_e}{\varrho_e \mu_e x}}\varrho, \tag{C.15}$$

2. Integration in transformed domain [39] eq.6.4:

$$\dot{S}_a = \int_0^y (\dot{S}_v)dy \qquad \frac{\partial \eta}{\sqrt{\frac{u_e}{\varrho_e \mu_e x}}\varrho} = \partial y, \tag{C.16}$$

3. Putting all inside the Cd expression the final forulation is obtained:

$$C_d = \sqrt{\frac{\varrho_e \mu_e x}{u_e}} \int_o^\delta [\frac{T_e}{T}\frac{C}{x}(f")^2]d\eta, \tag{C.17}$$

The parameter expressed in this terms reveals all the physical meaning. The properties of fluids are contained in Chapman-Rubesin parameter (viscosity) and the ratio of temperature. The flow kinetic properties are contained in the shear stress parameter. The horizontal coordinate determines the typical decrease shape of C_d along the surface. Moreover the transformation coordinate shows clearly how compressibility increase the thickness of boundary layer, universal behavior [66, 81]. As shown in section 4.4 the important parameter is the temperature ratio which is a function of fluid nature.
At this point is necessary introducing the turbulent implementation. In this section a further improvement from theoretical point of view will be presented: dissipation coefficient as formulated by Denton is a entropy dimensionless coefficient however in terms of energetic systems can be very important also the exergetic point of view. Exergy is the maximum theoretical work obtainable from an overall apparatus consisting of a system and the environment as the system comes into equilibrium with the environment (passes to the dead state) [78]. The general definition of exergy for system state is the following:

$$Ex = U + P_0V - T_0S + \sum_i \mu_i n_i \tag{C.18}$$

Where U, V S are respectively the internal energy, volume and entropy of the system P_0, T_0 are the pressure and the temperature of the environment and finally the summation is for the chemical exergy amount. Neglecting the last part and focusing on the first one: Using the Gouy-Stodola theorem:

$$\dot{W} = \dot{W}_{rev} - T_0\dot{S} \ , \tag{C.19}$$

which states that the mechanical work is given by the ideal (reversible) one minus the generation of entropy multiplied by the environment temperature.
The question is: how can we connect this thermodynamic concept to our study? Through the dissipation coefficient itself because:

$$C_d = \frac{T_e S_a}{\varrho u^3}_e \tag{C.20}$$

Making simply:

$$1 - C_d = \frac{\varrho u^3 - TS_a}{\varrho u^3} \ , \tag{C.21}$$

This represents a second law efficiency for boundary layer which represent the destruction of exergy (mechanical work): the other face of entropy generation due to viscous flow phenomena in boundary layer. This is the typical approach used in the contemporary power system.

C.2 The problem of entropy transport in turbulent flow

The turbulent regime has been investigated from the beginning of the boundary layer theory though the poor fluid mechanics knowledge about such complexity phenomenon as turbulence did not allow a deep comprehension of its manifestation in the layer. The impossibility to develop a totally analytically theory was challenged by many authors and the first results and discovers were formulated only in '50 with Van Driest, Klebanoff and then Schlichting. The work of Moore [57] gives a clear framework related to this problem. In fact in the laminar regime the concept of energy cascade is not present [71, 44] otherwise in turbulent regime, this fact increases the complexity of the phenomenon. The eqaution proposed by Moore is the following:

$$\sigma = \varrho Ds + \nabla \cdot (\frac{q}{T}) - \frac{\psi}{T} \tag{C.22}$$

This is the most general approach since the production of entropy (σ) is given by increase of entropy itself, the heat flux and subtracted the radiation phenomena.
Woods' analysis which we use is for laminar flow. In laminar flow, shear work results directly in entropy production; there is no intermediate turbulence kinetic energy. In turbulent flow, however, some of the shear work results directly in entropy production while the rest is temporarily stored as kinetic energy of turbulence. Thus, in turbulent flow, shear work at one point in the flow can result in entropy production downstream; the loss process then has history and is no longer a local phenomenon. In particular the concept of instantaneous values is applied to each quantities, scalar and vectorial ones.

$$\sigma = \overline{\sigma} + \sigma' \qquad T = \overline{T} + T' \qquad u = \overline{u} + u', \tag{C.23}$$

And the dissipation integral becomes:

$$D = \int_0^e \mu(\frac{\partial u}{\partial y})^2 dy + \int_0^e \epsilon dy + \frac{\varrho}{dx} \int_0^e \overline{u} \frac{q^2}{2} dy, \tag{C.24}$$

In turbulence field the dissipation is caused also by the ϵ typical parameter of the energy cascade. Looking at the Schlicthing [66] the energy transport equation:

$$\underbrace{\varrho c_p(\overline{u}\frac{\partial\overline{T}}{\partial x}+\overline{v}\frac{\partial\overline{T}}{\partial y}\overline{w}\frac{\partial\overline{T}}{\partial z})}_{\text{convection}}$$
$$=\underbrace{k(\frac{\partial^2\overline{T}}{\partial x^2}+\frac{\partial^2\overline{T}}{\partial y^2}\frac{\partial^2\overline{T}}{\partial z^2})}_{\text{molecular heat tranport}}\underbrace{-\varrho c_p(\frac{\partial\overline{u'T}}{\partial x}+\frac{\partial\overline{v'T}}{\partial y}+\frac{\partial\overline{w'T}}{\partial z})}_{\text{turbulent heat transport}}+$$
$$\underbrace{+\mu[2(\frac{\partial\overline{u}}{\partial x})^2+2(\frac{\partial\overline{v}}{\partial y})^2+2(\frac{\partial\overline{w}}{\partial z})^2+(\frac{\partial\overline{u}}{\partial y}+\frac{\partial\overline{v}}{\partial x})^2+(\frac{\partial\overline{u}}{\partial z}+\frac{\partial\overline{w}}{\partial x})^2+(\frac{\partial\overline{v}}{\partial z}+\frac{\partial\overline{w}}{\partial y})^2]}_{\text{direct dissipation}}+\underbrace{\varrho\tilde{\epsilon}}_{\text{turbulent dissipation}}, \tag{C.25}$$

Therefore, looking at the Navier- Stokes the dissipation in turbulent regime is higher than in laminar and this causes an increase of temperature. At this point a closure problem is needed, in other words a turbulence model is required. The typical RANS model are described in whatever CFD book [43, 44, 71]; in the case of this thesis work a 0-equation model is used, the Cebeci-Smith [40, 79].
The cascade phenomena complicates strongly the theoretical frame since part of the energy is directly dissipated in the mean flow C.25 and another part passes to smaller scale towards the Kolmogorov structure. To conclude the dissipation concept is not easy to manage in turbulence field, now, if the temperature becomes so high the radiation interactions become important and therefore the complexity of the analysis explodes since the radiation is non-local phenomena.

Appendix D

Turbulence model in CFD validation

The Menter Shear Stress Transport Turbulence Model

This model is a 2-equations model proposed by Menter in 1994 to overcome the severe limitations of $k-\varepsilon$ and $k-\omega$ [82]. A great source of information about the model and its application is https://turbmodels.larc.nasa.gov/sst.html. It is a 2-equations model which means that the fluid mechanics phenomena are studied with the Navier-Stokes plus two more turbulent equations respectively the turbulent kinetic energy (TKE) k-equation equation and the turbulence frequency ω-equation close to the wall. In formulas:

$$\underbrace{\frac{\partial(\varrho k)}{\partial t}}_{(\mathrm{I})}+\underbrace{\frac{\partial(\varrho u_j k)}{\partial x_j}}_{\mathrm{II}}=\underbrace{P}_{\mathrm{III}}-\underbrace{\beta^*}_{\mathrm{IV}}+\underbrace{\frac{\partial}{\partial x_j}[(\mu\sigma_k\mu_t)\frac{\partial k}{\partial x_j}]}_{\mathrm{V}} \tag{D.1}$$

$$\underbrace{\frac{\partial(\varrho\omega)}{\partial t}}_{(\mathrm{I})}+\underbrace{\frac{\partial(\varrho u_j\omega)}{\partial x_j}}_{(\mathrm{II})}=\underbrace{\frac{\gamma}{\nu_t}P}_{(\mathrm{III})}\underbrace{-\beta\varrho\omega^2}_{(\mathrm{IV})}+\underbrace{\frac{\partial}{\partial x_j}[(\mu\sigma_\omega\mu_t)\frac{\partial\omega}{\partial x_j}]}_{(\mathrm{V})}+\underbrace{2(1-F_1)\frac{\varrho\sigma_{\omega 2}}{\omega}\frac{\partial(\varrho k)}{\partial x_j}\frac{\partial(\varrho k)}{\partial x_j}}_{(\mathrm{VI})} \tag{D.2}$$

Where:

- (I) Rate of change of transport quantities
- (II) Transport by convection
- (III) Production: $\tau_{ij}\frac{\partial u_i}{\partial_j}$
- (IV) Destruction

- (V) Transport by diffusion
- (VI) Cross diffuesion term

And through the Prandtl-Kolmogorov relation modified:

$$\mu_t = \frac{\varrho a_1 k}{max(a_1 \omega\, \Omega F_2)} \tag{D.3}$$

The blending function is fundamental to make possible the connection between k-ω and the k-ε at certain point:

$$\phi = F_1 \Phi_1 + (1 - F_1)\Phi_2 \ , \tag{D.4}$$

where

$$F_1 = tanh(min[max(\frac{\sqrt{k}}{\beta^* \omega d} \ \ \frac{500\nu}{d^2\omega}) \ \ , \ \frac{4\varrho\sigma_{\omega 2} k}{CD_{k\omega} d^2}]) \ , \tag{D.5}$$

and:

$$CD = max(\varrho\sigma_{\omega 2} \ \frac{1}{\omega}\frac{\partial k}{\partial x_j}\frac{}{\frac{\omega}{x_j}} \ \ , \ 10^{-20}) \ , \tag{D.6}$$

The boundary conditions are:

$$\frac{U_\infty}{L} < \omega_{farfield} < 10\frac{U_\infty}{L} \tag{D.7}$$

$$\frac{10^{-5} U_\infty^2}{Re_L} < k_{farfield} < \frac{0.1 U_\infty^2}{Re_L} \tag{D.8}$$

$$\omega_{wall} = 10\frac{6\nu}{\beta_1(\delta d_1)^2} \ \ \text{and} \ \ \ k_{wall} = 0 \ , \tag{D.9}$$

where L is the approximate length of the computational domain, and the combination of the two far field values should yield a free stream turbulent viscosity between 10^{-5} and 10^{-2} times free stream laminar viscosity. Thus, the far field turbulence boundary conditions are somewhat open to interpretation. Note that the turbulence variables decay (sometimes dramatically) from their set values in the far field for external aerodynamic problems.
The constants are:

$$\sigma_{k1} = 0.85 \qquad \sigma_{\omega 1} = 0.5 \qquad \beta_1 = 0.075 \ , \tag{D.10}$$

$$\sigma_{k2} = 1 \qquad \sigma_{\omega 2} = 0.856 \qquad \beta_2 = 0.0828\ , \tag{D.11}$$

$$\beta^* = 0.09 \qquad \kappa = 0.41 \qquad a_1 = 0.31\ , \tag{D.12}$$

The model is totally closed. The final description is about the fundamental hypothesis t compute the Reynolds shear stress: the Boussinesq's hypothesis:

$$\tau_{ij} = 2\mu_\tau(S_{ij} - \frac{1}{3}\frac{\partial u_k}{\partial x_k}) - \frac{2}{3}\varrho k\delta_{ij} \tag{D.13}$$

Appendix E

Similitude concept and loss models

The general concept is reducing the complexity of the system introducing dimensionless group. The Buckingham theorem provides a method for computing sets of dimensionless parameters from given variables, even if the form of the equation remains unknown. However, the choice of dimensionless parameters is not unique; Buckingham's theorem only provides a way of generating sets of dimensionless parameters and does not indicate the most physically meaningful. Two systems for which these parameters coincide are called similar; they are equivalent for the purposes of the equation, and the experimentalist who wants to determine the form of the equation can choose the most convenient one. Most importantly, Buckingham's theorem describes the relation between the number of variables and fundamental dimensions. There are different category about similarity behavior [83]:

- **Geometric similarity**: the model must be the same shape as the prototype, but may be scaled by some constant factor.
- **Kinematic similarity**: the velocity at any point in the model flow must be proportional by a constant scale factor to the velocity at the homologous point in the prototype flow. (That is, the flow streamlines must have the same shape.)
- **Dynamic similarity**: all forces in the model flow must scale by a constant factor to the corresponding forces in the prototype flow. In other words, the relative importance of different types of forces (e.g., viscous and inertial forces) must be the same for the model and prototype. This requires that the model and prototype have the same dimensionless parameters (e.g., the same Reynolds number), although they may (and usually do) have different dimensional variables. Mathematically, for all p (π) groups that can be defined for two different flow situations, dynamic similarity requires that

$$\prod_{k,model} = \prod_{k,prototype} \qquad k = 1, 2, ..., p \ . \tag{E.1}$$

Thus, geometric and kinematic similarity are necessary but insufficient conditions for dynamic similarity. That is, it is possible to have geometric and kinematic similarity, but

not dynamic similarity.
Dimensional analysis applied to turbomachines has two further important uses:

- prediction of a prototype's performance from tests conducted on a scale model (similitude);
- determination of the most suitable type of machine, on the basis of maximum efficiency, for a specified range of head, speed, and flow rate;

An important difference is between incompressible and compressible fluid machines i.e thermal ones and hydraulic. Naturally the analysis is simpler for the first class since the number of variables of the system is lower. From the point of view of the flow, it can be considered incompressible if Ma < 0.3 [53]: in this case if the process is exploited at sufficiently high Reynold number, the dynamic similarity is achieved once the flow coefficient is the same. Obviously this thesis deals with thermal turbines therefore the interest is only about a compressible fluid analysis. Also for the most simple fluid model (ideal gas) two further characteristics are required: a_0, the stagnation speed of sound at the inlet machine and the γ ($\frac{c_p}{c_v}$), the ratio of specifics heats. Moreover if density has a important variation along the machine one the best variables selected are the mass flow rate $\dot{m}$ and the isentropic stagnation enthalpy change Δh_{0s}. The final functional form is the following [53]:

$$\Delta h_{0s}, \eta, P = f(\mu, N, D, \dot{m}, \varrho_{01}, c_{01}, \gamma) \tag{E.2}$$

Where Δh_{0s} is the total-to-static enthalpy drop, η is the efficiency and P is the power. In the right member there are: μ viscosity, N rotational speed, $\dot{m}$ mass flow rate, ϱ_{01} total density, c_{01} sonic velocity, γ ratio of specific heats.

$$\eta_{TS} = f(\underbrace{\Delta h_{TT}, h_0, h_1, h_2}_{\text{thermodynamic variables}}, \underbrace{\omega, D_0, D_1, D_2}_{\text{speed and size}}, \underbrace{u_{ax0}, v_{ax1}, v_{ax2}, v_0, w_2}_{\text{velocity triangles}}, \underbrace{\mu_1, \mu_2, \varrho_0, \varrho_1, \varrho_2, c_0, c_1, c_2}_{\text{fluid properties}} \underbrace{\Delta P_{Tstator}, \Delta P_{Trotor}}_{\text{losses}}), \tag{E.3}$$

The several groups include multiple variables, in total 24 where Δh is the enthalpy drop, v is velocity, D diameter, μ viscosity, ϱ is density, ω rotational speed, ΔP the power drop due to losses. The subscripts are: 0 for inlet, 1 stator outlet, 2 exit stage. The next step is applying the dimensionless analysis and selecting the group $\prod_1 = \frac{\Delta h_{TT}}{\omega^2 D_1^2}$. The benefits are multiple: first the number of variables will decrease, second we will obtain groups which represent different concepts; therefore the final form is:

Loss models

Soderberg model

The model of Soderberg [53] joins all the losses in a unique group only distinguishing rotor and stator. Such a system was developed by Soderberg (1949) from a large number of tests performed on steam turbines and on cascades and extended to fit data obtained from small turbines with very low aspect ratio blading (small height–chord). Soderberg found that with the optimum space–chord ratio (using Zweifel's criterion), turbine blade losses could be correlated with space–chord ratio, blade aspect ratio, blade thickness–chord ratio and Reynolds number. For turbine blade rows operating at this load coefficient, with a Reynolds number of 10^5 and aspect ratio $\frac{H}{b}$ blade height/axial chord of 3, the "nominal" loss coefficient, ζ^* is a simple function of the fluid deflection angle, $\varepsilon = \alpha_{in} + \alpha_{out}$, for a given thickness–chord ratio ($\frac{t_{max}}{l}$):

$$\zeta^* = 0.04 + 0.06\left(\frac{\varepsilon}{100}\right)^2 \qquad \text{deflection losses} \tag{E.4}$$

$$1 + \zeta = (1 + \zeta^*)\left(0.993 + 0.021\frac{b}{H}\right) \qquad \text{nozzle} \tag{E.5}$$

$$1 + \zeta = (1 + \zeta^*)\left(0.975 + 0.075\frac{b}{H}\right) \qquad \text{rotor} \tag{E.6}$$

Since this set of equation is based on a certain flow regime (Re $\approx 10^5$) a correction is necessary.

$$\zeta_2 = \frac{10^5}{Re} \tag{E.7}$$

Soderberg's method of loss prediction gives turbine efficiencies with an error of within 3 % over a wide range of Reynolds numbers and aspect ratios when additional corrections are included to allow for tip leakage and disc friction. The intrinsic limitation of this approach is the totally lack of knowledge about physical phenomena. No phenomenon about boundary layer is take into account.

Craig Cox

The other important classical model is the Craig Cox one [84]. In the table E.1 all the several groups are contained.

Group 1	**Group 2**
Guide profile loss	Guide gland leakage loss
Runner profile loss	Balance hole loss
Guide secondary loss	Rotor type leakage loss
Runner secondary loss	Lacing wire loss

Table E.1: Craig Cox groups of losses

This loss model is the most complex but comprehensive system of computation since it takes into account a wide class of phenomena. A major fact is that this model (like the previous) is valid for

The profile loss consists of an incompressible basic profile loss corrected by multiplying factors accounting for the Reynolds number, the incidence angle and the trailing edge. Further, the effect of Mach number, the suction trailing side curvature and the trailing edge thickness are added. The formula for calculating the profile loss coefficient is as follows:

$$\zeta_P = \chi_R \chi_{Te} \chi_i \zeta_{PO} + \Delta\zeta_{P,H} + \zeta_{P,SE} + \zeta_{P,TE} \tag{E.8}$$

The basic profile loss term ζ_{PO} is a function of a modified blade lift parameter C_L, which in turn depends on the flow turning and cascade solidity, and a contraction ratio CR which denotes the ratio of the inlet width to the throat width of the internal blade passage. While the Reynolds number factor χ_R depends only on the Re, the trailing edge thickness factor χ_{Te} depends on the fluid outlet angle as well as the ratio of trailing edge thickness to the blade pitch. Furthermore, the loss increment due to outlet Mach number for supersonic flows is accounted by the term χ_{PM} , which is a function of the outlet Mach number, blade pitch, throat width and trailing edge thickness. An additional term $\chi_{P,se}$ appears for the blades with curvature suction surfaces near trailing edges as opposed to straight suction back. This term depends on the outlet Mach number, the blade pitch and the camber line length. The last term $\chi_{P,Tt}$ depends on the blade pitch and trailing edge thickness which gives the loss increment due to trailing edge thickness.

Traupel

The Traupel model [85] is also based on the classical distinction between profile, secondary and tip leakage losses.

$$\zeta = \zeta_p + \zeta_s + \zeta_{tl} \ , \tag{E.9}$$

Focusing on profile losses field:

$$\zeta_p = \chi_R \chi_M \zeta_{PO} + \zeta_{Te} + \zeta_c \ , \tag{E.10}$$

χ_{PO} is the basic profile loss, which is a function of the inlet and outlet flow angles, χ_R is the Reynolds number multiplier which depends on the Reynolds number and the surface roughness, χ_M is the Mach number multiplier, depending on the free stream velocity, χ_{Te} is the trailing edge loss, generated due to the mixing of boundary layers in the wake and χ_C is the Carnot shock loss created during the sudden expansion of a fluid after the trailing edge. The trailing edge loss depends on the trailing edge thickness, outlet flow angle, basic profile loss, Reynolds number and the Mach number. This loss is generally proportional to the tangential projection of the trailing edge. The larger this projection is, the thicker the profile, or in other terms, at large outlet flow angle corresponds large loss due to the broader wake. The Carnot shock loss depends on the trailing edge thickness and flow angle at outlet of cascades as given by the formula below:

$$\zeta_C = \langle \frac{\Delta a}{1 - \Delta a} \rangle sin^2(\alpha_1) \qquad \text{where } \Delta a = \frac{t}{t \ sin(90° - \alpha_1)} \tag{E.11}$$

Glassman

Glassman derived expressions for two dimensional and three dimensional kinetic energy loss coefficient for the stator and rotor of a radial turbine . The two dimensional loss coefficient is as shown below

$$\overline{e}_{2D} = \frac{\psi_{tot}}{scos(\phi) - \delta_{tot} - t} \tag{E.12}$$

$$\phi = \begin{cases} \alpha_1 & \text{for stator} \\ \beta_1 & \text{for rotor} \end{cases} \tag{E.13}$$

And H is the shape factor and E is the energy factor [86]. It should be noted that the Glassman's loss coefficient is a function of the boundary layer parameters such as energy thickness and displacement thickness as shown below:

$$\begin{cases} \psi = E\theta \\ \delta = H\theta \end{cases} \tag{E.14}$$

The momentum thickness per unit surface length is expressed as a function of the Reynolds number:

$$\frac{\theta_{tot}}{l} = C\left(\frac{\theta_{TOT}}{l}\right)_{ref}\left(\frac{Re}{Re_{ref}}\right)^{-0.2}, \tag{E.15}$$

where C is a factor used to modify the loss level whenever required Finally the passage between two dimensional to three dimensional:

$$\frac{\overline{e}_{3D}}{\overline{e}_{2D}} = \frac{A_{3D}}{A_{2D}} \tag{E.16}$$

The area ratio for the stator and the rotor can be found from the geometric parameters such as inlet radius, outlet radius, surface length, chord length and the blade pitch:

$$\left(\frac{\overline{e}_{3D}}{\overline{e}_{2D}}\right) = \begin{cases} 1 + \frac{r_0^2 - r_1^2}{2r_1\left(\frac{l}{c}\right)\left(\frac{c}{s}\right)h_s} & \text{stator} \\ 1 + \frac{A_{wtr}+A_{whr}}{A_{br}}, & \text{rotor} \end{cases} \tag{E.17}$$

There are others loss model however they are not specific with the subject treated in this work. In particular Chen-Baines [31] deals with mixed flow machines, taking into account the loss mechanisms through the skin friction coefficient c_f.
All these methods presented have some limitations in particular the oldest ones. The semi-empirical nature manifests all its limitation for new technology or cases. This is one of the reason to develop a physical based approach able to describe generally the phenomena itself Denton proposed it [1].

Bibliography

[1] J.D Denton. Loss mechanisms in turbomachines. 322(10):891–921, 1905.

[2] J Do Denton and NA Cumpsty. Loss mechanisms in turbomachines. *Journal of Turbomachinery. Transactions of the ASME*, 115(4):621–656, 1993.

[3] Ashish Patel, Bendiks J Boersma, and Rene Pecnik. The influence of near-wall density and viscosity gradients on turbulence in channel flows. *Journal of Fluid Mechanics*, 809:793–820, 2016.

[4] RD Stieger and HP Hodson. Unsteady dissipation measurements on a flat plate subject to wake passing. *Proceedings of the Institution of Mechanical Engineers, Part A: Journal of Power and Energy*, 217(4):413–419, 2003.

[5] Piero Colonna, Emiliano Casati, Carsten Trapp, Tiemo Mathijssen, Jaakko Larjola, Teemu Turunen-Saaresti, and Antti Uusitalo. Organic rankine cycle power systems: from the concept to current technology, applications, and an outlook to the future. *Journal of Engineering for Gas Turbines and Power*, 137(10):100801, 2015.

[6] P Colonna and TP Van der Stelt. Fluidprop: a program for the estimation of thermo physical properties of fluids. *Energy Technology Section, Delft University of Technology, Delft, The Netherlands, http://www. FluidProp. com*, 2004.

[7] G Angelino, M Gaia, and E Macchi. A review of italian activity in the field of organic rankine cycles. *VDI-Berichte*, (539):465–482, 1984.

[8] E Macchi and A Perdichizzi. Efficiency prediction for axial-flow turbines operating with nonconventional fluids. *Journal of engineering for power*, 103(4):718–724, 1981.

[9] Ennio Macchi and Marco Astolfi. *Organic rankine cycle (ORC) power systems: Technologies and applications*. Woodhead Publishing, 2016.

[10] Giacomo Persico, Matteo Pini, Vincenzo Dossena, and Paolo Gaetani. Aerodynamics of centrifugal turbine cascades. *Journal of Engineering for Gas Turbines and Power*, 137(11):112602, 2015.

[11] Matteo Pini, Giacomo Persico, Emiliano Casati, and Vincenzo Dossena. Preliminary design of a centrifugal turbine for organic rankine cycle applications. *Journal of Engineering for Gas turbines and power*, 135(4):042312, 2013.

[12] Teemu Turunen-Saaresti, Antti Uusitalo, and Juha Honkatukia. Design and testing of high temperature micro-orc test stand using siloxane as working fluid. In *Journal of Physics: Conference Series*, volume 821, page 012024. IOP Publishing, 2017.

[13] Emiliano Casati, Salvatore Vitale, Matteo Pini, Giacomo Persico, and Piero Colonna. Centrifugal turbines for mini-organic rankine cycle power systems. *Journal of Engineering for Gas Turbines and Power*, 136(12):122607, 2014.

[14] Matteo Burigana. Fluid dynamic design and optimization of a mini-orc turbine for high temperature application, 2016-2017.

[15] P Colonna, S Rebay, J Harinck, and A Guardone. Real-gas effects in orc turbine flow simulations: influence of thermodynamic models on flow fields and performance parameters. In *ECCOMAS CFD 2006: Proceedings of the European Conference on Computational Fluid Dynamics, Egmond aan Zee, The Netherlands, September 5-8, 2006*. Delft University of Technology; European Community on Computational Methods in Applied Sciences (ECCOMAS), 2006.

[16] Adam Joseph Head, Carlo De Servi, Emiliano Casati, Matteo Pini, and Piero Colonna. Preliminary design of the orchid: a facility for studying non-ideal compressible fluid dynamics and testing orc expanders. In *ASME Turbo Expo*, pages V003T25A001–V003T25A001, 2016.

[17] P Colonna, NR Nannan, A Guardone, and TP Van der Stelt. On the computation of the fundamental derivative of gas dynamics using equations of state. *Fluid Phase Equilibria*, 286(1):43–54, 2009.

[18] P Colonna and A Guardone. Molecular interpretation of nonclassical gas dynamics of dense vapors under the van der waals model. *Physics of Fluids*, 18(5):056101, 2006.

[19] Hans Albrecht Bethe. On the theory of shock waves for an arbitrary equation of state. In *Classic papers in shock compression science*, pages 421–495. Springer, 1998.

[20] J Harinck, A Guardone, and P Colonna. The influence of molecular complexity on expanding flows of ideal and dense gases. *Physics of fluids*, 21(8):086101, 2009.

[21] Philip A Thompson. A fundamental derivative in gasdynamics. *The Physics of Fluids*, 14(9):1843–1849, 1971.

[22] Konstantine C Lambrakis and Philip A Thompson. Existence of real fluids with a negative fundamental derivative γ. *The Physics of Fluids*, 15(5):933–935, 1972.

[23] DG Ainley and G Cr Mathieson. A method of performance estimation for axial-flow turbines. Technical report, AERONAUTICAL RESEARCH COUNCIL LONDON (UNITED KINGDOM), 1951.

[24] SL Dixon. Fluid mechanics, thermodynamics of turbomachinery. butterworth, 1998.

[25] SC Kacker and U Okapuu. A mean line prediction method for axial flow turbine efficiency. *Journal of engineering for power*, 104(1):111–119, 1982.

[26] John D Denton. Entropy generation in turbomachinery flows. Technical report, SAE Technical Paper, 1990.

[27] A Kluwick. Non-ideal compressible fluid dynamics: A challenge for theory. In *Journal of Physics: Conference Series*, volume 821, page 012001. IOP Publishing, 2017.

[28] SF Smith. A simple correlation of turbine efficiency. *The Aeronautical Journal*, 69(655):467–470, 1965.

[29] Francisco Palacios, Michael R Colonno, Aniket C Aranake, Alejandro Campos, Sean R Copeland, Thomas D Economon, Amrita K Lonkar, Trent W Lukaczyk, Thomas WR Taylor, and Juan J Alonso. Stanford university unstructured (su2): An open-source integrated computational environment for multi-physics simulation and design. *AIAA Paper*, 287:2013, 2013.

[30] Prof. Matteo Pini. Similarity criteria fot turbines operating non-ideal compressible flows, 2015.

[31] H Chen and NC Baines. The aerodynamic loading of radial and mixed-flow turbines. *International journal of mechanical sciences*, 36(1):63–79, 1994.

[32] Carlo Osnaghi. *Teoria delle turbomacchine*. Società Editrice Esculapio, 2013.

[33] LE Brown. Axial flow compressor and turbine loss coefficients: A comparison of several parameters. *Journal of Engineering for Power*, 94(3):193–201, 1972.

[34] Ronald H Aungier. *Preliminary Aerodynamic Design of Axial-Flow Turbine Stages*. ASME press, 2006.

[35] J Dunham and PM Came. Improvements to the ainley-mathieson method of turbine performance prediction. *Journal of Engineering for Power*, 92(3):252–256, 1970.

[36] Edward M Greitzer, Choon Sooi Tan, and Martin B Graf. *Internal flow: concepts and applications*, volume 3. Cambridge University Press, 2007.

[37] Frank M White and Isla Corfield. *Viscous fluid flow*, volume 3. McGraw-Hill Higher Education Boston, 2006.

[38] D.D. Dijkshoorn. Matlab code validation and verification, 2018.

[39] Darwin W Clutter and AM Smith. Solution of the general boundary-layer equations for compressible laminar flow, including transverse curvature. Technical report, DOUGLAS AIRCRAFT CO LONG BEACH CA AIRCRAFT DIV, 1963.

[40] Tuncer Cebeci. Calculation of laminar and turbulent boundary layers for two-dimensional time-dependent flows. 1977.

[41] Hermann Schlichting, Klaus Gersten, Egon Krause, and Herbert Oertel. *Boundary-layer theory*, volume 7. Springer, 1955.

[42] Itiro Tani. On the approximate solution of the laminar boundary-layer equations. *Journal of the Aeronautical Sciences*, 21(7):487–495, 1954.

[43] David C Wilcox et al. *Turbulence modeling for CFD*, volume 2. DCW industries La Canada, CA, 1998.

[44] Stephen B Pope. Turbulent flows, 2001.

[45] C Dijkshoorn D.D Pizzi, F De Servi. A boundary layer code for real gas computation, 2018.

[46] Herbert B Keller. Numerical methods in boundary-layer theory. *Annual Review of Fluid Mechanics*, 10(1):417–433, 1978.

[47] Tuncer Cebeci and LW Carr. A computer program for calculating laminar and turbulent boundary layers for two-dimensional time-dependent flows. 1978.

[48] AR Wazzan, C Gazley Jr, and Apollo Milton Olin Smith. Hr/x/method for predicting transition. *AIAA Journal*, 19:810–812, 1981.

[49] AM Smith and Tuncer Cebeci. Numerical solution of the turbulent-boundary-layer equations. Technical report, DOUGLAS AIRCRAFT CO LONG BEACH CA AIRCRAFT DIV, 1967.

[50] Tuncer Cebeci. *Convective heat transfer*. Springer, 2002.

[51] Tuncer Cebeci. *Analysis of turbulent boundary layers*, volume 15. Elsevier, 2012.

[52] John D Coull and Howard P Hodson. Blade loading and its application in the mean-line design of low pressure turbines. *Journal of Turbomachinery*, 135(2):021032, 2013.

[53] SL Dixon and C Hall. Fluid mechanics and thermodynamics of turbomachinery retrieved from http://canterbury. eblib. com. au/patron. *FullRecord. aspx*, 2010.

[54] O Zweifel. The spacing of turbo-machine blading, especially with large angular deflection. *Brown Boveri Rev.*, 32(12):436–444, 1945.

[55] John David Anderson Jr. *Fundamentals of aerodynamics*. Tata McGraw-Hill Education, 2010.

[56] Giovanni Lozza. A comparison between the craig-cox and the kacker-okapuu methods of turbine performance prediction. *Meccanica*, 17(4):211–221, 1982.

[57] John Moore and Joan G Moore. Entropy production rates from viscous flow calculations: Part i—a turbulent boundary layer flow. In *ASME 1983 International Gas Turbine Conference and Exhibit*, pages V001T01A032–V001T01A032. American Society of Mechanical Engineers, 1983.

[58] WN Dawes. A comparison of zero and one equation turbulence modelling for turbomachinery calculations. *ASME paper*, (90-GT):303, 1990.

[59] Mark Drela and Michael B Giles. Viscous-inviscid analysis of transonic and low reynolds number airfoils. *AIAA journal*, 25(10):1347–1355, 1987.

[60] Mark Drela. Power balance in aerodynamic flows. *AIAA journal*, 47(7):1761, 2009.

[61] William Sutherland. Lii. the viscosity of gases and molecular force. *The London, Edinburgh, and Dublin Philosophical Magazine and Journal of Science*, 36(223):507–531, 1893.

[62] Clarence B Cohen and Eli Reshotko. Similar solutions for the compressible laminar boundary layer with heat transfer and pressure gradient. Technical report, FLIGHT PROPULSION RESEARCH LAB CLEVELAND OH, 1955.

[63] Leslie Howarth. On the solution of the laminar boundary layer equations. In *Proceedings of the Royal Society of London A: Mathematical, Physical and Engineering Sciences*, volume 164, pages 547–579. The Royal Society, 1938.

[64] Luigi Crocco. Boundary layer of gases along a flat plate. *Rendiconti Mat., Univ. Roma, ser. V*, 2:138, 1941.

[65] Ec R Van Driest. Investigation of laminar boundary layer in compressible fluids using the crocco method. 1952.

[66] Hermann Schlichting (Deceased) and Klaus Gersten. *Unsteady Turbulent Boundary Layers*, pages 645–651. Springer Berlin Heidelberg, Berlin, Heidelberg, 2017.

[67] MF Shahab, G Lehnasch, TB Gatski, and P Comte. Statistical characteristics of an isothermal, supersonic developing boundary layer flow from dns data. *Flow, turbulence and combustion*, 86(3):369–397, 2011.

[68] Alfred Kluwick. Internal flows of dense gases. *Acta mechanica*, 169(1):123–143, 2004.

[69] JCj Rotta. Turbulent boundary layers in incompressible flow. *Progress in Aerospace Sciences*, 2(1):1–95, 1962.

[70] Alfred Walz. Compressible turbulent boundary layers with heat transfer and pressure gradient in flow direction. *J. Research Natl. Bur. Standards*, 63, 1959.

[71] Henk Kaarle Versteeg and Weeratunge Malalasekera. *An introduction to computational fluid dynamics: the finite volume method*. Pearson Education, 2007.

[72] H Tennekes. Law of the wall for turbulent boundary layers in compressible flow. *AIAA Journal*, 5(3):489–492, 1967.

[73] ER Van Driest. Turbulent boundary layer in compressible fluids. *Journal of the Aeronautical Sciences*, 18(3):145–160, 1951.

[74] ER Van Driest. On turbulent flow near a wall. *Journal of the Aeronautical Sciences*, 23(11):1007–1011, 1956.

[75] Alexander J Smits and Jean-Paul Dussauge. *Turbulent shear layers in supersonic flow*. Springer Science & Business Media, 2006.

[76] Soshi Kawai. Direct numerical simulation of transcritical turbulent boundary layers at supercritical pressures with strong real fluid effects. In *54th AIAA Aerospace Sciences Meeting*, page 1934, 2016.

[77] J Rotta. Schubspannungsverteilung und energiedissipation bei turbulenten grenzschichten. *Ingenieur-Archiv*, 20(3):195–207, 1952.

[78] Michael J Moran, Howard N Shapiro, Daisie D Boettner, and Margaret B Bailey. *Fundamentals of engineering thermodynamics*. John Wiley & Sons, 2010.

[79] Tuncer Cebeci. *Analysis of turbulent flows with computer programs*. Butterworth-Heinemann, 2013.

[80] Theodore L Bergman and Frank P Incropera. *Fundamentals of heat and mass transfer*. John Wiley & Sons, 2011.

[81] Tuncer Cebeci. *Turbulence models and their application: efficient numerical methods with computer programs*. Springer Science & Business Media, 2003.

[82] Florian R Menter. Two-equation eddy-viscosity turbulence models for engineering applications. *AIAA journal*, 32(8):1598–1605, 1994.

[83] Yunus A Cengel. *Fluid mechanics*. Tata McGraw-Hill Education, 2010.

[84] HRM Craig and HJA Cox. Performance estimation of axial flow turbines. *Proceedings of the Institution of Mechanical Engineers*, 185(1):407–424, 1970.

[85] Walter Traupel. *Thermische Turbomaschinen: Thermodynamisch-strömungstechnische Berechnung*. Springer-Verlag, 2012.

[86] Peter L Meitner and Arthur J Glassman. Off-design performance loss model for radial turbines with pivoting, variable-area stators. Technical report, NATIONAL AERONAUTICS AND SPACE ADMINISTRATION CLEVELAND OH LEWIS RESEARCH CENTER, 1980.